INFORMATION TO USERS

This manuscript has been reproduced from the microfilm master. UMI films the text directly from the original or copy submitted. Thus, some thesis and dissertation copies are in typewriter face, while others may be from any type of computer printer.

The quality of this reproduction is dependent upon the quality of the copy submitted. Broken or indistinct print, colored or poor quality illustrations and photographs, print bleedthrough, substandard margins, and improper alignment can adversely affect reproduction.

In the unlikely event that the author did not send UMI a complete manuscript and there are missing pages, these will be noted. Also, if unauthorized copyright material had to be removed, a note will indicate the deletion.

Oversize materials (e.g., maps, drawings, charts) are reproduced by sectioning the original, beginning at the upper left-hand corner and continuing from left to right in equal sections with small overlaps.

ProQuest Information and Learning
300 North Zeeb Road, Ann Arbor, MI 48106-1346 USA
800-521-0600

The Involvement of Mitochondria in the Cell Death Process:

Communication from Mitochondria to the Nucleus

Michael Lynn Adams

A dissertation submitted in partial fulfillment of the requirements for the degree of

Doctor of Philosophy

University of Washington

2003

Program Authorized to Offer Degree:
School of Pharmacy, Department of Medicinal Chemistry

In presenting this dissertation in partial fulfillment of the requirements for the Doctoral degree at the University of Washington, I agree that the Library shall make copies freely available for inspection. I further agree that extensive copying of the dissertation is allowable only for scholarly purposes, consistent with "fair use" as prescribed in the U.S. Copyright Law. Requests for copying or reproduction of this dissertation may be referred to Proquest Information and Learning, 300 North Zeeb Road, Ann Arbor, MI 48106-1346, to whom the author has granted "the right to reproduce and sell (a) copies of the manuscript in microform and/or (b) printed copies of the manuscript made from microform."

Signature 

Date 3/3/03

University of Washington
Graduate School

This is to certify that I have examined this copy of a doctoral dissertation by

Michael Lynn Adams

and have found that it is complete and satisfactory in all respects, and that any and all revisions required by the examination committee have been made.

Chair of Supervisory Committee

Sidney D. Nelson

Reading Committee

Sidney D. Nelson

Sam A. Bruschi

Terrence J. Kavanagh

Date: 3/3/03

University of Washington

Abstract

The Involvement of Mitochondria in the Cell Death Process:
Communication from Mitochondria to the Nucleus

Michael Lynn Adams

Chair of Supervisory Committee:
Professor Sidney D. Nelson
Department of Medicinal Chemistry

A thorough understanding of the mechanisms of cell death could open the door to numerous opportunities for therapeutic modulation. In addition to disease state treatment options, cell death modulation may also have benefit in toxicological research of xenobiotics. The studies described here focus on two extensively studied compounds: acetaminophen (APAP) and *S*-(1,1,2,2-tetrafluoroethyl)-L-cysteine (TFEC). Investigations into the toxicity of these compounds have suggested a critical role for the mitochondria in cell death related to direct effects on this organelle. The function that the mitochondria play in the cellular-mediated, as well as the xenobiotic-induced process, is generating wide interest. In particular, different pathways that hinge on the mitochondria in cell death processes have been identified, especially during apoptosis. Additionally, specific changes in HSP60, a nuclear encoded, mitochondrial protein, have been identified after TFEC dosing, indicating a communication pathway from the site of damage, in mitochondria, to the nucleus. The general background for this type of communication, called retrograde regulation in yeast is described in Chapter 1. Chapter 2 details our search for a mammalian system similar to the yeast retrograde regulation system through the use of Southern blots and degenerate primer RT-PCR. This search identified mitochondrial cytochrome *b*, an integral part of the mitochondrial electron

transport chain complex III, as a possible reporter protein. The effects of TFEC and APAP on complex III activity in mammalian cells, as a means to characterize a role for cytochrome *b* in the cell death process, are described in Chapter 3. Complex III activities in mice that overexpress the anti-apoptotic BCL-2 after dosing with APAP were evaluated in Chapter 4. Although our data suggest a potential role for cytochrome *b* in a cell death process, the exact role remains elusive.

Table of Contents

List of Figures ____ iii

List of Tables ____ v

List of Abbreviations ____ vi

Chapter 1 The Involvement of Mitochondria in the Cell Death Process: Communication from Mitochondria to the Nucleus

Section 1.1 Cell Death Overview ____ 1
Section 1.2 Study Compounds ____ 3
Section 1.2.1 Tetrafluoroethyl cysteine ____ 3
Section 1.2.2 Acetaminophen ____ 7
Section 1.3 Mitochondria ____ 11
Section 1.3.1 Mitochondrial Structure and Function ____ 11
Section 1.3.2 Mitochondrial Roles in Cell Death ____ 12
Section 1.4 Retrograde Regulation ____ 19
Section 1.5 Unfolded Protein Response ____ 20
Section 1.6 Mammalian Retrograde System: Mitochondria to Nucleus Communication ____ 22

Chapter 2 Searching for a Mammalian Retrograde Homologue

Section 2.1 Introduction ____ 37
Section 2.2 Materials and Methods ____ 38
Section 2.2.1 Materials ____ 38
Section 2.2.2 Cloning of RTG genes ____ 39
Section 2.2.3 Probe Synthesis and Southern Blots ____ 40
Section 2.2.4 Degenerate Primer Design and RT-PCR ____ 42
Section 2.3 Results ____ 44
Section 2.3.1 Cloning of RTG genes ____ 44
Section 2.3.2 Probe Synthesis and Southern Blots ____ 44
Section 2.3.3 Degenerate Primer RT-PCR ____ 45
Section 2.4 Discussion ____ 47

Chapter 3 Exploring Cytochrome *b*: Physical and Functional Characterization

Section 3.1 Introduction ____ 62
Section 3.2 Materials and Methods ____ 63
Section 3.2.1 Materials ____ 63
Section 3.2.2 TFEC synthesis ____ 63
Section 3.2.3 Tissue Culture ____ 64
Section 3.2.4 Immunoblot detection of cytochrome *b* ____ 65

Section 3.2.5 Peptide antibody design and use ____ 66
Section 3.2.6 Identification of epitope unmasking ____ 67
Section 3.2.7 Examination of Complex III activities & viability 70
Section 3.3 Results ____ 71
Section 3.3.1 Western Blots using Cytochrome *b* antibody ____ 71
Section 3.3.2 Epitope Unmasking identification ____ 73
Section 3.3.3 Complex III activities *in vitro* ____ 74
Section 3.4 Discussion ____ 75
Section 3.4.1 Physical Characterization of Cytochrome *b* ____ 75
Section 3.4.2 Functional Characterization measuring ____ 79

Chapter 4 Enhanced Acetaminophen Hepatotoxicity in Transgenic Mice Overexpressing BCL-2

Section 4.1 Introduction ____ 98
Section 4.2 Methods and materials ____ 101
Section 4.2.1 Materials ____ 101
Section 4.2.2 Animal care and dosing protocols ____ 101
Section 4.2.3 Isolation of subcellular fractions and immunoblotting procedures ____ 101
Section 4.2.4 Transaminase activities ____ 102
Section 4.2.5 Assessment of hepatotoxicity by histopathology 102
Section 4.2.6 Assessment of cellular morphology by electron microscopy ____ 103
Section 4.2.7 Determination of reduced (GSH) and oxidized (GSSG) liver glutathione ____ 103
Section 4.2.8 Caspase activation ____ 104
Section 4.2.9 Determination of mitochondrial respiration ____ 104
Section 4.2.10 Statistical analysis ____ 104
Section 4.3 Results ____ 105
Section 4.3.1 Altered processing and subcellular levels of BAX after drug treatment ____ 105
Section 4.3.2 Assessment of liver damage ____ 105
Section 4.3.3 Histopathological analyses ____ 106
Section 4.3.4 Characterizations of BCL-2 overexpression ____ 108
Section 4.3.5 Immunoblot detection of BCL-2 ____ 109
Section 4.3.6 Caspase activation ____ 109
Section 4.3.7 Complex III activities ____ 110
Section 4.4 Discussion ____ 111
Section 4.5 End Notes ____ 116

References ____ 124

List of Figures

Figure 1.1	Study Compounds	24
Figure 1.2	Metabolism of tetrafluoroethylene to tetrafluoroethyl cysteine	25
Figure 1.3	Formation of tetrafluoroethyl cysteine adducted proteins	26
Figure 1.4	Acetaminophen metabolic profile	28
Figure 1.5	N-acetyl-*m*-aminophenol metabolic profile	31
Figure 1.6	Mitochondrial structure	32
Figure 1.7	A schematic overview of ETC and MPTP	33
Figure 1.8	Mitochondrial roles in cell death	33
Figure 1.9	Summary of retrograde communication pathway	34
Figure 1.10	Summary of yeast unfolded protein response	35
Figure 1.12	Heat shock protein 60 up-regulation	36
Figure 2.1	Vector Map for pCRII-TOPO	54
Figure 2.2	Retrograde degenerate primer design	55
Figure 2.3	Ethidium bromide stained photograph of retrograde PCR products	56
Figure 2.4	Full-Length non-isotopic probe hybridization	57
Figure 2.5	RT-PCR results using degenerate primers	57
Figure 2.6	DNA sequence of RT-PCR products insert into plasmid	58
Figure 2.7	Cytochrome *b* peptide sequence deduced from DNA	59
Figure 2.8	Complex bc_1 crystal structure	60
Figure 2.9	Schematic view of Complex III activity	61
Figure 3.1	Nuclear magnetic resonance of TFEC	85
Figure 3.2	Initial peptide antibody screening against TAMH cells	86

Figure 3.3 Peptide antibody screening both *in vivo* and *in vitro* 86

Figure 3.4 Peptide antibody screened against TAMH cells 87

Figure 3.5 DEAE column elution profile 87

Figure 3.6 DEAE fractions screened with LOOP antibody & silver stained gel 88

Figure 3.7 Silver stained gel for trypsin digest 88

Figure 3.8 Mass spectrum of 54 kDa band 90

Figure 3.9 Protein sequence for protein disulfide isomerase 91

Figure 3.10 Peptides from 54 kDa band identified as PDI 92

Figure 3.11 Mass spectrum of 46 kDa band 93

Figure 3.12 Protein sequence for ATP synthase, β-subunit 94

Figure 3.13 Peptides from 46 kDa band identified as ATP synthase, β-subunit 95

Figure 3.14 Complex III & viability of TAMH cells after APAP treatment 96

Figure 3.15 Complex III dose response of TAMH cells after APAP treatment 96

Figure 3.16 Complex III & viability of TAMH cells after TFEC treatment 97

Figure 3.17 Complex III & viability of TAMH cells after $NaAsO_2$ 97

Figure 4.1 Mitochondrial alterations induced by APAP & AMAP 117

Figure 4.2 Assessment of hepatotoxicity by morphology 119

Figure 4.3 Cellular morphology changes observed by electron microscopy 120

Figure 4.4 Biochemical characterization 121

Figure 4.5 Confirmation of BCL-2 transgene overexpression & caspase-3 activities 122

Figure 4.6 Complex III activity 123

List of Tables

Table 1.1 Identification of tetrafluoroethyl cysteine adducted proteins ____ 27

Table 1.2 Identification of acetaminophen adducted proteins ____ 29

Table 1.3 Acetaminophen adducts identified by two-dimensional gel electrophoresis and mass spectrometry ____ 30

Table 1.4 N-acetyl-*m*-aminophenol adducts identified by two-dimensional gel electrophoresis and mass spectrometry ____ 32

Table 2.1 Retrograde primer design ____ 53

Table 2.2 Retrograde plasmid restriction digest products ____ 55

Table 2.3 Retrograde degenerate primers ____ 56

Table 3.1 Proteins identified from the 54 kDa immunoreactive band ____ 89

Table 3.2 Proteins identified from the 47 kDa immunoreactive band ____ 89

Table 4.1 Plasma Transaminase Activities ____ 118

List of Abbreviations

2D-GE	Two-dimensional gel electrophoresis
ACO1	Aconitase
ADP	Adenosine diphosphate
AIDS	Acquired immunodeficiency syndrome
AIF	Apoptosis initiating factor
ALT	Alanine aminotransferase
AMAP	N-acetyl-*m*-aminophenol
ANT	Adenine nucleotide translocase
Apaf-1	Apoptosis activating factor-1
APAP	N-acetyl-*p*-aminophenol; acetaminophen
AST	Aspartate aminotransferase
ATF6	Activating transcription factor 6
ATP	Adenosine triphosphate
BA	Bongkrekic acid
CAR	Constitutive androstane receptor
CIT1	Mitochondrial citrate synthase
CIT2	Non-mitochondrial citrate synthase
CSA	Cyslosporin A
CYP	Cytochrome P450
CyP-D	Cyclophilin D
DEAE	diethylaminoethyl
DFTAL	Difluorothioamidyl lysine
DISC	Death-inducing signaling complex
DNA	Deoxyribonucleic acid
DP	Dipeptidase
$\Delta\Psi_m$	Mitochondrial inner membrane potential
EDTA	ethylenediaminetetraacetic acid
EF1-α	Elongation factor 1-α
ER	Endoplasmic reticulum
ERSE	ER-stress response elements
EST	Expressed sequence tag
ETC	Electron transport chain
GAPDH	Glyceraldehyde 3-phosphate dehydrogenase
GSH	Glutathione (reduced)
GSSG	Glutathione (oxidized)
GST	Glutathione *S*-transferase
γ-GTP	γ-Glutamyl transpeptidase

HIV	Human immunodeficiency virus
HRP	Horse radish peroxidase
HSP60	Heat shock protein 60 kDa
IAP	Inhibitors of apoptosis proteins
IDH1 & *IDH2*	Isocitrate dehydrogenase 1 & 2
Ire1p	Inisitol requiring 1 protein
kDa	Kilodaltons
αKDH	α-Ketogluterate dehydrogenase
KLH	Keyhole limpit hemacyanin
MIM	Mitochondrial inner membrane
MOM	Mitochondrial outer membrane
MMP	Mitochondrial processing peptidase
MPT	Mitochondrial permeability transition
MPTP	Mitochondrial permeability transition pore
mRNA	Messenger ribonucleic acid
NADH	Nicotinamide adenine dinucleotide
NADPH	Nicotinamide adenine dinucleotide phosphate
NAPQI	N-acetyl-*p*-quinone imine
NCBI	National Center for Biotechnology Information
NMR	Nuclear magnetic resonance
PBS	Phosphate buffered saline
PCR	Polymerase chain reaction
PDI	Protein disulfide isomerase
PERK/PEK	Protein kinase R-like ER kinase/ pancreatic eIF2α kinase
PLP	Pyridoxal 5'-phosphate
RT-PCR	Reverse transcriptase PCR
SDS	Sodium dodecyl sulfate
SRB	Sulforhodamine B
SSC	3M NaCl, 0.3M sodium citrate
TCA	Tricarboxylic acid cycle or Trichloroacetic acid
TCP	T-complex protein
TFA	Trifluoroacetic acid
TFE	Tetrafluoroethylene
TFE-GS	TFE-glutathione
TFEC	*S*-(1,1,2,2-tetrefluoroethyl)-L-cysteine
TMPD	*N, N, N, N*- tetra methyl-*p*-phenylene diamine

UAS_r	Upstream activation site (R box)
UPR	Unfolded protein response
UPRE	Unfolded protein response element
UV	Ultraviolet
VDAC	Voltage-dependent anion channel
WT	Wild type
Xbp-1	X box binding protein

Acknowledgments

I would like to thank all the faculty, staff and students of the Department of Medicinal Chemistry, past and present, who assisted me with their knowledge, experience, or willingness to listen.

Specifically, I would like to thank:

My supervisory committee, Sid Nelson, Sam Bruschi, Terry Kavanagh, Bill Atkins, and David Cummings for their willingness to spend their precious time on my scientific development.

The Nelson Lab, both past and present, for allowing me to be myself and work in an exciting environment.

Michael Mohutsky and Jason Boer, my comrades, for their boundless support and encouragement, both scientifically and personally. This long, hard road was a much more pleasant journey with friends like these by my side during the good times and the bad. Their countless acts of friendship will never be forgotten.

Dedication

To my parents, Clifton and Joy Adams

To my wife, Dina

for their faith, love, and support.

To the memory of my brother, Eddie

Chapter 1

The Involvement of Mitochondria in the Cell Death Process: Communication from Mitochondria to the Nucleus

1.1 Cell Death Overview

Although cell death may have a negative connotation associated with pathological situations, the process of cell death is crucial in many physiological situations as well. The study of developing animals has indicated that programmed cell death is vital to the formation or deletion to particular structures, the regulation of cell numbers, and the elimination of abnormal cells (Baehrecke 2002). The disruption of programmed cell death leads to abnormalities in development indicating the tight regulation required for proper embryogenesis (Zakeri 1998). Cell death dependent structure formation is evident in the development of digits forming the interdigital space (Zakeri *et al.* 1994; Chautan *et al.* 1999) while cell death dependent structure deletion is observed in mice and humans *via* a testosterone dependent death of mammary cells in males (Kratochwil and Schwartz 1976). In addition, the regulation of cell number is a delicate balance between cell proliferation and cell death that is developmentally important in the nervous system of many different species (Klambt *et al.* 1991; Barres *et al.* 1992). These are only a few of the examples highlighting the essential physiological role that cell death plays in the development of both vertebrate and invertebrate organisms.

The dysregulation of programmed cell death, either during development or during the maintenance of homeostasis, may lead to pathologies ranging from cancer and

autoimmune diseases to acquired immunodeficiency syndrome (AIDS) and neurodegenerative disorders. Cancer and autoimmune diseases are often examples of an attenuated apoptotic process. For example, most human follicular lymphomas express the BCL-2 gene, which inhibits the cellular response to apoptotic signals (Bakhshi *et al.* 1985; Cleary and Sklar 1985; Tsujimoto *et al.* 1985). As a result of this apoptosis resistance, homeostasis is perturbed leading to an accumulation of lymphocytes and ultimately leukemia. Another potential example of cancer induced by apoptosis perturbations is the p53 system of deoxyribonucleic acid (DNA) repair. In normal cells, the p53 gene product induces apoptosis in cells that have experienced irreparable DNA damage (Clarke *et al.* 1993; Lee and Bernstein 1993; Lowe *et al.* 1993). Cells deficient in p53 are resistant to the homeostatic apoptotic process; therefore, p53-deficient cells continue to grow after DNA damage and may develop into cancers resistant to apoptotic inducing treatments such as chemotherapy or radiation (Thompson 1995). The study of autoimmune disease in mice has demonstrated the etiological importance of dysregulated apoptosis within the immune system. In particular, a disruption in Fas-mediated apoptosis, either by a mutation on the Fas receptor or the Fas ligand, may allow the development of self-reactive lymphocytes causing a fatal systemic lupus erythematosus in mice (Watanabe-Fukunaga *et al.* 1992; Suda *et al.* 1993).

In contrast to the cancer and autoimmunity examples of attenuated apoptosis, AIDS and neurodegenerative disorders may be the result of excessive apoptosis. Human immunodeficiency virus (HIV), the virus that causes AIDS, appears to cause lymphocyte depletion by making the T-lymphocyte more susceptible to apoptotic stimuli (Ameisen and Capron 1991; Groux *et al.* 1992; Gougeon and Montagnier 1993). The depletion of

T-lymphocytes makes the host more susceptible to other opportunistic infections and therefore the clinical presentation of AIDS. Neurodegenerative disorders such as Alzheimer's disease, Parkinson's disease, and amyotrophic lateral sclerosis are caused by a gradual loss of specific sets of neurons (Heintz 1993; Isacson 1993). The neuronal loss is hypothesized to be the result of specific situations like oxidative stress, calcium toxicity, or deficiency of survival factors that predispose the neurons to apoptosis, ultimately causing symptoms of disease (Choi 1992; Ziv *et al.* 1994).

A thorough understanding of the mechanisms of cell death could open the door to numerous opportunities for therapeutic modulation. The therapeutic potential for cell death modulation is not only in prevention of cell death, as in the examples of AIDS and neurodegenerative disorders, but also in the promotion of cell death in dysregulated systems like cancer and autoimmune disease. In addition to these organic events, cell death modulation may also have benefit in areas of xenobiotic toxicity evaluation and treatment, e.g., drug overdose or acute exposure to a toxic substance.

1.2 Study Compounds

To further examine the process of cell death, two extensively studied test compounds will be used. These compounds are *S*-(1,1,2,2-tetrafluoroethyl)-L-cysteine (TFEC), a product of the industrial gas tetrafluoroethylene, and acetaminophen (N-acetyl-*p*-aminophenol, APAP), a widely used analgesic (Fig. 1.1).

1.2.1 Tetrafluoroethyl cysteine

The industrial gas tetrafluoroethylene (TFE), the precursor of Teflon™, is anticipated to be a human carcinogen (TFE 1999; NTP 2002) and is known to be a multiorgan rodent carcinogen particularly with chronic, long term inhalation (NTP 1997)

TFEC, the cysteine conjugate of TFE, is the major metabolic product and is known to produce renal toxicity and mild hepatic perturbations in mammals (Lock and Ishmael 1998). Sequential metabolism of TFE by glutathione *S*-transferase, γ-glutamyl transpeptidase, and cysteinylglycine-dipeptidase produces the corresponding nontoxic cysteine conjugate (Fig. 1.2).

The mechanism of TFEC-induced cell death and organ damage is expected to follow the "Covalent Binding Hypothesis" originally proposed by Brodie and colleagues during their study of bromobenzene (Brodie *et al.* 1971). This hypothesis proposes that the covalent modification of critical proteins by reactive intermediates of metabolism inhibits target protein function and ultimately results in organ damage. For example, TFEC can be bioactivated in the renal proximal tubular epithelium by a cysteine *S*-conjugate β-lyase to an unstable α-fluorothiolate, tetrafluoroethanethiolate (Anders and Dekant 1998). Collapse of the thiolate yields a transient, but potent, acylating species, 2,2-difluorothioacetyl fluoride, which covalently modifies lysyl ε-amino groups of neighboring proteins to produce difluorothioamidyl-lysine (DFTAL) modified proteins (Commandeur *et al.* 1989) (Fig. 1.3).

The identity of one specific β-lyase responsible for the cleavage of TFEC and its toxicity has not been determined although several different β-lyase proteins have been identified. Interestingly, although all of the identified TFEC-adducts have been detected in the mitochondria, β-lyase activity has been identified both in the mitochondrial and the cytosolic compartments. The identified cytosolic β-lyase proteins include kynureniase, glutamine transaminase K (kynurenine aminotransferase), aspartate aminotransferase, alanine aminotransferase, and branched-chain amino acid aminotransferase. The

mitochondrial β-lyase proteins include aspartate aminotransferase, branched-chain amino acid aminotransferase, and alanine-glyoxylate aminotransferase isozyme II (Cooper *et al.* 2002). In addition, a high-Mr β-lyase, consisting of mitochondrial HSP70 and protein disulfide isomerase, has been localized both in the cytosolic and mitochondrial compartments (Abraham *et al.* 1995). Although a pyridoxal 5'-phosphate (PLP)-component of the high-Mr β-lyase has not been identified, all other characterized β-lyases are PLP-dependent enzymes with most having characterized roles in amino acid metabolism.

The identification of the TFEC produced DFTAL-adducts was facilitated by the use of a trifluoroacetic acid (TFA) antibody developed for the study of halothane hepatotoxicity that also selectively binds to the DFTAL-adducts (Hayden *et al.* 1991). All the predominant TFA antibody reactive DFTAL-modified proteins were identified through various techniques. The identified DFTAL-adducts and the methods of identification are listed in Table 1.1. As an indication of the mechanism of cell death, all of the identified adducts were localized to the mitochondria. In addition to identification, two adducted-enzymes that have assayable activities demonstrate a decrease in function after TFEC dosing, supporting the covalent binding hypothesis. After dosing with TFEC, both α-ketogluterate dehydrogenase (αKDH) and aconitase activities are inhibited both *in vivo* and *in vitro* by 30 to 60% (Bruschi *et al.* 1998; James *et al.* 2002).

In addition to the localization of DFTAL-adducts to the mitochondria, further evidence suggests the critical role of the mitochondria, particularly the mitochondrial permeability transition pore (MPTP) in TFEC-induced cell death. MPTP is a multi-component pore that when open causes a permeabilization of the otherwise impermeable

mitochondrial inner membrane. This mitochondrial permeability transition (MPT) causes a collapse of the mitochondrial inner membrane potential ($\Delta\Psi_m$), inhibition of oxidative phosphorylation, and matrix swelling. Electron micrograph evidence of mitochondrial swelling after TFEC dosing suggests the early opening of the MPTP (James *et al.* 2002). The protective effect of bongkrekic acid (BA), a specific MPTP inhibitor, on TFEC-induced cell death *in vitro* also further suggests a possible role for the MPTP (James *et al.* 2002). Finally, the *in vitro* overexpression of BCL-x_L, a BCL-2 family member shown to inhibit MPTP (Shimizu *et al.* 1999), also protects against cell death after extreme doses of TFEC (400μM) (Ho, Hu, & Bruschi, manuscript in preparation). The role of the MPTP is further supported by the dose related decrease in the $\Delta\Psi_m$ (Bruschi, unpublished results) that is rapidly dissipated during the MPT after opening of the MPTP. This data suggests that TFEC-induced cytotoxicity requires an early MPT that is modulated both by classic pore inhibitors (i.e., BA) and apoptotic modulators (i.e., BCL-x_L). These observations further support the vital role of the MPTP and the mitochondria in TFEC-induced cell death processes.

There is accumulating data that points to the mitochondria as the key in the toxicity associated with TFEC. This evidence includes the localization of all the identified adducts to the mitochondria and the alterations to mitochondrial function, specifically, the perturbation of the tricarboxylic acid (TCA) cycle and collapse of $\Delta\Psi_m$. Therefore, TFEC appears to be an exclusively mitochondrial toxicant and excellent model to study the mitochondrial role in xenobiotic-induced cell death processes.

1.2.2 Acetaminophen

Acetaminophen (APAP) is a commonly prescribed and over-the-counter analgesic and antipyretic with a relatively safe toxicity profile. APAP was first used in the late 1800's but did not gain widespread use throughout the United States and the United Kingdom until the 1950's when it was used for a wide array of ailments (Prescott 1996). Although considered very safe, there is one caveat only recognized after widespread use of APAP. A serious hepatotoxicity is associated with APAP overdose and other predisposing conditions. This APAP-associated hepatotoxicity was first reported in Scotland in 1966 as an attempted suicide (Prescott 1996). Soon after, other reports of APAP-associated hepatotoxicity appeared in the literature describing a characteristic centrilobular necrosis. Today the exact cause of APAP-hepatotoxicity is still uncertain but many different possibilities have been proposed and studied extensively.

The first evidence to explain the toxic mechanism of APAP was the observation that APAP-induced hepatotoxicity was dependent on nicotinamide adenine dinucleotide phosphate (NADPH)-dependent microsomal cytochrome P450 (CYP) metabolism. Mitchell and colleagues (Jollow *et al.* 1973; Mitchell *et al.* 1973a; Mitchell *et al.* 1973b; Potter *et al.* 1973) demonstrated this clearly with their ability to modulate APAP-induced hepatotoxicity by inhibiting or inducing CYP activity. The inhibition of CYP activity in mice and rats with cobaltous chloride or piperonyl butoxide protected the liver, while induction with phenobarbitone or 3-methylcholanthrene increased liver sensitivity to APAP-associated hepatotoxicity (Mitchell *et al.* 1973b). The dependence on metabolism for APAP-induced hepatotoxicity has been further demonstrated in studies with the xenobiotic receptor called the constitutive androstane receptor (CAR). APAP binding to

CAR in mice causes the induction of two CYPs, CYP1A2 and 3A11, that result in increased liver sensitivity similar to that observed with phenobarbital induction while CAR null mice are resistant to APAP toxicity (Zhang *et al.* 2002).

In addition to CYP dependent metabolism, a crucial role was recognized for the state and concentrations of hepatic glutathione in APAP-hepatotoxicity. Glutathione was proposed to protect from hepatotoxicity *via* its conjugation to the reactive metabolite therefore preventing tissue arylation and ultimately toxicity (Jollow *et al.* 1973; Mitchell *et al.* 1973c; Potter *et al.* 1974). This hypothesis was further supported by the observation that the extent of hepatic necrosis was associated with the proportional, dose-dependent extent of covalent binding (Jollow *et al.* 1973) as well as the dose-dependent depletion of glutathione (Tirmenstein and Nelson 1989).

The recognition of a CYP mediated toxicity led to the close investigation of the metabolic profile of APAP for the "offending" metabolite. Early proposed toxic metabolites included an aromatic epoxide intermediate, N-hydroxy APAP, and N-acetyl-*p*-quinone imine (NAPQI). The possibility of an epoxide intermediate as the toxic metabolite was eliminated with radiolabel studies indicating no $^{18}O_2$ incorporation or loss of ^{18}O loss from labeled APAP (Hinson *et al.* 1979a). Also the addition of epoxide hydrolase failed to block covalent binding of the reactive intermediate of APAP metabolism again indicating that the epoxide is not responsible for APAP-induced hepatotoxicity (Hinson *et al.* 1980; Steele *et al.* 1983). N-hydroxy APAP was thought to rapidly decompose to NAPQI but after synthesis was found to be relatively stable at physiological pH. The lack of decomposition, toxicity, and the absence of N-hydroxy APAP in the blood or urine indicated that it was not the metabolite responsible for

toxicity (Gemborys *et al.* 1978; Healey *et al.* 1978; Hinson *et al.* 1979b; Nelson *et al.* 1980; Calder *et al.* 1981). The electrochemical synthesis and characterization of NAPQI indicated that it was the most probable reactive intermediate (Miner and Kissinger 1979). In addition to forming adducts indistinguishable from the microsomal metabolism of APAP (Miner and Kissinger 1979), NAPQI was more toxic than APAP and its covalent binding could be reduced by the addition of glutathione or ascorbic acid (Dahlin and Nelson 1982; Dahlin *et al.* 1984). These observations strongly suggest that NAPQI is the toxic metabolite of APAP.

APAP metabolism has been extensively characterized and is summarized in Figure 1.4 (for review see (Prescott 1996)). The major metabolites after use in humans are the glucuronide and sulfate conjugates accounting for between 70 to 90% of the dose (Prescott 1996). At higher doses of APAP, the conjugation pathways become saturated allowing more CYP dependent metabolism of APAP to the 3-hydroxy APAP, also known as the catechol, and NAPQI.

Even with the proof of principle that NAPQI can lead to toxicity, the exact mechanism of formation and its toxic mechanism are still unknown. The proposed mechanisms of NAPQI induced toxicity include general oxidative stress, disruption of calcium homeostasis, cellular thiol oxidation, and covalent binding of macromolecules. There have been extensive studies on all the possible mechanisms but recent opinion favors the combination of thiol oxidation and covalent binding (Prescott 1996).

The identification of APAP covalently bound to proteins and its proportionality to toxicity, indicated that APAP toxicity might be mediated by covalent binding (Jollow *et al.* 1973). The covalent binding hypothesis suggests that critical cellular proteins are

adducted and the loss of activity leads to cell death (Brodie *et al.* 1971). Through the years, many of the adducted proteins have been identified by various methods. The major adducts identified by classical techniques are listed in Table 1.2. It is still uncertain what the relative contribution of each protein target to the ultimate expression of toxicity since no one critical target appears to be solely responsible for the resulting centrilobular injury.

One powerful study using two-dimensional gel electrophoresis (2D-GE) identified mouse proteins adducted with ^{14}C radiolabeled APAP after intraperitoneal injection (Qiu *et al.* 1998). This study identified 23 proteins, listed in Table 1.3, constituting a wide range of cellular targets throughout many different compartments. Targets included cytosolic, mitochondrial, and nuclear proteins, and confirmed the adduction of three proteins, selenium-binding protein, aldehyde dehydrogenase, and glutathione *S*-transferase, identified by other more classical techniques. Again, these results offered no single target resulting in the toxicity.

In an effort to better understand the mechanism of APAP-associated hepatotoxicity, study of its relatively non-hepatotoxic regioisomer, N-acetyl-*m*-aminophenol (AMAP), has often paralleled the study of APAP. AMAP was shown to have a similar metabolic profile when compared to APAP (Fig. 1.5). Although AMAP can form reactive quinone metabolites, it was unable to deplete mitochondrial glutathione, disrupt the mitochondrial ability to sequester calcium, or oxidize thiols to the same level as APAP (Tirmenstein and Nelson 1989, 1990). Conversely, AMAP was able to covalently adduct cellular proteins to a similar or greater extent than APAP with the most notable difference being the lower concentration of AMAP adducts localized to the

mitochondria (Tirmenstein and Nelson 1989; Nelson *et al.* 1991). The differences in mitochondrial adducts were further supported by the identification of twelve ^{14}C radiolabeled AMAP adducts by 2D-GE (Table 1.4) (Qiu *et al.* 2001). Although fewer AMAP adducts were detected, the mitochondrial proteins identified with APAP were completely absent. A decreased stability of the AMAP adducts in the 2D-GE procedures has been proposed to explain the lower overall numbers in AMAP-adducts while other reports show similar or higher levels of AMAP-adducts when compared to APAP (Tirmenstein and Nelson 1989).

Thus, effects on the mitochondria seem to be one of the major differences between the ability of APAP, and the decreased ability of AMAP, to induce hepatotoxicity. These observations further emphasize the importance of this organelle in the cell death processes.

1.3 Mitochondria

With the intense study of cell death, the function that the mitochondria play in the cellular-mediated, as well as the xenobiotic-induced process, is generating wide interest. Mitochondria have long been studied and recognized as important organelles responsible for the production of energy, in the form of adenosine triphosphate (ATP), from the aerobic metabolism of carbohydrates and fatty acids *via* the TCA and oxidative phosphorylation cycles.

1.3.1 Mitochondrial Structure and Function

Two mitochondrial membranes, the outer membrane and the inner membrane, create four distinct areas within a mitochondrion. These regions, starting from the exterior, are called the mitochondrial outer membrane (MOM), the intermembrane space,

the mitochondrial inner membrane (MIM), and the matrix (Fig. 1.6). The shape of the mitochondrion is formed by the MOM, which is characterized by the localization of the transmembrane protein porin, also called the voltage-dependent anion channel (VDAC), the most abundant protein of the outer membrane. Porin proteins form channels that allow the free diffusion of molecules, with molecular weights of approximately 10 kDa or less, into and out of the intermembrane space. Localized within the intermembrane space are many different proteins including cytochrome *c*, part of the electron transport chain (ETC), and ATP dependant enzymes like creatine kinase and adenylate kinase. The MIM is an impermeable membrane that forms a complex structure of folds called cristae. The MIM contains multiple protein complexes involved in the ETC. The ETC utilizes electrons released from the TCA cycle in the form of nicotinamide adenine dinucleotide (NADH) to expel protons from the matrix generating a proton gradient across the impermeable MIM producing the inner membrane potential ($\Delta\Psi_m$). The $\Delta\Psi_m$ is utilized to drive enzymatic oxidative phosphorylatoin *via* ATP-synthase (Complex V of the ETC). A schematic overview of the ETC is included in Figure 1.7. Inside the MIM is the matrix that contains TCA cycle enzymes, fatty acid oxidation enzymes, circular mitochondrial DNA, and the ribosomes and enzymes required for mitochondrial protein expression.

1.3.2 Mitochondrial Roles in Cell Death

With the known role that the mitochondria play in cellular energy production, much interest has surrounded the mitochondria and its role in cell death. In particular, different pathways that hinge on the mitochondria in the cell death processes have been identified, especially in apoptosis. The first observation directly connecting the

mitochondria to apoptosis was the observed requirement of cytochrome *c* to initiate the apoptotic process (Liu *et al.* 1996). Since then, much more has been learned about the role mitochondria play in the process of apoptotic cell death.

In both the extrinsic (initiated from a cell surface receptor) or intrinsic (initiated from the mitochondria) apoptosis pathways, a potential role for mitochondria has been elucidated. The extrinsic pathway involves the ligand-activated recruitment of various proteins to form a death-inducing signaling complex (DISC). As a result of its association within the DISC, caspase-8 is activated and either directly cleaves other caspase family members without further mitochondrial involvement (type I cells) or recruits the mitochondria to amplify the signal by cleaving the pro-apoptotic BCL-2 family member BID (type II cells) (Scaffidi *et al.* 1998). While the extrinsic pathways can lead to the involvement of the mitochondria, the intrinsic pathway requires alteration in the mitochondria that causes the release of apoptosis initiators (see below).

A structurally related group of proteins called the BCL-2 family are able to influence both the intrinsic and extrinsic apoptotic pathways. Within the BCL-2 family are pro-apoptotic (BAX, BAK, BID) and anti-apoptotic (BCL-2, BCL-x_L) proteins thought to work by exerting their particular effect on the permeabilization of the mitochondria (Gross *et al.* 1999a). As indicated above, death receptor induced cleavage of pro-apoptotic BID to tBID allows for its insertion into the MOM initiating the apoptotic process (Li *et al.* 1998; Luo *et al.* 1998; Gross *et al.* 1999b). Although tBID lacks a proposed channel-forming domain (Zou *et al.* 1997), it can form channels in synthetic lipid vesicles (Desagher and Martinou 2000). More recent work has demonstrated that tBID-induced apoptosis requires either BAX or BAK and their

oligomeric insertion into the MOM to induce apoptosis (Wei *et al.* 2000; Wei *et al.* 2001; Zong *et al.* 2001). In addition to cooperation with tBID, BAX has demonstrated the ability to redistribute itself from the cytosol to the mitochondria after apoptotic stimuli (Hsu *et al.* 1997; Wolter *et al.* 1997) and may be a critical step in the mitochondrial initiation of apoptosis. Although these observations have indicated a critical role for pro-apoptotic BCL-2 family members, the exact role is still unknown. The same is true for the anti-apoptotic BCL-2 family members, which are able to counter the effects of the pro-apoptotic members. The possible mechanisms of action include heterodimerization with pro-apoptotic members such as BAX (Yin *et al.* 1994; Antonsson *et al.* 1997), antioxidant effects (Hockenbery *et al.* 1993), or the blockage of BAX formed pores (Shimizu *et al.* 1999). Regardless of the exact mechanism, the BCL-2 family members play a critical role in the modulation of apoptosis *via* their effects on mitochondrial permeability.

It is generally thought that caspase-dependent initiation of the intrinsic apoptosis execution process relies on a change in mitochondrial permeability and the release of multiple factors. The first factor observed, and most classically studied, is cytochrome *c* (Liu *et al.* 1996). This redistribution of the 15 kDa cytochrome *c* begins the apoptotic process by its activation of a family of enzymes called caspases (Liu *et al.* 1996; Zou *et al.* 1997). Caspases are cysteine aspartic acid-specific proteases that initiate, amplify, or execute the apoptotic process. Caspase-9 is an initiator caspase and is activated through its association with the cytosolic apoptosis activating factor-1 (Apaf-1), cytochrome *c* and dATP/ATP to form an oligomeric complex referred to as the "apoptosome" (Zou *et al.* 1999). After the formation of the apoptosome, active caspase-9 activates the effector

caspases, including caspases-3 and -7 by cleaving their inhibitory prodomains. This leads to a cascade of caspase activation and ultimately the characteristic morphology of apoptosis (Li *et al.* 1997; Zou *et al.* 1997; Zou *et al.* 1999). The initiation of the caspase cascade is potently inhibited by HSP70 binding to Apaf-1 therefore preventing apoptosome formation and caspase activation (Beere *et al.* 2000; Saleh *et al.* 2000).

In addition to the mitochondrial release of cytochrome *c*, other factors are also released from the mitochondria to initiate the apoptotic process yielding the apoptotic morphology. One factor is SMAC/DIABLO, a 29 kDa protein, which inhibits the activities of the cytosolic inhibitors of apoptosis proteins (IAP), and therefore facilitates the activation of the caspase cascade (Du *et al.* 2000; Verhagen *et al.* 2000). Another mitochondrial factor released from the intermembrane space is the 57 kDa flavoprotein called apoptosis initiating factor (AIF), which is involved in DNA degradation (i.e., chromatin condensation and DNA fragmentation) (Susin *et al.* 1999). Omi/HtrA2, a 37 kDa protein with both serine protease activity and an IAP binding domain, is also released from the mitochondria after an apoptotic trigger (Van Loo *et al.* 2002). Finally, endonuclease G, a 30 kDa protein proposed to participate in mitochondrial DNA replication, is released after various apoptotic stimuli and facilitates nuclear DNA breakdown (Wang 2001; Van Loo *et al.* 2002). In addition to the proteins listed above with known functions contributing to the apoptotic process, many other mitochondrial proteins are also released indicating that the increased permeability may not be a selective process.

Although the apoptotic function of several proteins released from the mitochondria are known, the precise mechanism of release is still un-identified. Here we

will examine four leading proposals to explain the mitochondrial membrane permeabilization or the MPT. They include (1) the formation of a non-specific pore causing matrix swelling and MOM rupture, (2) BAX induced VDAC opening to selectively release cytochrome *c*, (3) BAX oligomerization and insertion into the MOM to form a selective cytochrome *c* pore, or (4) closure of the VDAC with BCL-2 pore formation leading to MOM rupture (Kroemer and Reed 2000).

The most extensively studied model of MPT is non-specific pore formation most commonly known as MPTP. The MPTP is made by the associations of cyclophilin D (CyP-D) from within the matrix, adenine nucleotide translocase (ANT) in the MIM and possibly the VDAC in the MOM (Crompton 1999; Halestrap *et al.* 2000). The physiological function of this pore has not been conclusively determined but once open, it allows the free movement of solutes < 1.5 kDa through the impermeable MIM and ultimately causes a collapse of the mitochondrial inner membrane potential ($\Delta\Psi_m$) (Zoratti and Szabo 1995). The prolonged opening of the MPTP causes mitochondrial matrix swelling that may rupture the MOM and allows the release of the inner membrane space contents, particularly cytochrome *c* (Friberg *et al.* 1998).

MPTP involvement in MPT is supported by the ability of cyclosporin A (CsA), a MPTP inhibitor that binds to CyP-D, in isolated mitochondria (Friberg *et al.* 1998) and bongkrekic acid, which binds to ANT in a cell free system, to inhibit apoptotic morphology (Zamzami *et al.* 1996). Additional evidence is that BCL-2 family members interact with ANT. For example, BAX associates with the MPTP purified from rat brain (Marzo *et al.* 1998b) and BCL-2 associates with the contact sites between the MIM and MOM that make up the MPTP (de Jong *et al.* 1994). The specificity of this interaction

was demonstrated by the ability to coimmunoprecipitate ANT in mammalian cells lines with BAX and by the interactions of BAX, BAK, and BCL-2 with ANT in a yeast two-hybrid system (Marzo *et al.* 1998a). Although these observations suggest a role for ANT and the BCL-2 family in MPT, the exact mechanism has not been determined.

The non-specific pore induced release of cytochrome *c* suggests that the rupture of the MOM is the essential step in the initiation of apoptosis; however, the time course is not always in agreement with caspase activation. Caspase activation, often dependent on cytochrome *c* inclusion in the apoptosome, is well underway before the opening of MPTP and loss of $\Delta\Psi_m$ (Bossy-Wetzel *et al.* 1998). This discrepancy suggests that matrix swelling may be dependent on cytochrome *c* release rather than the cause.

The MPTP has also been suggested to be the pore by which cytochrome *c* is released into the cytosol *via* short openings signaling the induction of apoptosis while extended opening results in necrosis (Halestrap *et al.* 1998). This proposal is in agreement with the hypothesis that ATP levels dictate whether apoptosis (normal ATP levels) or necrosis (low ATP levels) occurs (Leist *et al.* 1997) but the mechanism by which cytochrome *c* can be released through the MPTP is not known since only molecules < 1.5 kDa freely move through the MPTP.

The second proposed model is closely related to the first, and suggests a direct interaction of BAX or BAK with VDAC to induce its opening and the release of cytochrome *c*. This proposal is supported by two different reports of BAX or BAK coimmunoprecipitating with VDAC from isolated mitochondria (Narita *et al.* 1998; Shimizu *et al.* 1999). Additionally, both BAX and BAK were able to induce the opening of VDAC in liposomes allowing cytochrome *c* release without liposomal rupture. This

opening could be prevented by the anti-apoptotic BCL-2 family member, BCL-x_L binding directly to VDAC (Shimizu *et al.* 1999). Although these observations suggest a role for VDAC, the question remains if these interactions occur *in vivo.*

Another proposal involves only BAX and its oligomerization to form pores. This has been demonstrated by the ability of recombinant BAX to cause cell lysis within 6 hours after addition to cell cultures or erythrocytes (Antonsson *et al.* 1997). The addition of BAX to liposomes also induced the BCL-2 inhibitable release of carboxyfluorescein further indicating its ability to form pores (Antonsson *et al.* 1997). The large pores formed by BAX are predicted to interact as homodimers or oligomers (Saito *et al.* 2000) and therefore allow for the release of cytochrome *c* and the other inner membrane space proteins to activate the apoptotic process. Although the formation of BAX pores has not been directly demonstrated *in vivo*, the ability of BAX to induce apoptosis by dimerization in cells after the withdrawal of interleukin-3, and inhibition of apoptosis by BCL-2 and BCL-x_L has been demonstrated (Gross *et al.* 1998).

The final proposal involves the hyperpolarization of the matrix resulting in the closure of the VDAC. Hyperpolarization causes matrix swelling and MOM rupture to release cytochrome *c*. This proposal has been supported by the ability of BCL-x_L to prevent apoptosis in growth factor deprived cells by allowing the normal function of the VDAC and ANT to exchange adenosine diphosphate (ADP) and ATP (Vander Heiden *et al.* 1999).

Regardless of the exact roles of all the proposed players and the interplay between pathways, it is apparent from these studies that the mitochondria play a critical role in the process of cell death. A brief overview of mitochondrial involvement in cell death is

shown in Figure 1.8. Further study on the contributions of the BCL-2 family, MPTP components, and as yet unknown factors will undoubtedly only further support the role of mitochondria in the control of cell death and offer targets for therapeutic manipulation.

1.4 Retrograde Regulation

While the mitochondria have DNA that is required for synthesis of several proteins in the electron transport chain (ETC), the majority of the proteins are encoded in the nucleus. Mitochondrial biogenesis requires the NRF transcription factors, among others, to induce the expression of the nuclear ETC genes (Scarpulla 2002). This mitochondrial requirement for nuclear input has long been recognized but the prospect of communication from the mitochondria to the nucleus is a novel idea proposed by Butow *et al.* (1988). This system of communication is called "retrograde regulation" and has been observed in the yeast *Saccharomyces cerevisiae* (Butow *et al.* 1988; Liao and Butow 1993). It appears that retrograde regulation is a "homeostatic or stress response mechanism by which cells adapt to alterations in the mitochondrial state," and is found predominantly in ρ° petites (yeast cells lacking mitochondrial DNA) (Chelstowska *et al.* 1999). This pathway requires three genes named *RTG1*, *RTG2*, and *RTG3*, for the up-regulation of target genes in response to altered mitochondrial function. *RTG1* codes for a 177 amino acid protein, RTG1p, that has a predicted similarity to a basic helix-loop-helix transcription factor, while *RTG2* codes for a protein, RTG2p, of 394 amino acids with no observed homology to any known motifs (Liao and Butow 1993). *RTG3* also codes for a protein with similarity to a basic helix-loop-helix transcription factor with 486 amino acids (Jia *et al.* 1997). Although the initiation signals of mitochondrial communication are not clear at this point, it has been proposed that one method may be

through glutamate levels produced by the TCA (Sekito *et al.* 2000). These signals are then transmitted to the regulatory RTG2p that interacts with the cytosolic RTG1p/RTG3p complex. Highly phosphorylated RTG3p dissociates from RTG1p and is dephosphorylated. This dephosphorylation allows for the translocation of the RTG1p/dephosphorylated RTG3p complex into the nucleus where it binds with an upstream activation site called the R box (UAS_r) (Sekito *et al.* 2000). (See summary in Figure 1.9).

Binding of the RTG1p/RTG3p complex to the UAS_r induces the transcription of several genes. The genes up-regulated include non-mitochondrial citrate synthase (*CIT2*) involved in the glyoxylate shunt (Liao *et al.* 1991). Mitochondrial citrate synthase (*CIT1*), aconitase (*ACO1*), isocitrate dehydrogenase 1 and 2 (*IDH1* & *IDH2*) are also up-regulated by RTG during compromised energy production by the mitochondria instead of the normal *HAP* transcription factors (Liu and Butow 1999). It appears that the up-regulation of these genes is a response to maintain high glutamate levels in order to maintain anabolic growth. Another gene, not directly involved in the production of glutamate, is also up-regulated and codes for an isoform of D-lactate dehydrogenase (Chelstowska *et al.* 1999).

1.5 Unfolded Protein Response

The yeast retrograde regulation is not the only example of a communication pathway from an organelle to the nucleus. One system that has been well characterized in yeast and extensively studied in mammals is the unfolded protein response (UPR). The UPR is induced following the accumulation of unfolded proteins within the lumen of

the endoplasmic reticulum (ER) and results in the up-regulation of genes involved in protein folding.

The yeast UPR is relatively simple in that it only requires four components: Ire1p, BiP, Rlg1p, and *HAC1*. Inisitol requiring 1 protein (Ire1p), an ER-localized transmembrane protein, is the initiator of the process. The N-terminal domain of Ire1p is localized within the ER lumen while the C-terminal domain, which has both kinase and endoribonuclease activities, is localized in the cytoplasm. With the accumulation of unfolded proteins within the ER lumen, BiP, an ER chaperone that associates with the N-terminal domain of Ire1p, is recruited and allows the oligomerization of Ire1p. Upon oligomerization and phosphorylation, Ire1p cleaves the constitutively expressed $HAC1^u$ (uninduced) messenger ribonucleic acid (mRNA) to eliminate a 252 nucleotide region. The remaining mRNA, $HAC1^i$ (induced), is then spliced by Rlg1p, a tRNA ligase which allows for the overexpression of Hac1p, a transcription factor which binds to the unfolded protein response element (UPRE) (Ma and Hendershot 2001). The result is an increased expression in BiP to correct the accumulation of unfolded proteins. (See summary in Figure 1.10).

In mammalian systems, the UPR is more complicated as a result of redundancies that ultimately lead to the clearance of unfolded proteins as well as discontinuation of protein synthesis. Like the yeast Ire1p, mammals have two ER transmembrane proteins, Ire1α and Ire1β, which regulate the splicing of the X box binding protein (*Xbp-1*) mRNA. After the removal of 26 nucleotides the mRNA is translated to make active Xbp-1. Xbp-1 is a transcription factor that binds to and up-regulates genes with the ER-stress response elements (ERSEs) (Ma and Hendershot 2001).

In addition to these observations and similar to the yeast UPR, two other pathways are involved in mammals. These pathways include activating transcription factor 6 (ATF6) and the protein kinase R-like ER kinase/pancreatic eIF2α kinase (PERK/PEK). ATF6 is a transcription factor localized to the ER by its lumenal association with the mammalian chaperone BiP. In response to unfolded proteins, ATF6 moves to the Golgi and is cleaved by S1P and S2P proteases which free ATF6 to translocate to the nucleus to bind to ERSEs and induce the UPR (Shen *et al.* 2002). By phosphorylating eIF2α, PERK/PEK prevents the 80S ribosomal initiating complexes from translating mRNA, thereby inhibiting further protein synthesis rather than correcting protein folding (Harding *et al.* 1999; Kaufman 1999).

1.6 Mammalian Retrograde System: Mitochondria to Nucleus Communication

Previous investigations into the molecular events associated with TFEC nephrotoxicity, in particular the adduction and apparent up-regulation of the nuclear encoded mitochondrial heat shock protein 60 kDa (HSP60) after a sub-lethal dose (Bruschi, unpublished observations), suggested that a mammalian communication pathway from the damaged mitochondria to the nucleus may exist (Fig. 1.11). The observed up-regulation of HSP60, a heat shock protein that attempts to correct damaged or misfolded protein, occurs within the regions of kidney most damaged by the mitochondrial specific toxicant TFEC (i.e., damage demonstrated by anti-TFA immunoreactivity is co-localized with increased anti-HSP60 immunoreactivity, see Fig. 1.11). Further support for HSP60 up-regulation was obtained by DNA microarray analysis after *in vitro* dosing of TFEC. The HSP60 mRNA, in addition to several other mitochondrial proteins, was up-regulated further supporting the proposition of a

"retrograde type" communication in mammals (Ho, Hu, & Bruschi, manuscript in preparation). With these observations in hand, we have attempted to identify and characterize a homologous mammalian pathway to the previously described yeast retrograde communication (flow of information from the mitochondria to the nucleus) using APAP and TFEC as tools in the process.

In Chapter 2 our investigations focused on searching for a mammalian retrograde homologue through Southern blots and degenerate primers designed for reverse transcriptase polymerase chain reaction (RT-PCR). The *in vitro* physical characterization of a potential homologue, cytochrome *b*, after dosing with both APAP and TFEC is described in Chapter 3 while *in vivo* characterization of APAP dosed mice is explored in Chapter 4.

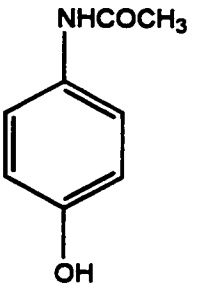

N-acetyl-*p*-aminophenol (APAP)

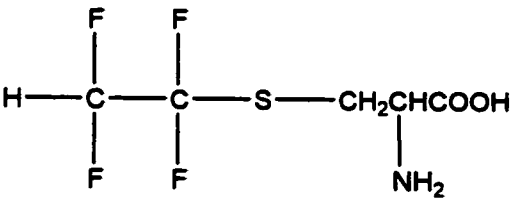

S-(1,1,2,2-tetrafluoroethyl)-L-cysteine (TFEC)

Figure 1.1. Study Compounds. Acetaminophen (APAP) and *S*-(1,1,2,2-tetrafluoroethyl)-L-cysteine (TFEC).

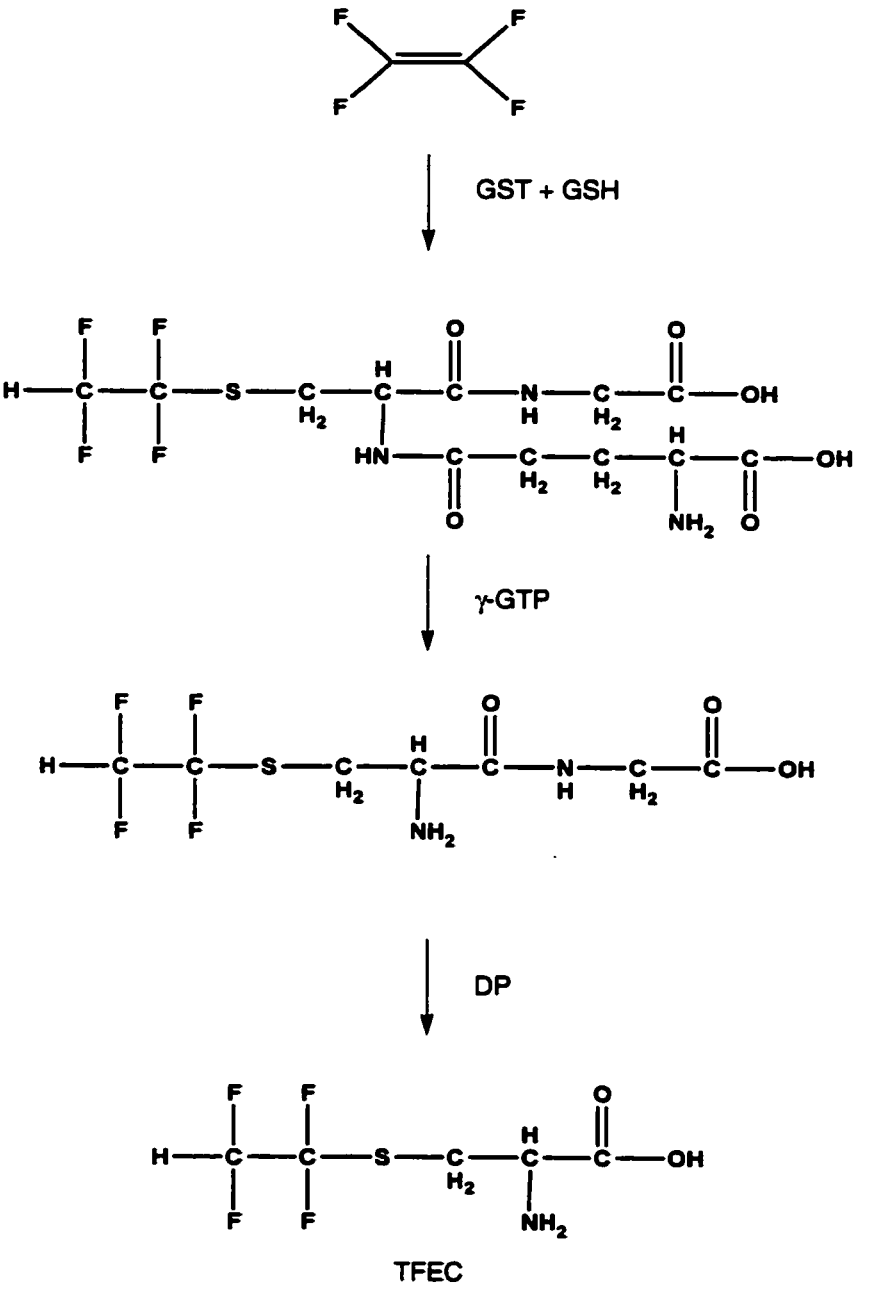

Figure 1.2. Metabolism of tetrafluoroethylene (TFE) to tetrafluoroethyl cysteine (TFEC). Glutathione (GSH) is added to TFE by glutathione S-transferase (GST) forming the TFE-glutathione adduct (TFE-GS). TFE-GS adduct is metabolized by γ-glutamyltranspeptidase (γ-GTP) forming the TFE-cysteinylglycine conjugate, which is processed by cysteinylglycine dipeptidase (DP) to TFEC.

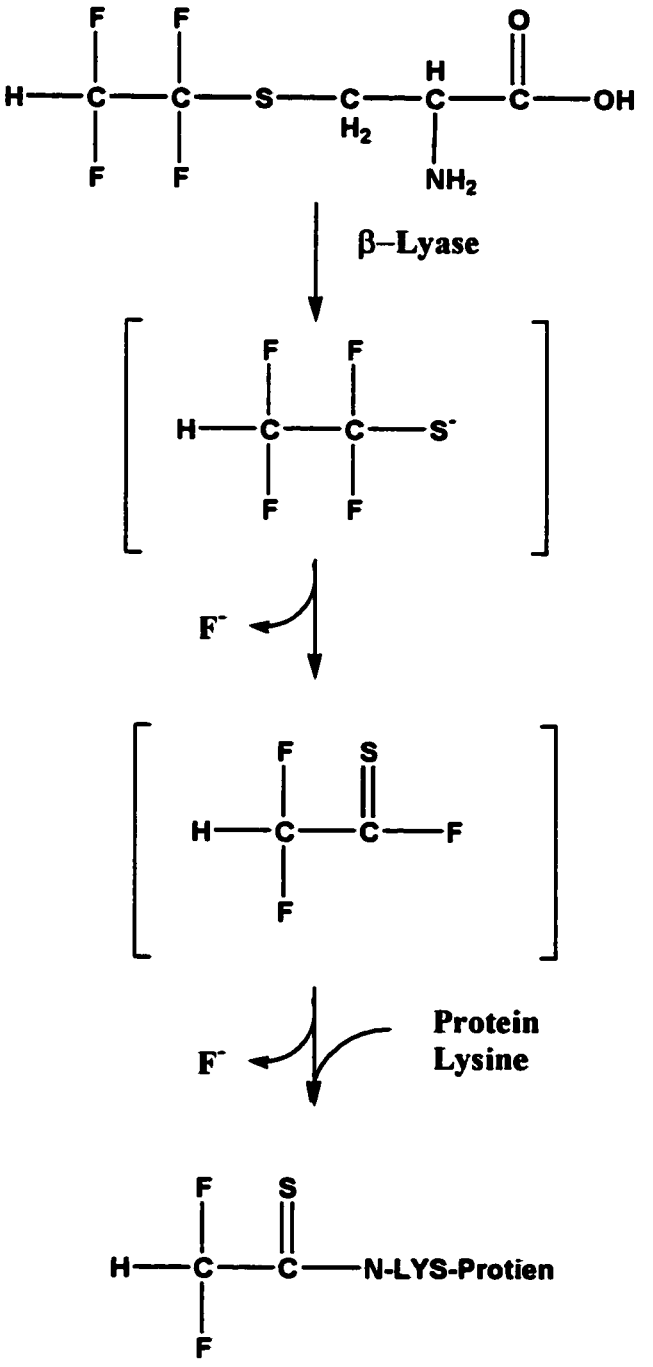

DFTAL

Figure 1.3. Formation of tetrafluoroethyl cysteine adducted proteins. A β-lyase is proposed to convert TFEC to the reactive tetrafluoroethanethiolate that rearranges to difluorothioacetyl fluoride. This reactive difluorothioacetyl fluoride covalently binds to proteins at lysine residues forming the difluorothioacetyl-lysine adduct (DFTAL).

Table 1.1. Identification of tetrafluoroethyl cysteine adducted proteins.

Protein	Identification Method	Function	Reference
mtHSP70 (Mortalin)	N-terminal sequencing	Stress Protein	(Bruschi *et al.* 1993)
HSP60	N-terminal sequencing	Stress Protein	(Bruschi *et al.* 1993)
Dihydrolipoamide dyhydrogenase (E3o) subunit (αKDH)	N-terminal sequencing	TCA enzyme	(Bruschi *et al.* 1998)
Dihydrolipoamide dyhydrogenase (e3) subunit (BCKDK)	N-terminal sequencing	Intermediary metabolism	(Bruschi *et al.* 1994)
Lipoamide succinyltransferase (E2o) subunit (αKDH)	N-terminal sequencing	TCA enzyme	(Bruschi *et al.* 1998)
Aspartate aminotransferase (AspAT)	N-terminal sequencing	Intermediary metabolism	(Bruschi *et al.* 1993)
L-arginine:glycine amidinotransferase	N-terminal sequencing	Creatine synthesis	Bruschi, unpublished data
Mitochondrial aconitase	In gel digest & Mass Spectrometry	TCA enzyme	(James *et al.* 2002)

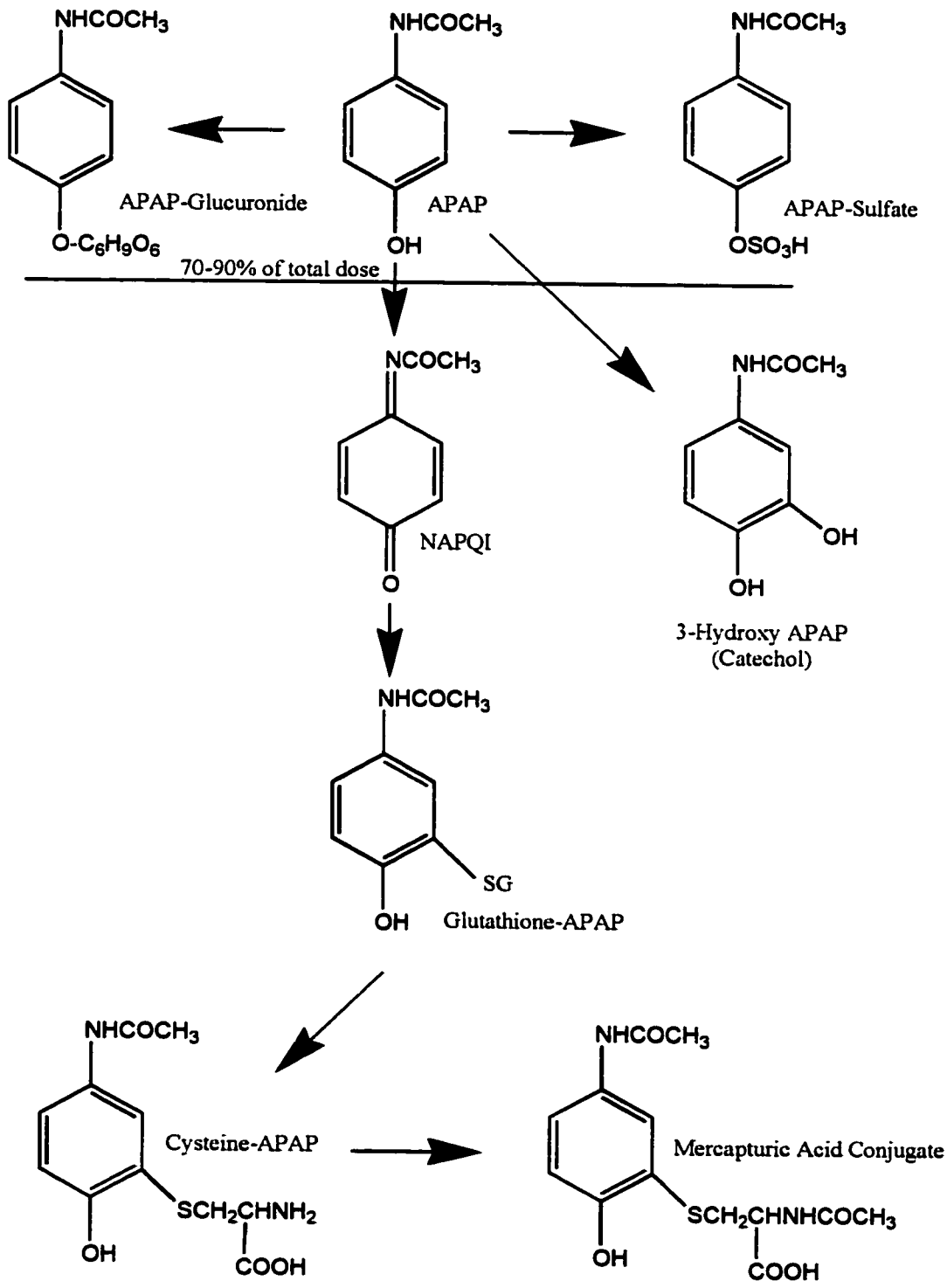

Figure 1.4. Acetaminophen metabolic profile. Phase II conjugation of APAP to the glucuronide and sulfate make up approximately 70 to 90% of the total dose. CYP metabolism is responsible for the formation of the catechol and the proposed toxic metabolite N-acetyl-*p*-quinone imine (NAPQI). Figure adapted from Prescott (1996).

Table 1.2. Identification of acetaminophen adducted proteins by classical techniques.

Protein	Identification Method	Function	Reference
Glutamine synthetase	Tryptic digest then N-terminal sequencing	Gln synthesis	(Bulera *et al.* 1995)
Lamin A	Immunochemically	Nuclear lamina structure	(Hong *et al.* 1994)
Selenium-binding protein	Tryptic digest then N-terminal sequencing	Scavenger of electrophiles	(Bartolone *et al.* 1992; Pumford *et al.* 1992)
Glutamate dehydrogenase	N-terminal sequencing	Glu synthesis	(Halmes *et al.* 1996)
Aldehyde dehydrogenase	Tryptic digest then N-terminal sequencing	Oxidation of aldehydes	(Landin *et al.* 1996)
N-10-formyl tetrahydro-folate dehydrogenase	Tryptic digest then N-terminal sequencing	Donation of one-carbon units in biosynthesis	(Pumford *et al.* 1997)
Carbamyl phosphate synthetase I	N-terminal sequencing	Ammonia consumption	(Gupta *et al.* 1997)
Calreticulin	Tryptic digest then N-terminal sequencing	Calcium regulation	(Zhou *et al.* 1996)
Glutathione *S*-transferase	N-terminal sequencing	Electrophile detoxification	(Weis *et al.* 1992)
Thiol:Protein disulfide oxidoreductase	Tryptic digest then N-terminal sequencing	Posttranslational modifications	(Zhou *et al.* 1996)
Glyceraldehyde-3-phosphate dehydrogenase	N-terminal sequencing and Mass Spectrometry	Glycolytic pathway (ATP synthesis)	(Dietze *et al.* 1997)

Table 1.3. Acetaminophen adducts identified by two-dimensional gel electrophoresis and mass spectrometry (Qiu *et al.* 1998).

Identified Protein	Location
glutathione reductase (peroxidase)	cytoplasmic & **mitochondrial**
housekeeping (thioredoxin reductase?)	**mitochondrial**
thioether S-methyltransferase	cytoplasmic or ER
dEST homology:aryl sulfotransferase	cytoplasmic
homology: bovine pyrophosphatase	?
tropomyosin 5	cytoskeletal
selenium-binding protein	cytoplasmic
selenium-binding liver protein	cytoplasmic
acetaminophen-binding protein	cytoplasmic
homology: proteasome subunit C8	cytoplasmic
methionine adenosyltransferase	cytoplasmic
protein synthesis initiation factor 4A	ribosomal
aldehyde dehydrogenase class I & II	**mitochondrial** & cytoplasmic
ATPase α-subunit	**mitochondrial**
urate oxidase	peroxisomal
homology: 2,4-dienoyl-CoA reductase	**mitochondrial** & ER
macrophage 23kD stress protein	cytoplasmic
GSH transferase pi	cytoplasmic, **mitochondrial,** & ER
homology: glycine N-methyl-transferase	cytoplasmic
homology: 3-hydroxy anthraniolate 3,4 dioxygenase	cytoplasmic
carbonic anhydrase III	cytoplasmic
Sorbitol dehydrogenase precursor	cytoplasmic
db EST:2049563 Life Technologies mouse embryo 8 c DNA clone	?

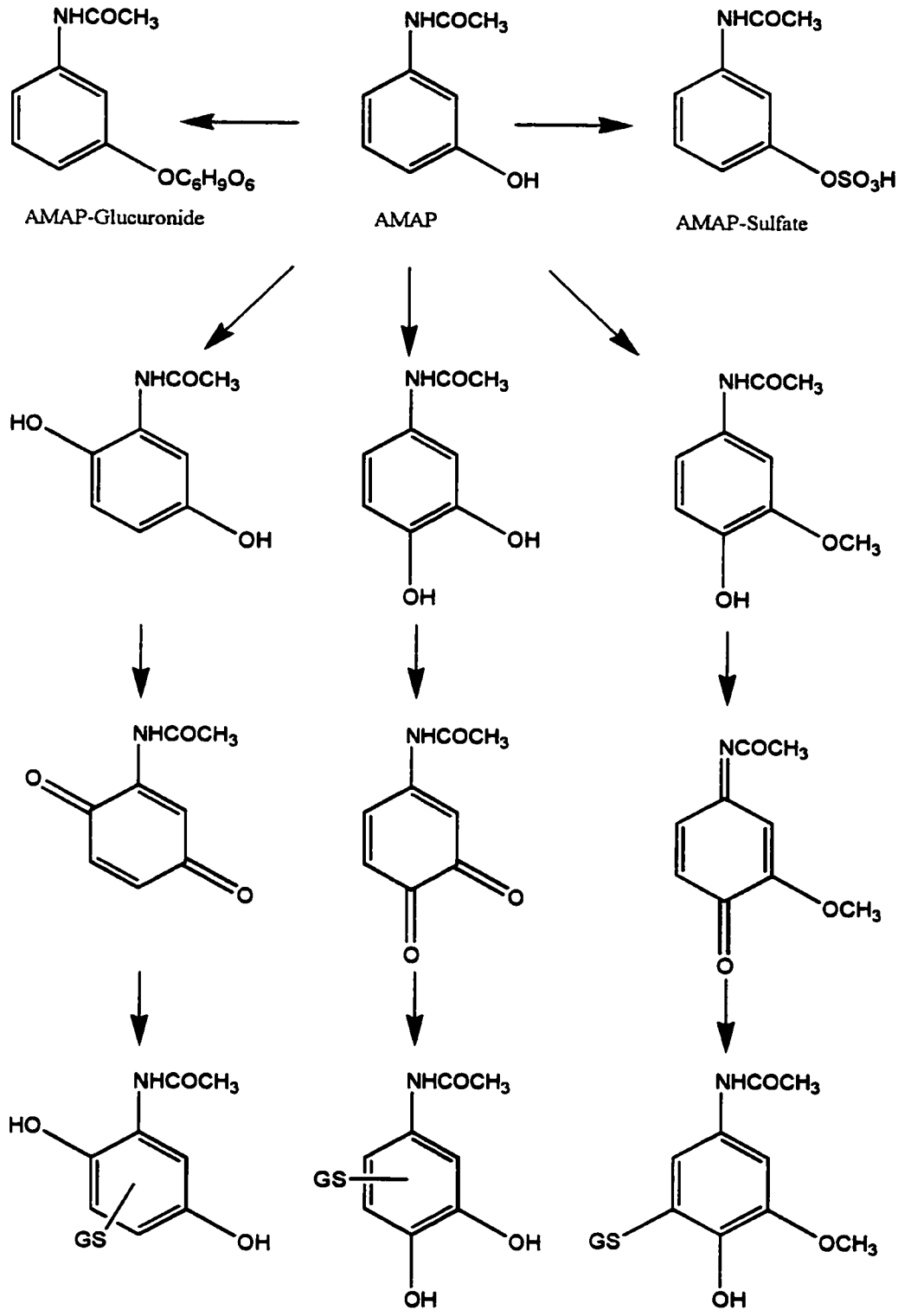

Figure 1.5. N-acetyl-*m*-aminophenol metabolic profile. Profile summarized from Rashed *et al.* (1990).

Table 1.4. N-acetyl-*m*-aminophenol adducts identified by two-dimensional gel electrophoresis and mass spectrometry (Qiu *et al.* 2001).

Identified Protein	Location
methionine adenosyltransferase	cytoplasmic
selenium-binding liver protein	cytoplasmic
acetaminophen-binding protein	cytoplasmic
selenium-binding protein	cytoplasmic
Endoplasmic reticulum transmembrane protein precursor	ER membrane
Protein disulfide isomerase/thyroid hormone binding protein	ER lumen
HMA CoA synthase	cytoplasmic
homology: proteasome subunit C8	cytoplasmic
alpha-1 protease inhibitors 1, 3, & 5	cytoplasmic
db EST:2049563 Life Technologies mouse embryo 8 c DNA clone	?

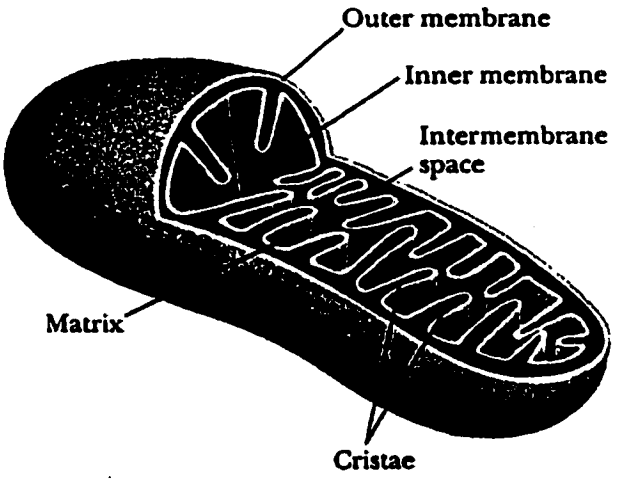

Figure 1.6. Mitochondrial structure. Two mitochondrial membranes create four distinct regions called the mitochondrial outer membrane (MOM), intermembrane space (IMS), mitochondrial inner membrane (MIM), and the matrix. The folds in the MIM form the cristae. Figure taken from Garrett and Grisham (1995).

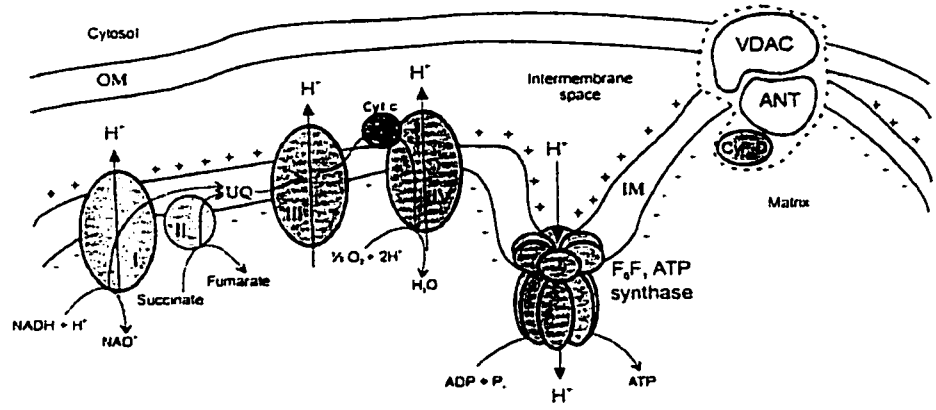

Figure 1.7. A schematic overview of the electron transport chain and the constituents of the mitochondrial permeability transition pore. Figure taken from Robertson and Orrenius (2002).

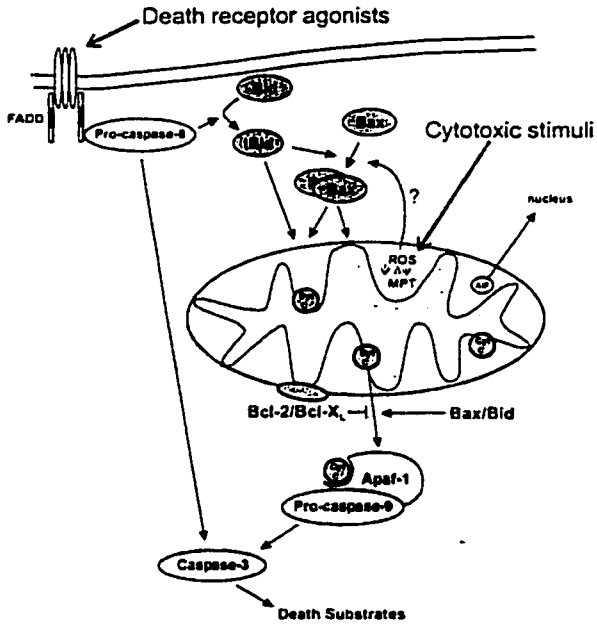

Figure 1.8. Mitochondrial roles in cell death. Figure taken from Robertson and Orrenius (2002).

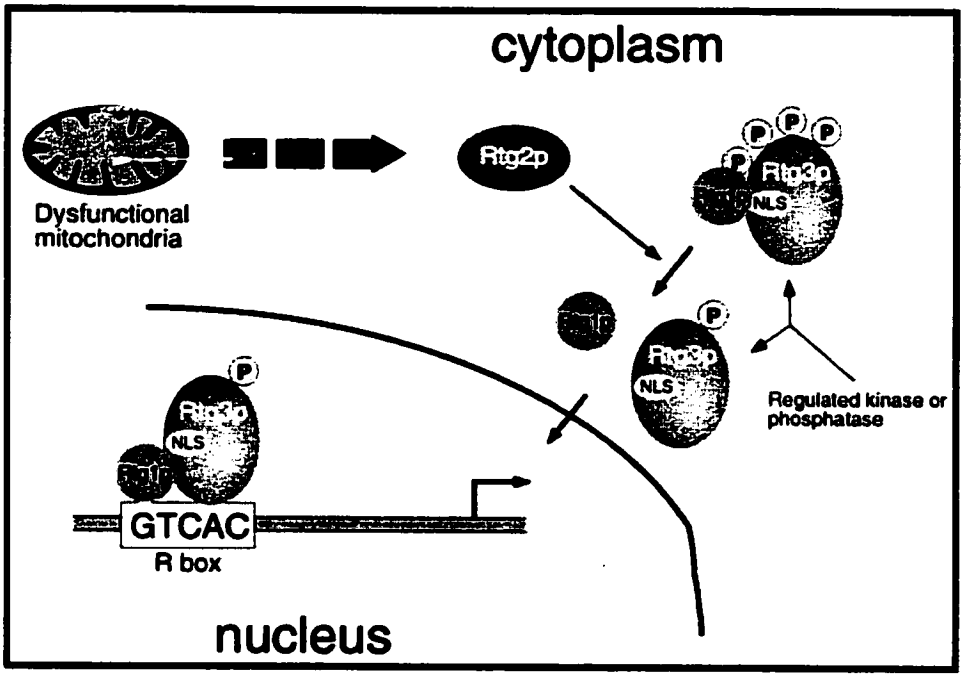

Figure 1.9. Summary of retrograde communication pathway. Signals of mitochondrial dysfunction are transmitted through an unknown mechanism to activate RTG2p. Active RTG2p interacts with the cytosolic RTG1p/RTG3p complex and results in their dissociation. RTG3p is dephosphorylated and translocated, with RTG1p, into the nucleus to bind to the upstream activation site of retrograde target genes. The ultimate result being increased mRNA and protein for target genes. Figure taken from Sekito *et al.* (2000).

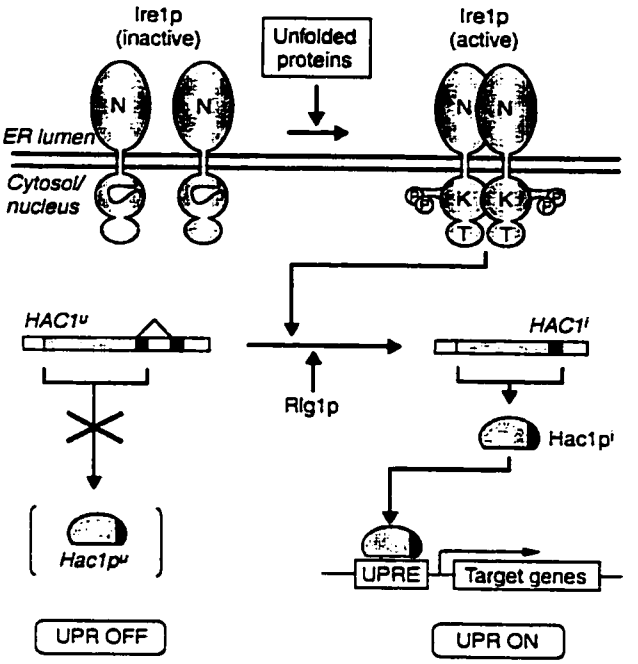

Figure 1.10. Summary of yeast unfolded protein response (UPR). The endoplasmic reticulum portion of inisitol requiring 1 protein (Ire1p) oligomerizes in response to unfolded proteins. After oligomerization, the cytosolic portion of Ire1p is activated by self-phosphorylation. The endoribonuclease activity of cytosolic Ire1p then processes the uninduced mRNA, *HAC1*^{u}, to the active form *HAC1*^{i} encoding for Hac1p^{i}. Hac1p^{i} binds to the unfolded protein response element (UPRE) for up-regulation of target genes. Figure taken from Patil and Walter (2001).

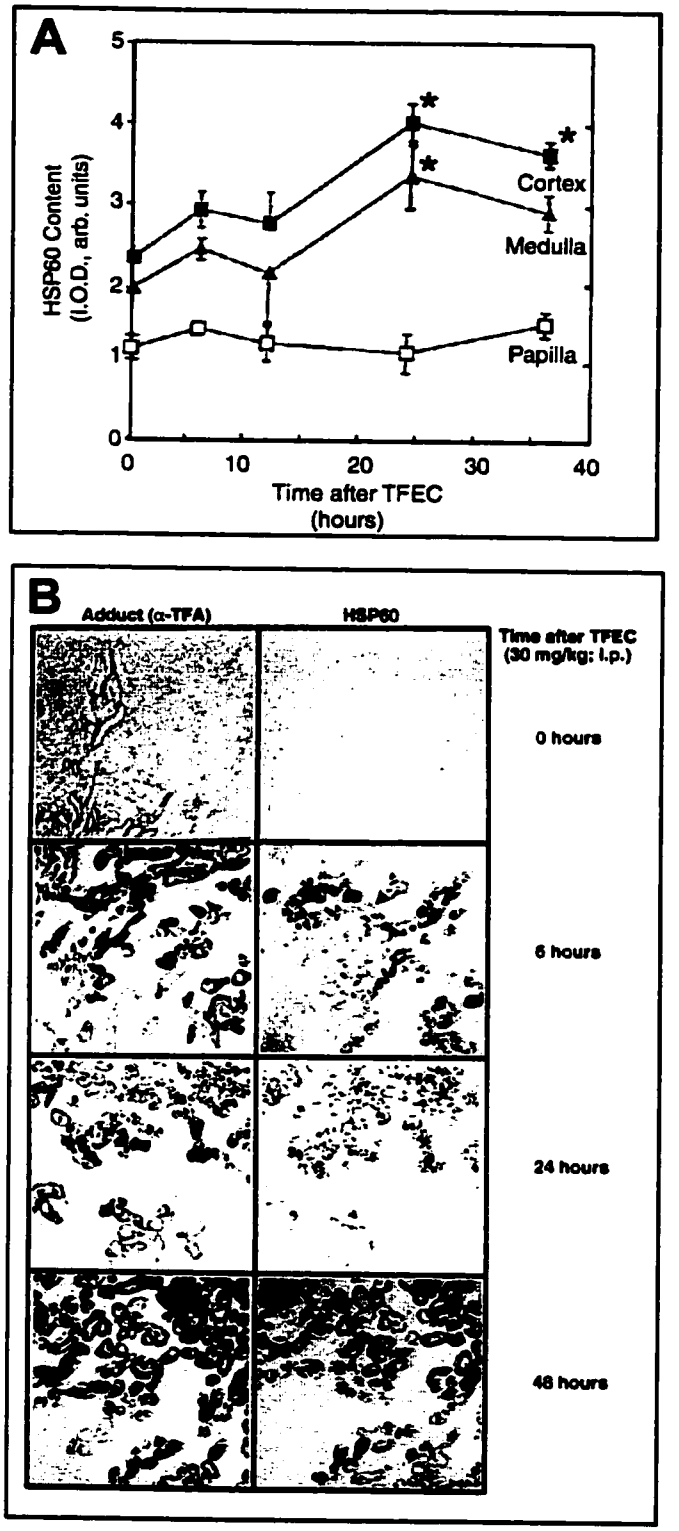

Figure 1.11. Heat shock protein 60 up-regulation. (A) densitometry of HSP60 from Western blot analysis and (B) immunohistochemistry of serial rat kidney sections after sub-lethal TFEC dose.

Chapter 2

Searching for a Mammalian Retrograde Homologue

2.1 Introduction

Butow and colleagues have characterized a homeostatic response to alterations in the mitochondrial state within the yeast *Saccharomyces cerevisiae* and coined the term "retrograde regulation" to describe this response pathway. These studies have identified three novel retrograde genes, named *RTG1*, *RTG2*, and *RTG3*, required for the proper function of this pathway (Butow *et al.* 1988; Liao *et al.* 1991; Liao and Butow 1993; Chelstowska *et al.* 1999). *RTG1* codes for a 177 amino acid protein with predicted structural similarity to a basic helix-loop-helix transcription factor containing a leucine zipper. *RTG2* codes for a 394 amino acid regulatory protein with an unknown mechanism of action and an ATP binding domain as the only recognized motif (Liao and Butow 1993). *RTG3* also codes for a protein of 486 amino acids with a predicted basic helix-loop-helix transcription factor structure (Jia *et al.* 1997). All three retrograde proteins are required for the retrograde response and up-regulation of the identified genes under retrograde control. Mitochondrial dysfunction, signaled though an unknown mechanism, results in the dephosphorylation of RTG3p and its translocation to the nucleus with RTG1p that then binds the UAS_r and induces the transcription of the target genes (Sekito *et al.* 2000).

The known importance of mitochondria in the maintenance of cellular homeostasis through energy production and calcium regulation, combined with our

understanding of its ever-growing importance in many different cell death processes, led us to wonder about the possible communication pathways that are utilized by mitochondria to indicate damage or functional alterations. This reverse flow of information through transcription factors or other protein-based modulators is obviously important but has been neglected in higher organisms. The identification and characterization of the retrograde regulation system in yeast suggests the possibility of the existence of a homologous mammalian system. Here we attempt to search for and identify a homologous system in a mammalian system using the known yeast proteins as a starting point.

2.2 Materials and Methods

2.2.1 Materials

Custom DNA primers were purchased from Gibco BRL Life Technologies (Rockville, MD). Yeast, mouse, and human genomic DNA was purchased from Promega (Madison, WI). Genomic DNA from *C. elegans* was a kind gift from Jim Thomas (Department of Genetics, University of Washington). Unless otherwise noted, polymerase chain reactions (PCR) were performed using the "Ready-to-go®" PCR Beads from Amersham Biosciences (Piscataway, NJ). Cloning was performed with TOPO-TA cloning into the pCRII-TOPO vector and transformed into "TOP10 One Shot" competent *E. coli* cells purchased from Invitrogen (Carlsbad, CA). Plasmid DNA was isolated using either the Wizard Mini-Preps from Promega (Madison, WI) or the QIAgene Mini-preps (Valencia, CA). EcoRI, SacI, SpeI, and BglII were purchased from New England BioLabs (Beverly, MA). DNA sequencing was performed using the ABI Prism™ Big Dye™ Terminator Cycle Sequencing Ready Reaction kit (Perkin Elmer Applied

Biosystems-Foster City, CA). Centri-Sep Columns were purchased from Princeton Separations (Adelphia, NJ). Non-radioactive full-length DNA probes were generated using the Renaissance® Labeling Kit (du Pont) purchased from New England Nuclear Life Science Products (Boston, MA). GeneScreen™ nylon membrane was purchased from New England Nuclear Research Products (Boston, MA). SV Total RNA Isolation System was purchased from Promega and the MasterAmp™ RT-PCR kit was purchased from Epicentre Technologies (Madison, WI). DNA hybridization was performed in a Model 2000 Micro Hybridization Incubator purchased from Robbin Scientific (Sunnyvale, CA). β-Agarase I from *Pseudomonas atlantica* was purchased from Calbiochem-Novabiochem (San Diego, CA). All other materials were purchased either from Sigma (St. Louis, MO) or other common suppliers.

2.2.2 Cloning of RTG genes

Primers for the Yeast retrograde genes were designed with the aid of the Oligo version 4.05 Primer Analysis Software (National Biosciences, Plymouth, MN) and the published protein sequences. The accession numbers for RTG1, RTG2, and RTG3 are M97690, M97691, and U46012, respectively. Yeast actin (accession number X62630) and glyceraldehyde 3-phosphate dehydrogenase (GAPDH-I-acc. #V01302) were used as positive controls. Each primer set is described in Table 2.1. Primers were diluted in 10 mM Tris pH 8.0 / 1 mM ethylenediaminetetraacetic acid (EDTA) (TE) to a working concentration ranging from 5.65 to 7.41 pmol/μL. Twenty-five pmol of each primer were used with Ready-to-go® PCR beads to amplify 50 ng of genomic yeast DNA. The PCR cycle was as follows: 95°C for 5 min then 35 cycles of 95°C for 1 min, 48°C for 1 min, and 72°C for 2 min followed by a 10 min extension at 72°C. Amplified products were

separated by 1% agarose gel electrophoresis in 1x TBE (Tris-Borate-EDTA) running buffer and visualized by ethidium bromide staining under ultraviolet (UV) light.

The resultant PCR products were cloned into the pCRII-TOPO Vector (Fig. 2.1) and transfected into "TOP10 One Shot" competent *E. coli* cells as directed by the Invitrogen TOPO-TA cloning protocol. Plasmid DNA was isolated using the Promega Wizard Mini-preps as directed by the protocol. The inserts were screened for orientation in the plasmid by predicted restriction digest products (see Table 2.2 for details). Each insert was amplified by PCR utilizing the plasmid M13 sites (FM13-20 and RM13) and the resultant PCR products were purified with the PCR DNA preparation purification kit (Promega) and sequenced with the ABI Prism™ Big Dye™ Terminator sequencing kit with 6 μL PCR product, 3.2 pmol Reverse M13 primer and the appropriate concentration of the dye master mix. Cycle reactions were carried out for 25 cycles at 96°C for 30 sec, 50°C for 15 sec, and 60°C for 4 min. Unincorporated dye from these reactions was removed using Centri-Sep Columns and sequences were analyzed by sequencing gel in the Molecular Biomarkers Laboratory, Department of Environmental Health at the University of Washington on a 377 Perkin Elmer/Applied Biosystems DNA Sequencer.

2.2.3 Probe Synthesis and Southern Blots

The non-isotopic Renaissance® labeling kit utilizes random primers and biotinylated nucleotides for labeling and streptavidin-horse radish peroxidase (HRP) with luminol reagent for detection on X-ray film. This system retains a high level of sensitivity without radioactive components. Full-length probes to target genes *RTG1*, *RTG2*, and *RTG3* as well as a control gene, *GAPDH-I*, were produced following the manufacturer's protocol. Approximately 500 ng of purified DNA from a PCR sample

were incubated with the random primers, biotinylated nucleotides, and Klenow fragment overnight at room temperature to incorporate labels. After ethanol precipitation of DNA from the reaction mixture, DNA concentrations were estimated and standardized to 6.25 pg/μL. Serial dilutions from 6.25 pg/μL to 0.025 pg/μL were prepared and cross-linked to nylon membrane (GeneScreen™) to determine the labeling efficiency by chemiluminesence.

Probing conditions were optimized using slot blots with denatured yeast genomic DNA ranging from 1 μg to 10 pg cross-linked to nylon membrane (GeneScreen™). Membranes were wetted with 2X SSC (3 M NaCl, 0.3 M sodium citrate) for 15 min then equilibrated for 1 h at 42°C in hybridization buffer (2X SSC, 0.5% Blocking reagent from the Renaissance kit, 5% dextran sulfate, 0.1% sodium dodecyl sulfate (SDS), and 50% formamide) with 50 μg/mL sheared salmon sperm DNA. During equilibration, the hybridization solution (probing solution) was prepared by adding full-length biotin labeled probes (final concentration 20 ng/mL) to the hybridization buffer with 50 μg/mL sheared salmon sperm DNA. Hybridization was performed at 42°C for 16 h in a rotating micro hybridization oven. The membranes were washed with 2X SSC with 1% SDS then 0.2X SSC with 0.1% SDS each for 15 min at 42°C and exposed to X-ray film after treatment with chemiluminescence reagent. Using this hybridization method, we were able to detect target sequences in as little as 1 ng denatured genomic yeast DNA in a slot blot probe (data not shown).

E. coli, human, mouse, yeast, and *C. elegans* genomic DNA were digested separately with EcoRI for 4 h at 37°C. Digested DNA was precipitated with ethanol and 10 μg were separated using electrophoresis with a 0.7% agarose gel in 1X TBE. The

agarose gel separated DNA was transferred to GeneScreen™ nylon membrane by the following procedure. The gel was equilibrated for 10 min in 0.25N HCl then rinsed with deionized water. Next the gel was agitated in 0.4N NaOH / 0.6M NaCl for 30 min followed by 30 min in 1.5M NaCl / 0.5M Tris-HCl pH 7.5. A capillary blot using 20X SSC and a filter paper wick was used to transfer the DNA to the nitrocellulose. DNA was UV cross-linked to the membrane. Probing was performed as described above. Alternate techniques were tried to modify the stringency including hybridizing at 65°C with no formamide, changing the wash to 2X SSC with 1% SDS at 65°C only, and altering the hybridization buffer to 3X and 6X SSC.

2.2.4 Degenerate Primer Design and RT-PCR

Two sets of degenerate primers were designed against the published DNA sequences and anchored within the predicted structural motifs for each of the three known yeast retrograde proteins, RTG1, RTG2, and RTG3 (see Fig. 2.2 and Table 2.3). Degenerate primer design utilized National Center for Biotechnology Information (NCBI) Genetic Codon Genetic Code tables (http://www.ncbi.nlm.nih.gov/Taxonomy/) and Codon Usage Database (http://www.kazusa.or.jp/codon/) to account for codon differences observed between yeast and humans. Additionally, the third nucleotide position with the codon, often called the wobble position, was either substituted with multiple nucleotides for major codons or with deoxyinosine for universal nucleotide matches. These primers were used for RT-PCR against human fetal liver mRNA to search for mammalian homologues to the yeast retrograde proteins. Primers were diluted in water to a concentration ranging from 7.67 to 15.33 pmol/μL.

Total RNA was isolated from human fetal livers using the published protocol for the SV Total RNA Isolation Kit. Briefly, approximately 30 mg of –80°C tissue was cracked with a pestle while in liquid nitrogen, diluted and applied to a proprietary spin column to bind the RNA. A DNase step was included and the isolated RNA was eluted from the column with sterile RNase free water and stored at –80°C until use. RNA quality was evaluated by agarose gel electrophoresis and UV absorbance at 260 and 280 nm. RNA concentration was estimated from the absorbance at 260 nm and the standard of 1 absorbance unit at 260 nm equivalent to approximately 40 μg/mL single stranded RNA.

RT-PCR was performed following the protocol provided with the MasterAmp™ RT-PCR kit from Epicentre Technologies. Total RNA (2 μg) was used as a template for the RT-PCR with 25 pmol of each forward and reverse degenerate primer described above. The reverse transcriptase reaction was performed at 60°C for 30 min then followed by the PCR cycle (95°C for 1 min, 48°C for 1 min, 72°C for 1 min for 35 cycles then 72°C for 10 min). As a positive control and to check for DNA contamination, a set of primers capable of recognizing human, rat, and mouse GAPDH was ordered from Clontech. These primers yield a 475 bp fragment in both PCR and RT-PCR.

Products generated reproducibly from RT-PCR were excised after separation using low temperature agarose gel electrophoresis. The excised agarose band was melted at 65°C for 10 min then digested with 1 unit agarase at 40°C for 1 h. The agarase incubation was terminated by the addition of sodium acetate to a final concentration of 300 mM and chilling on ice for 15 min. The resultant mixture was centrifuged at 14,000 rpm for 15 min to remove any undigested agarose. The DNA in the supernatant was

precipitated in ethanol, cloned into the pCRII-TOPO vector, and sequenced as described above. Sequence results were searched using the BLASTN (version 2.0.6 on http://www.ncbi.nlm.nih.gov) against both the non-redundant and expressed sequence tag (EST) database.

2.3 Results

2.3.1 Cloning of RTG genes

PCR, using yeast DNA as a template and the designed *RTG1*, *RTG2*, and *RTG3* primers, resulted in single bands of the predicted sizes of the amplification products indicating the specificity of the primers under the conditions used (Fig. 2.3). The resultant PCR products for *RTG1* and *RTG2* were successfully cloned into at least one vector in the correct orientation as predicted by restriction digest (data not shown). Screening 40 *RTG3* colonies revealed only plasmids with *RTG3* in the reverse orientation. The significance of this observation is unclear but since the purpose of this cloning was manipulation and not expression, the reverse orientation sufficed for further steps. The orientation and identity of the inserts were further confirmed by DNA sequencing and were in complete agreement (100% identity) with the published DNA sequences of all three genes through at least 500 bp of insert.

2.3.2 Probe Synthesis and Southern Blots

Full-length probes for *RTG1*, *RTG2*, *RTG3*, and *GAPDH* were successfully synthesized and the lower limit of probe detection by chemiluminesence was in the range of 0.1 to 0.4 pg of probe cross-linked to nylon membrane, indicating efficient incorporation of the biotin label. The concentration of the probes was estimated to range from 23.1 to 46.2 ng/μL based on protocol guidelines.

Full-length non-isotopic *RTG1* and *RTG3* probes demonstrated specific hybridization bands to single copy genes of the target yeast genomic DNA while the *RTG2* probe bound to two specific hybridization bands (Fig. 2.4). The two specific hybridization bands detected using the full-length non-isotopic *RTG2* probe is the result of an internal EcoRI site within the coding region. The non-isotopic *GAPDH* positive control probe demonstrated three specific hybridization bands corresponding to the three coding sequences and three isoforms for this enzyme. The identity of the three bands is consistent with the different *GAPDH* isoforms since all three isoforms of *GAPDH* lack an internal EcoRI site as observed with *RTG2*. All three yeast *GAPDH* isoforms have ~89% similarity while cross species *GAPDH* have ~60-65% identity as determined by sequence alignment. The *GAPDH* positive control provided useful information regarding the sensitivity of the full-length probes. Regardless of the adjustments in probing conditions or wash stringency *via* changes in formamide, salt or detergent concentrations, or temperature, the *GAPDH* probe was unable to detect cross species *GAPDH* with relatively high identity (60-65%). Therefore, it is not unreasonable to anticipate that the full-length probes lacked the sensitivity to detect the weak homologies expected between the yeast retrograde system and a homologous mammalian system.

2.3.3 Degenerate Primer RT-PCR

Total RNA was isolated from human fetal liver (kindly provided by Dr. J. Rhim, Department of Pathology, University of Washington) and evaluated for integrity by agarose gel electrophoresis and UV absorption. The ethidium bromide stained gel showed a smear of material with two bands expected at approximately 750 and 1500 bp indicating the 18S and 28S ribosomal RNA (data not shown). UV absorbance gave 260

nm / 280 nm ratios ranging from 1.7 to 1.9 and estimated concentrations ranging from 0.093 to 0.51 μg/μL.

RT-PCR using human fetal liver total RNA as a template and the degenerate primer sets for *RTG1*, *RTG2*, and *RTG3* only yielded one consistent, reproducible band of approximately 450 bp using primer set 6 directed to *RTG3* (Fig. 2.5). The other five primer sets failed to produce a band, while the *GAPDH* positive control generated the predicted band of 475 bp during only the RT-PCR, indicating no DNA contamination (data not shown). After excising the band from the agarose gel by agarase digestion and cloning, the insert was sequenced from both ends. Ten different plasmids were sequenced using the forward (FM13-20) and reverse (RM13) primers. Of the 20 possible sequences, 15 were readable through at least 230 bp of the insert (Fig. 2.6). All 15 readable sequences were searched by BLASTN (version 2.0.6 on http://www.ncbi.nlm.nih.gov/BLAST) against both the non-redundant and EST database. Against the non-redundant database, 13 of the 15 were strong matches for human mitochondrial genome cytochrome *b*, each with a low probability of a match by chance (Fig. 2.7). The expected values, the probability of a match by chance, ranged from 0 to e-125. The other two sequenced plasmids were identified, one as the pCRII vector, and the other weakly matched a *C. elegans* cosmid Y17G7B in the non-redundant database with an expected value of 0.28 and an unknown human clone in the EST database with an expected value of 0.23. By far, the most significant, reliable hits were for the human mitochondrial genome cytochrome *b*.

2.4 Discussion

The first attempt to search for a mammalian system homologous to the previously described yeast system of retrograde regulation (Sekito *et al.* 2000) utilized full-length non-isotopic DNA probes generated from the known retrograde yeast genes *RTG1*, *RTG2*, and *RTG3*. Although the probes were sensitive enough to detect a single copy of the gene in the yeast genomic DNA, there was not enough cross-reactivity to detect the weak homologies predicted to occur across species (Fig. 2.4). In the *GAPDH* positive control, there was enough cross reactivity to detect the three different yeast isoforms (~89% identity) but not enough cross reactivity to detect isoforms from mouse or human (~60-65% similarity). This limitation could not be overcome by adjustments to probing or wash stringency indicating this method would not be useful in the identification of a mammalian retrograde system with weak homology to the yeast system.

Although the first attempt was unsuccessful, an alternative attempt at identifying a mammalian retrograde system was pursued. Six sets of degenerate primers directed at the RTG genes were synthesized for RT-PCR. These degenerate primers were directed at the predicted structural motifs, if any, within the deduced protein sequence of each of the identified retrograde genes. Specifically, degenerate primers were anchored within the predicted basic helix-loop-helix motif and leucine zipper of *RTG1* and *RTG3*, respectively (Liao and Butow 1993; Jia *et al.* 1997). These degenerate primers were designed in an attempt to correct for the codon usage preferences in humans versus yeast as indicated in the methods section.

Of the six sets of degenerate primers designed (Fig 2.2), only primer set 6, targeted to the 3' region of *RTG3*, generated a consistent, reproducible RT-PCR product

(Fig 2.5). Sequencing and sequence searching identified the RT-PCR product as a portion of the human mitochondrial cytochrome *b*, an integral part of the electron transport chain Complex III, also known as the cytochrome bc_1 complex or ubiquinone:ferrictyochrome *c* oxidoreductase (E.C. 1.10.2.2).

The solved crystal structure of bovine heart bc_1 complex, Complex III, reveals a dimer formation with each monomer consisting of 11 polypeptide subunits. The complex spans the MIM protruding into both the intermembrane space and the matrix (Fig. 2.8) (Iwata *et al.* 1998). The bc_1 complex functions as part of the ETC by accepting electrons from the membrane soluble electron carrier ubiquinol and reducing cytochrome *c*. Cytochrome *c* is not a subunit of the bc_1 complex but it associates with the bc_1 complex within the inter membrane space to accept electrons and transport them to cytochrome *c* oxidase (Complex IV). A scheme of the electron transfer within Complex III is shown in Figure 2.9. Cytochrome *b*, the Rieske (Fe-S) protein, and cytochrome c_1 are three bc_1 complex proteins containing prosthetic groups that electrons flow directly through and therefore, are crucial to the function of the bc_1 complex. Both cytochrome *b* and cytochrome c_1 are heme proteins while the Rieske protein has an iron-sulfur cluster that facilitates electron transfer. It is proposed that the other subunits are required for the proper membrane insertion and tertiary structure of the complex since, with the exception of subunit VI, deletion of any other subunit results in respiration-deficient phenotypes (Scheffler 1999).

Cytochrome *b* is a mitochondrial encoded, inner membrane embedded heme protein with eight transmembrane helices. The identified sequence is predicted to span two transmembrane helices and three loops connecting the helices based on the bovine

heart mitochondrial cytochrome bc_1 complex crystal structure (Iwata *et al.* 1998) and a predicted yeast cytochrome bc_1 complex model (Esposti *et al.* 1993) (Fig 2.8).

The exact significance of cytochrome *b* identification is not readily apparent. The identification of cytochrome *b* may be nothing more than a fortuitous finding since the primers used have no observed homology to cytochrome *b*. The primer set used to detect this fragment was directed toward a soluble basic helix-loop-helix transcription factor. Although the sequence identified contains a helix-loop-helix motif, the sequence differs substantially from the original sequence and a transcription factor-like activity seems unlikely as the entire cytochrome *b* protein is very hydrophobic. Nonetheless, the identification of cytochrome *b* is interesting because of its localization to the mitochondria. A primary role for cytochrome *b* in Complex III of the ETC has already been identified and extensively characterized (see above). Although a secondary function for cytochrome *b* beyond that in the ETC has not been identified at this time, its localization within the mitochondria and the involvement of this organelle in cell death is of particular interest.

With the recent intensive study of cell death, it is obvious that mitochondria have more functions than the classically recognized role of energy production through the TCA cycle and oxidative phosphorylation. The TCA cycle utilizes metabolic pyruvate either from glycoloysis or fatty acid oxidation to produce a small amount of ATP, and more importantly, reduced cofactors (NADH) for oxidative phosphrylation in an aerobic environment. The oxidation of these cofactors results in the reduction of oxygen through a complex set of reactions called the ETC. Electron flow through the ETC pumps protons across the impermeable MIM generating the $\Delta\Psi_m$ that is utilized to produce ATP.

One critical player in the ETC with a secondary function not directly related to its ETC role is the soluble electron transporter cytochrome *c*. Cytochrome *c* is localized within the mitochondrial intermembrane space and functions primarily as an electron shuttle from Complex III (ubiquinol:ferrictyochrome *c* oxidoreductase) to Complex IV (cytochrome *c* oxidase). The secondary function of cytochrome *c* involves its release from the mitochondrial intermembrane space and participation in apoptosome formation (Zou *et al.* 1999). This ultimately leads to the activation of the caspase cascade and the characteristic morphology of apoptosis.

Additionally, other mitochondrial proteins with known functions have been implicated in triggering, or at least participating in the execution of cell death, particularly the participation of ANT and VDAC as members of the MPTP. The primary role of the ANT is to transport ATP and ADP across the impermeable MIM. ANT association with inhibitors of MPTP, like BA that prevent cell death, has suggested a secondary role, the prevention of cell death (Zamzami *et al.* 1996). Furthermore, the proposed association of VDAC, the MOM porin, with ANT to form the MPTP also supports a dual role for both VDAC and ANT (Crompton 1999; Halestrap *et al.* 2000). The exact contribution of each to the MPTP components and their role in cell death is still unclear. Nonetheless, a dual role for ANT and VDAC is suggested. Therefore, it is not unreasonable to propose that cytochrome *b* has some, as of yet, unrecognized function in cell death.

Further evidence supporting a possible secondary biological function for the bc_1 complex comes from the observation that the mitochondrial bc_1 complex in the fungus *Neurospora* (Schulte and Weiss 1995), in the potato plant (Braun *et al.* 1992), and in

spinach leaf (Eriksson *et al.* 1994) have a mitochondrial processing peptidase (MPP) activity in addition to their primary activity in electron transport. The peptidase activity is thought to be involved in the import and processing of cytosolic proteins and is localized within the core 1 and core 2 proteins of the complex (Fig. 2.8-Cores 1 and 2 in cyan and magenta, respectively) (Braun *et al.* 1992; Schulte and Weiss 1995). The potato, as well as the bovine, core subunits have sequence identity to yeast MPP, but only the potato subunits retain MPP activity (Braun *et al.* 1992). The crystal structure and further study of bovine bc_1 complex suggests that the MPP activity contained in the core 1 and core 2 proteins is inhibited as the result of a peptide bound within the active site cleft (Deng *et al.* 1998; Iwata *et al.* 1998). This has been demonstrated by the ability to activate and characterize MPP activity by the addition of non-ionic detergent (Trition X-100) to the point where electron flow is completely disrupted. This disruption is proposed to result in the release of the peptide inhibitor (Deng *et al.* 1998). Several other hypotheses concerning an MPP function within the bc_1 complex have been proposed. These include;

a) the possibility that the mammalian MPP is "a relic of an ancient processing peptidase,"

b) an important, although low, MPP activity *in vivo*, or,

c) a MPP activity early in biogenesis that is terminated by its inclusion in the bc_1 complex (Deng *et al.* 1998).

A combination of all this evidence for secondary roles associated with mitochondrial proteins, as well as the conserved nature of cytochrome *b*, leaves open the possibility of its involvement in cell death processes. Although there is at present no

direct evidence for MPP cleavage of cytochrome *b*, the localization of the core 1 and core 2 subunits within the bc_1 complex hints at a possible cleavage and alteration within the complex. This may result in changes in the overall confirmation of the complex that would dramatically affect activity, as has been demonstrated by detergent and mutagenesis studies (Deng *et al.* 1998; Scheffler 1999). Such a possibility is addressed by our work described in the following chapter.

Table 2.1. Retrograde primer design.

Target	Forward Primer (5' to 3')	Reverse Primer (5' to 3')	Expected Product Size (bp)
RTG1	GCACAACACCAAACATGAGC	ATCGCCCTTGACTAACCACC	714
RTG2	GAAAAGTGTAGGCGTGCACA	GCAATTCCTATCAGCGCTC	1334
RTG3	CTGCACGGAATCATCAAGG	GCTAATAAGACCATAAACTACCCC	1649
Actin	GGAAGCGATCTTAAATCCCA	CGCTTTTTCTTCTTCAGTGTTCGT	1286
GAPDH	CCACGTGCAGATCAACATAGTC	ACCGTATTCGTTATCGTACCAG	1205

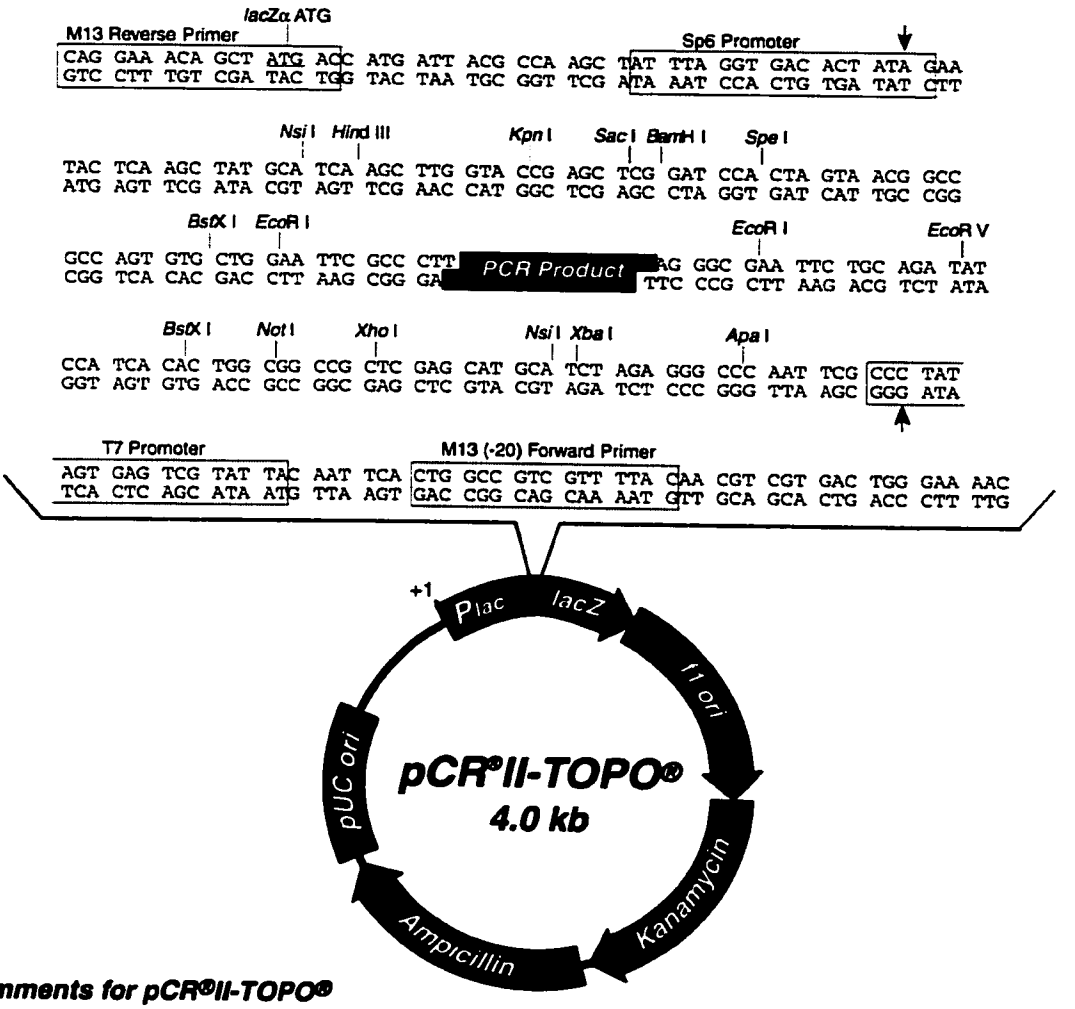

Comments for pCR®II-TOPO®
3973 nucleotides

LacZα gene: bases 1-589
M13 Reverse priming site: bases 205-221
Sp6 promoter: bases 239-256
Multiple Cloning Site: bases 269-383
T7 promoter: bases 406-425
M13 (-20) Forward priming site: bases 433-448
f1 origin: bases 590-1027
Kanamycin resistance ORF: bases 1361-2155
Ampicillin resistance ORF: bases 2173-3033
pUC origin: bases 3178-3851

Figure 2.1. Vector Map for pCRII-TOPO as proved by Invitrogen.

Table 2.2. Predicted retrograde plasmid restriction digest products.

Protein	Restriction Digest	Correct Orientation	Incorrect Orientation	EcoRI Digest
RTG1	SacI	539 bp 4100 bp	255 bp 4300 bp	731 bp
RTG2	SpeI	349 bp 4900 bp	1057 bp 4200 bp	507 bp 844 bp
RTG3	SacI	769 bp 4100 bp	970 bp 4600 bp	1666 bp

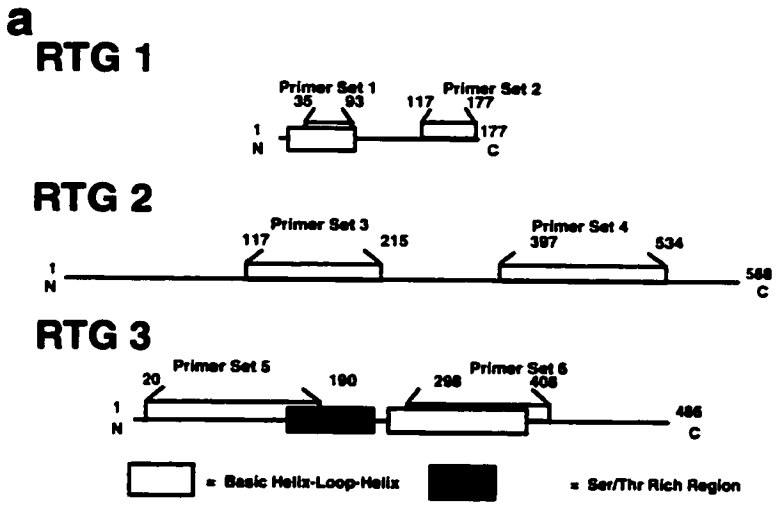

b

Primer Set Description

Name	Location (Res #)	Description
RTG 1		
Primer Set 1	35-93	bHLH
Primer Set 2	117-177	No Motif
RTG 2		
Primer Set 3	117-215	No Motif
Primer Set 4	397-534	No Motif
RTG 3		
Primer Set 5	20-190	Ser/Thr Rich
Primer Set 6	298-408	bHLH/Leu Zip

Figure 2.2. Retrograde degenerate primer design. A schematic view of the predicted structural motifs of each RTG gene with primer locations highlighted (a). A more detailed account of the degenerate primer localization (b).

Table 2.3. Retrograde degenerate primers.

Primer Target		Forward Primer (5' to 3')[a]	Reverse Primer (5' to 3')[a]
RTG1	Set 1	GYATIATICCIAARGAYTT	IATRTAYTCIACIGCYTGNG
	Set 2	CAARCARACIGGIACNAT	ICTICCRTTICCRTAYTCNC
RTG2	Set 3	TTYGTIAAYGCIGTNTAYGG	GCITCYTTRTAIGCYTC
	Set 4	TYGTICAYGCITCYTAYCC	IGTICTYTCYTCYTTNACYTT
RTG3	Set 5	AAYCARACIAARGTNCTNC	TRCTIGAIGAYAAIGANGARCT
	Set 6	GRGARTTIATIAARCARAA	IAAIGCRTTIGGIACNGAYCT

a-Nucleotide codes I = deoxyinosine
R = A & G
Y = C & T
N = A, C, G, & T

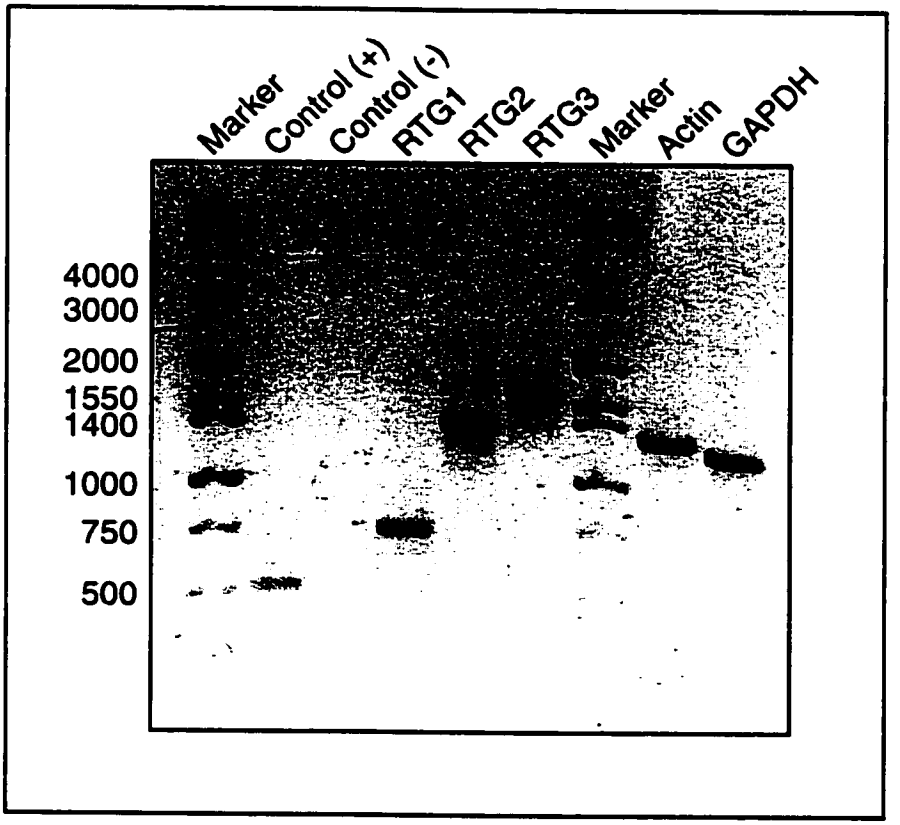

Figure 2.3. Ethidium bromide stained photograph of retrograde PCR products.

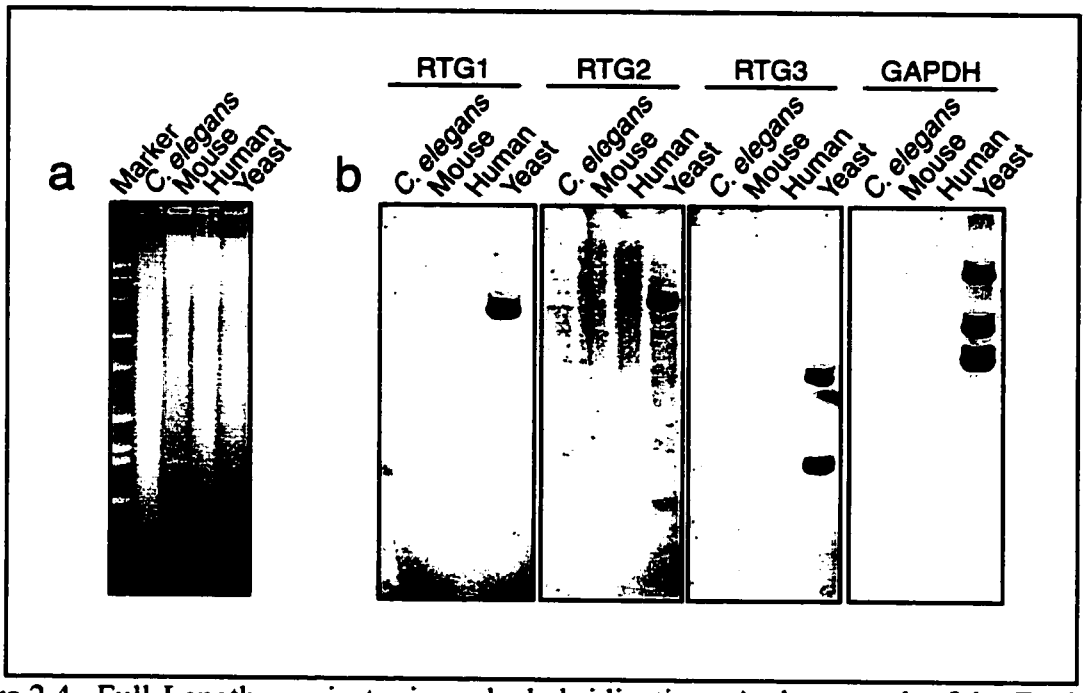

Figure 2.4. Full-Length non-isotopic probe hybridization. A photograph of the EcoRI digested genomic DNA separated on agarose before transfer to nylon membrane (a). Southern blots after probing with full-length biotin labeled probes visualized with chemiluminesence on X-ray film (b). Blots were probed with the corresponding RTG probe or GAPDH positive control listed.

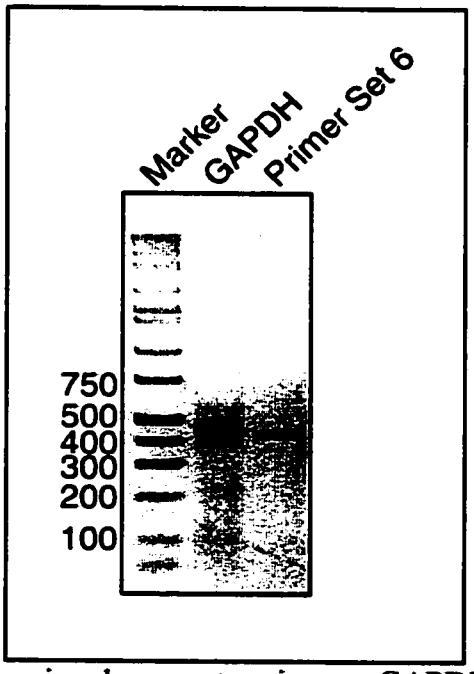

Figure 2.5. RT-PCR results using degenerate primers. GAPDH positive control yields a band approximately 475 bp while Primer Set 6 is approximately 425 bp.

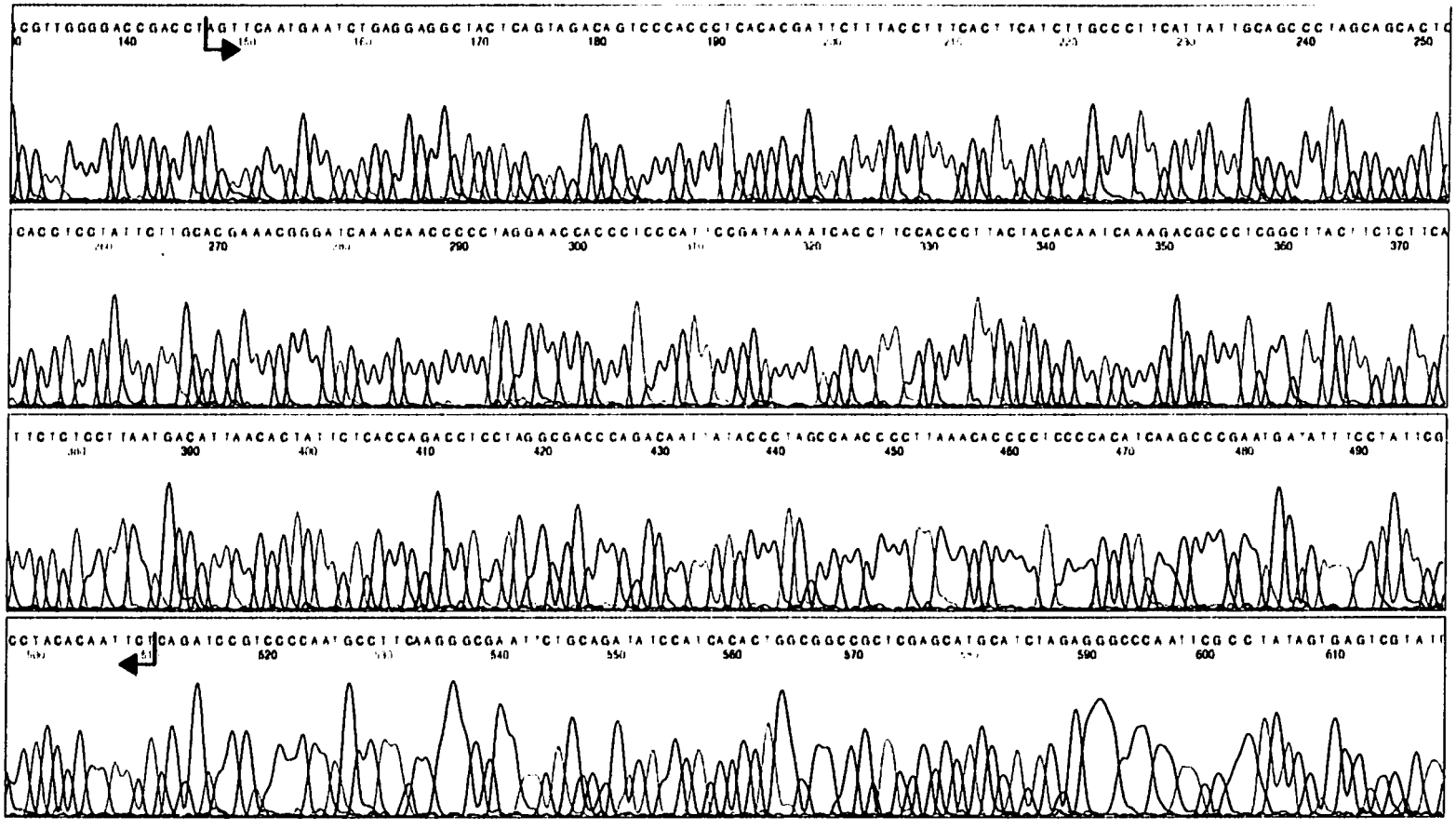

Figure 2.6. DNA sequence of RT-PCR product of Primer Set 6 after cloning into plasmid. The region between arrows was searched for sequence identity against the NCBI-nr database as described in the Methods section. This representative sequence demonstrated 98% identity with human cytochrome *b*.

```
        M  T  P  M  R  K  I  N  P  L  M  K  L  I  N  H  S  F  I  D  L  P
1       ccaatgaccc caatacgcaa aattaacccc ctaataaaat taattaacca ctcattcatc gacctcccca

        T  P  S  N  I  S  A  W  W  N  F  G  S  L  L  G  A  C  L  I  L  Q  I  T
71      ccccatccaa catctccgca tgatgaaact tcggctcact ccttggcgcc tgcctgatcc tccaaatcac

        T  G  L  F  L  A  M  H  Y  S  P  D  A  S  T  A  F  S  S  I  A  H  I
141     cacaggacta ttcctagcca tgcactactc accagacgcc tcaaccgcct tttcatcaat cgcccacatc

        I  R  D  V  N  Y  G  W  I  I  R  Y  L  H  A  N  G  A  S  M  F  F  I
211     actcgagacg taaattatgg ctgaatcatc cgctaccttc acgccaatgg cgcctcaata ttctttatct

        C  L  F  L  H  I  G  R  G  L  Y  Y  G  S  F  L  Y  S  E  T  W  N  I  G
281     gcctcttcct acacatcggg cgaggcctat attacggatc atttctctac tcagaaacct gaaacatcgg

        I  I  L  L  L  A  T  M  A  T  A  F  M  G  Y  V  L  P  W  G  Q  M  S
351     cattatcctc ctgcttgcaa ctatagcaac agccttcata ggctatgtcc tcccgtgagg ccaaatatca

        F  W  G  A  T  V  I  T  N  L  L  S  A  I  P  Y  I  G  T  D  L  V  Q
421     ttctgagggg ccacagtaat tacaaactta ctatccgcca tcccatacat tgggacagac ctagttcaat

        W  I  W  G  G  Y  S  V  D  S  P  T  L  T  R  F  F  T  F  H  F  I  L  P
491     gaatctgagg aggctactca gtagacagtc ccaccctcac acgattcttt acctttcact tcatcttgcc

        F  I  I  A  A  L  A  T  L  H  L  L  F  L  H  E  T  G  S  N  N  P  L
561     cttcattatt gcagccctag caacactcca cctcctattc ttgcacgaaa cgggatcaaa caacccccta

        G  I  T  S  H  S  D  K  I  T  F  H  P  Y  Y  T  I  K  D  A  L  G  L
631     ggaatcacct cccattccga taaaatcacc ttccaccctt actacacaat caaagacgcc ctcggcctac

        L  L  F  L  L  S  L  M  T  L  T  L  F  S  P  D  L  L  G  D  P  D  H  Y
701     ttctcttcct tctctcctta atgacattaa cactattctc accagacctc ctaggcgacc cagaccatta

        T  L  A  N  P  L  N  T  P  P  H  I  K  P  E  W  Y  F  L  F  A  Y  T
771     taccctagcc aaccccttaa acacccctcc ccacatcaag cccgaatgat atttcctatt cgcctacaca

        I  L  R  S  V  P  N  K  L  G  G  V  L  A  L  L  L  S  I  L  I  L  A
841     attctccgat ccgtccctaa caaactagga ggcgtccttg ccctattact atccatcctc atcctagcaa

        M  I  P  I  L  H  M  S  K  Q  Q  S  M  M  F  R  P  L  S  Q  S  L  Y  W
911     taatccccat cctccatata tccaaacaac aaagcataat atttcgccca ctaagccaat cactttattg

        L  L  A  A  D  L  L  I  L  T  W  I  G  G  Q  P  V  S  Y  P  F  T  I
981     actcctagcc gcagacctcc tcattctaac ctgaatcgga ggacaaccag taagctaccc ttttaccatc

        I  G  Q  V  A  S  V  L  Y  F  T  T  I  L  I  L  M  P  T  I  S  L  I
1051    attggacaag tagcatccgt actatacttc acaacaatcc taatcctaat accaactatc tccctaattg

        E  N  K  M  L  K  W  A
1121    aaaacaaaat actcaaatgg gcc
```

Figure 2.7. Cytochrome *b* peptide sequence deduced from DNA sequence (Accession number U09500). The underlined section was identified by sequencing of the RT-PCR fragment generated from Primer Set 6.

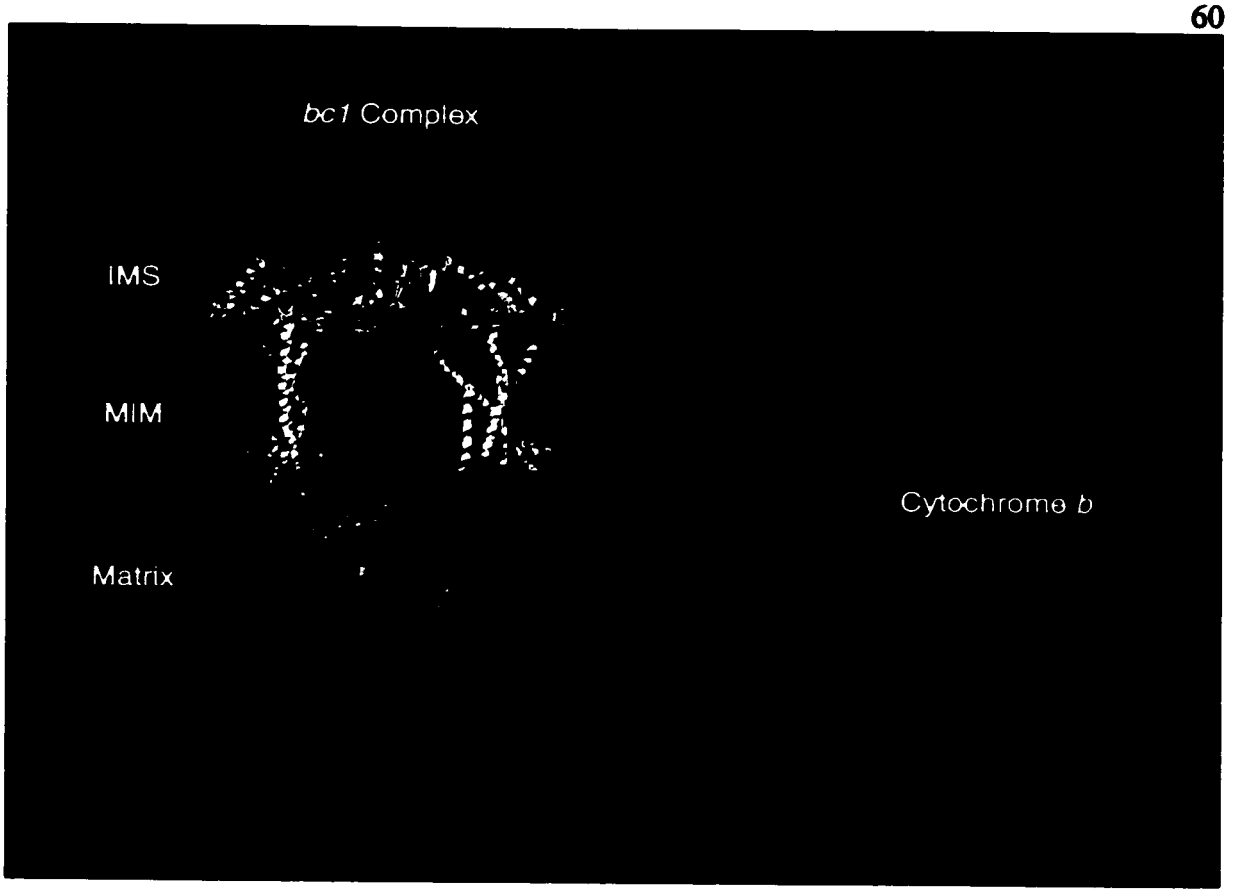

Figure 2.8. Complex bc_1 crystal structure. Cytochrome *b* is shown in green with a Cytochrome *b* monomer highlighted in the inset (hemes not shown in monomer). The estimated region amplified by Primer Set 6 RT-PCR is shown in red on the monomer. Cores 1 and 2 are shown in cyan and magenta, respectively, within the matrix. Both Cytochrome c_1 and the Fe-S protein are localized in the intermembrane space (IMS). Crystal structure solved by Iwata *et al.* (1998).

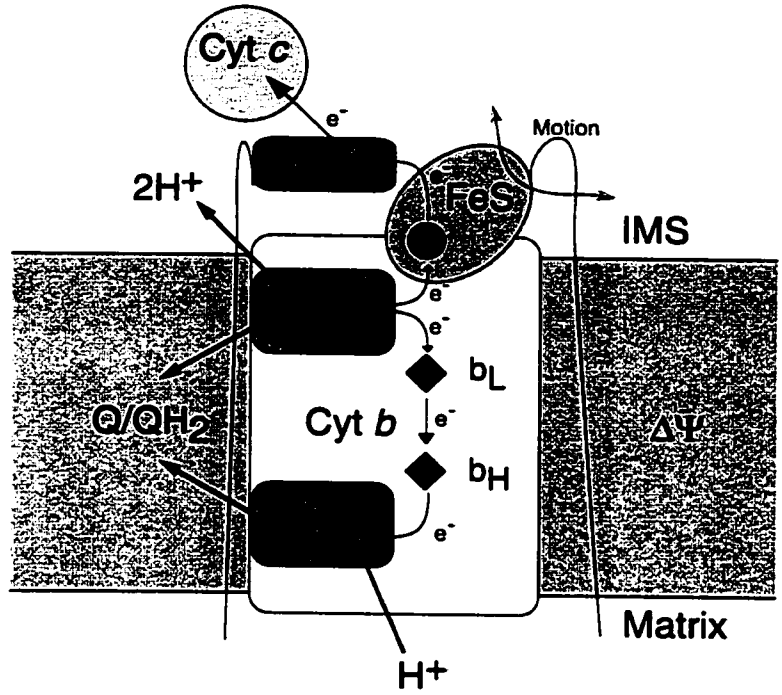

Figure 2.9. Schematic view of Complex III activity. Ubiquinol (QH_2) binds to cytochrome *b* (Q_o) while ubiquinone (Q) binds to Q_i. One electron flows from QH_2 bound at Q_o to the iron-sulfur (Fe-S) protein, which then moves to donate the electron to cytochrome c_1 and ultimately to cytochrome *c* in the intermembrane space (IMS). The second electron from QH_2 is transferred to the cytochrome *b* hemes (b_L and b_H) and ultimately reduces Q bound at Q_i to a semiquinone. The cycle is repeated with a new QH_2 binding to Q_o and reducing another cytochrome *c* molecule and the semiquinone bound at Q_i to QH_2. This process pumps protons into the IMS producing the inner membrane potential ($\Delta\Psi$) that drives ATP production. Figure adapted from Darrouzet *et al.* (2001).

Chapter 3

Exploring Cytochrome *b*:

Physical and Functional Characterization

3.1 Introduction

The potential involvement of mitochondrial cytochrome *b* in a communication pathway from the mitochondria to the nucleus is an intriguing proposition because of the growing interest in the mitochondria. In particular, the realization that many common proteins within the mitochondria have a secondary function related to the cell death process indicates the importance of this organelle. The significance of identifying cytochrome *b* as a possible contributor in cell communication as described in Chapter 2 is not immediately obvious, but here we will examine possible structural and functional changes that may indicate a role for cytochrome *b* in the cell death process or other homeostatic processes.

One possible mechanism to explain the fragment of cytochrome *b* identified in Chapter 2 is a system analogous to the mammalian UPR system (refer Chapter 1). Briefly, the UPR provides a communication pathway from the endoplasmic reticulum to the nucleus in response to accumulation of misfolded proteins in the ER. This pathway works through specific protein cleavage that results in differential mRNA splicing and ultimately changes in transcription and translation (for review see Sidrauski *et al.* 1998). Because of the close proximity of a MPP to cytochrome *b*, within the bc_1 complex, we investigated the possible cleavage of cytochrome *b* as an initiating step in a

communication of specific mitochondrial damage to the nucleus. Here we search for both structural and functional clues of such a change in cytochrome *b*.

3.2 Materials and Methods

3.2.1 Materials

Tetrafluoroethylene gas was purchased from SynQuest Laboratories (Alachua, FL). Cell culture media and gentamicin stock were purchased from Gibco BRL (Rockville, MD) while insulin, transferrin, and selenium (ITS) media additives were purchased from Collaborative Biomedical Products (Bedford, MA). "Complete-Mini®" protease inhibitor tablets with EDTA were purchased from Roche Diagnostics (Indianapolis, IN). Reagents for the Bradford assay were purchased from Bio-Rad Laboratories (Hercules, CA). Molecular weight markers were purchased either from MBI Fermentas (Hanover, MD) or New England Biolabs (Beverly, MA). Pure bovine heart bc_1 complex was a kind gift from Dr. Chang-An Yu (Oklahoma State University, Stillwater, OK). Secondary antibody coupled with HRP, Super-Signal West Dura chemiluminescent substrate, and CHAPS (3-(3-cholamidapropyl)dimethylammonio)-1-propanesulfonate) were purchased from Pierce Chemical Company (Rockford, IL). CNBr-activated sepharose 4B was purchased from Amersham Biosciences (Piscataway, NJ). Amicon® Ultra-4 centrifugal filters were ordered from Millipore (Bedford, MA). Sequencing grade modified trypsin was purchased from Promega (Madison, WI).

3.2.2 TFEC synthesis

TFEC was synthesized following the procedure previously published (Hayden *et al.* 1987; Hayden and Stevens 1990). Briefly, ~100 mL of methanol was degassed with nitrogen in a 200 mL round bottom flask. One g (0.006 mol) of anhydrous L-cysteine

hydrochloride was dissolved in methanol. To this solution, 3 equivalents of aqueous sodium hydroxide (5 N) were added drop wise. TFE gas was bubbled through the solution for five minutes. The reaction progress was monitored by thin layer chromatography (TLC) with 2-propanol: acetic acid: water (7:1:3) as the mobile phase. Products were visualized with 0.1% ninhydrin in acetone. Cysteine migrated with an R_f = 0.63 while TFEC migrated with an R_f = 0.81. Upon reaction completion as determined by the absence of cysteine in the reaction mixture, the methanol was evaporated under low pressure. The resultant crystals were resuspended in a minimal volume of aqueous 1 N NaOH. The product was recovered by isoelectric precipitation through the drop wise addition of 1 N HCl on ice until a white precipitate formed. The product was collected on a Buchner funnel and dried overnight under vacuum. Compound purity was confirmed by nuclear magnetic resonance (NMR, Varian Associates VXR 300, Palo Alto, CA) and mass spectrometry (MicroMass Quattro II, Manchester, UK). TFEC was successfully synthesized with a product yield of approximately 60%. The product identity was confirmed by mass determination (ESI $[MH]^+$ m/z 222). Product purity was confirmed and in agreement with NMR shifts as previously published (Hayden and Stevens 1990). (Fig. 3.1). ^1H NMR (D_2O, 300 MHz) δ: 3.4 (d of d, J_β = 14.9 Hz, J_α = 7.4 Hz, 1H), 3.6 (d of d, J_β = 15.1 Hz, J_α = 4.3 Hz, 1H), 4.1 (d of d, J_β = 3.9 Hz, J_α = 7.4 Hz, 1H), and 6.3 (t, J_{HF} = 53.0, 1H).

3.2.3 Tissue Culture

Serum-free culture of the differentiated mouse hepatocyte cell line expressing transforming growth factor-α, the TAMH cell line, was as previously described (Wu *et al.* 1994). Cells were grown and passaged in serum-free Dulbecco's modified Eagle's

medium/Ham's F12 supplemented with 5 μg/mL of insulin, 5 μg/mL of transferrin, 5 ng/mL of selenium, 0.1 μmol/L of dexamethasone, 10 mM of nicotinamide, and 50 μg/mL of gentamicin. Cultures were maintained in a humidified incubator with 5% carbon dioxide/95% atmospheric air and passaged when 70-90% confluent. Cells were treated when at 80-90% confluence.

Cells were treated with test compounds, 0.25 mM TFEC, 5 mM APAP, or 10 μM sodium (meta)arsenate ($NaAsO_2$) directly dissolved in supplemented TAMH media to avoid any cytotoxic effects of vehicle alone. Cells were harvested by scraping from the surface of the plate in minimal volume of Lysis Buffer (20 mM Tris pH 7.4, 0.25 M sucrose, 1 mM dithiothreitol (added fresh just before use), and one "Complete-Mini®" protease inhibitor tablet with EDTA per 10 mL solution). Supernatant was centrifuged and the pellet, if any, was added to the cells scraped from the plate surface. Lysates were stored at –80°C. Lysates were thawed then sonicated with a probe homongenizer (Series 4710 Ultra-sonic Homogenizer, Cole-Palmer) and protein content was determined using the Bradford microtiter plate assay with bovine serum albumin as a standard.

3.2.4 Immunoblot detection of cytochrome *b*

Denaturing polyacrylamide gel electrophoresis using the Mini-PROTEAN II system from Bio-Rad with 10-15% acrylamide gels separated 50 μg per lane of cell lysates. Prestained broad-range molecular weight markers were run concurrently. Resolved proteins were transferred to nitrocellulose membrane using a semidry transfer apparatus (Bio-Rad) and probed with varying concentrations of primary antibody (1:500 to 1:1000 in phosphate buffered saline (PBS), 0.1% Triton X-100 (v/v), 5% nonfat dry milk (w/v), pH 7.4). Secondary antibody directed to rabbit IgG was coupled with HRP

(1:50000 in PBS, 0.1% Trition X-100 (v/v), 5% nonfat dry milk (w/v), pH 7.4) for detection with enhanced chemiluminescence using Super-Signal West Dura substrate and exposure to X-ray film.

3.2.5 Peptide antibody design and use

Custom peptide antibodies for cytochrome *b* were prepared by Alpha Diagnostic International (ADI, San Antonio, TX) using one region identified by RT-PCR and a second region not included in the identified fragment as predicted from the deduced mouse protein sequence (Accession number-CAA24092). The antibody directed to the identified fragment (FRAG) region was predicted to fall within loop cd localized in the intermembrane space. The 20-mer peptide generated for the FRAG antibody started at peptide 251 with the N-terminal addition of Cys as a binding site for keyhole limpit hemocyanin (KLH) conjugation.

FRAG: 251-GDPDNYMPANPLNTPPHIK-269.

The second antibody (LOOP) was generated with 19 residues predicted to fall within loop ab localized in the intermembrane space starting with peptide 58 plus the N-terminal addition of a Lys residue for KLH conjugation.

LOOP: 58-DTMTAFSSVTHICRDVNYG-76.

Rabbits were injected with KLH-conjugated peptides and bled after 49 and 63 days. ELISA assays of the 49 day antisera against free peptide coated plates were performed by ADI. Antiserum was used for Western blotting in a concentration of 1:1000 or 1:500 is PBS with 0.1% Trition X-100 and 5% nonfat dry milk, pH 7.4.

To clarify the peptide antibody signal, antiserum was back adsorbed against control cell lysate. Briefly, approximately 5 mg of control TAMH cell lysate was diluted

in coupling buffer (0.1 M sodium bicarbonate, 0.5 M sodium chloride, pH 8.3) to a volume of approximately 2 mL. One-half g of cyanogen bromide (CNBr)-activated sepharose 4B was activated in 5 mL 1 mM HCl and washed on sintered glass filter for 15 min with approximately 200 mL 1 mM HCl. Activated CNBr-sepharose was combined with cell lysate in coupling buffer and mixed occasionally overnight at room temperature. After coupling, the gel was washed with 5 volumes of coupling buffer and blocked with 0.1 M Tris pH 8.0 with occasional mixing for 2 h at room temperature. The gel was finally washed with 5 cycles of 0.1 M acetate buffer pH 4.0, 0.5 M NaCl then 0.1 M Tris pH 8.0, 0.5 M NaCl. Samples of control TAMH cell lysate were obtained before and after coupling.

NaCl was added to antiserum to a final concentration of 65 mM and then passed through a 0.45 μ syringe filter. Filtered antiserum was added to column material prepared with TAMH control lysate and allowed to equilibrate for 3 h at 4°C. Coupling buffer eluted unbound antiserum in approximately eighteen 400 μL fractions. Protein content was estimated by UV absorbance at 280 nm. Fractions with UV absorbance greater than 1.25 au were combined, concentrated by lyophilization then reconstituted in 1 mL water. This "purified" antiserum was used as described above for Western blots.

3.2.6 Identification of epitope unmasking

Western blots of total cell lysates from APAP-treated TAMH cells were prescreened for epitope and these lysates were combined for further separation on diethylaminoethyl (DEAE)-speharose. A DEAE-sepharose column (2 cm X 10 cm) was poured with Running/Equilibration Buffer (20 mM Tris pH 7.4, 0.1 mM EDTA, 2 mM DTT, 0.1% CHAPS) and equilibrated at 4°C and ~0.8 mL/min for two hours. Combined

cell lysate was adjusted to 0.1% CHAPS then loaded onto the column. Five mL fractions were collected during the Running Buffer wash at ~0.8 mL/min for 2 h (fractions 1-20). After the 2 h wash, a 200 mL linear salt gradient (Running Buffer from 0 M to 0.7 M sodium chloride) was performed and ~5 mL fractions were collected (fractions 21-60). Twenty-five mL of 0.7 M sodium chloride Running Buffer was collected (fractions 61-65) then 50 mL of 1 M sodium chloride in Running Buffer was the final wash (fractions 65-74). Fractions were screened for protein content by UV absorbance at 280 nm and the Bradford assay as above.

Epitope localization in the DEAE fractions was determined by Western blot as previously described. Similar fractions were combined and concentrated using 10,000 MW cutoff Amicon® Ultra-4 centrifugal filter devices to a final volume of ~ 0.5 mL. Purified fractions were separated on duplicate 15% polyacrylamide gels. One gel was silver stained while the other was transferred to nitrocellulose for Western blot analysis as previously described. The silver staining protocol was adapted from published procedures by Shevchenko *et al.* (Shevchenko *et al.* 1996).

Silver stained bands corresponding to immunoreactive bands were excised from the gel and processed for tryptic in-gel digestion following a previously published protocol (Shevchenko *et al.* 1996). Briefly, excised bands were destained with three, 10 min washes of 6 mM potassium ferricyanide ($K_3Fe(CN)_6$) in water, then washed with 100 mM ammonium bicarbonate for 10 min. Next, gel pieces were dehydrated in 100% acetonitrile and rehydrated in 100 mM ammonium bicarbonate. At this point, slices were stored at –20°C prior to tryptic digestion.

To start tryptic digestion, hydrated gel pieces were dehydrated with 100% acetonitrile and dried for 30 min in a speed-vac. Gel pieces were transferred to 0.2 mL microcentrifuge tubes and incubated with 100 µL 10 mM DTT in 100 mM ammonium bicarbonate for 1 h at 60°C. The DTT solution was removed and replaced with 100 µL of freshly prepared 55 mM iodoacetamide in 100 mM ammonium bicarbonate for 45 min at room temperature. After 45 min, iodoacetamide solution was removed and the gel piece was washed twice for 10 min with 100 mM ammonium bicarbonate then dried for 30 min in a speed-vac. Cold trypsin solution (25 ng/µL in 50 mM ammonium bicarbonate) was prepared and stored on ice. Fifty µL of trypsin solution were added to each gel slice and incubated for 45 min on ice. After 45 min, the remaining trypsin solution around the gel piece was removed and replaced with 50 µL 20 mM ammonium bicarbonate at 37°C for overnight digestion.

The next morning, microcentrifuge tubes were centrifuged to collect and transfer the supernatant to a fresh microcentrifuge tube. Gel pieces were washed twice for 15 min with 50 µL acetonitrile containing 0.1% TFA to extract remaining peptides. The combined wash buffer and digestion liquid were dried by speed-vac. Dried digests were reconstituted in acetonitrile with 0.1% formic acid for mass spectrometry analysis.

Mass spectrometry analysis was performed in the University of Washington Mass Spectrometry Center on a MicroMass (Manchester, UK) atmospheric pressure ionization Quadrupole/Orthagonal accelerator Time-of-Flight Tandem Hybrid Mass Spectrometer (Q-Tof MS/MS) equipped with a Modular MicroMass capillary HPLC (CapLC) System. The resultant data were analyzed using the Mascot program as previously described (Perkins *et al.* 1999) and available at http://www.matrixsciences.com. Results were

searched against both the NCBI non-redundant database and the Swiss-Prot database in separate searches allowing up to two missed cleavage sites and reporting the top 20 protein hits.

3.2.7 Examination of Complex III activities and viability *in vitro*

In an effort to investigate a possible functional role for cytochrome *b* in a mitochondrial communication pathway, complex III activity was determined on treated cell lysates by a previously described method (Gudz *et al.* 1997). TAMH cells were treated with 5 mM APAP, 0.25 mM TFEC, or 10 μM $NaAsO_2$ dissolved in TAMH media for 48 h, 9 h, or 24 h, respectively in order to encompass the mid-range of cytotoxicity. Treated and control TAMH cells were harvested in lysis buffer and protein concentration was estimated as described above. Complex III activities were measured as the antimycin A-sensitive rate of cytochrome *c* reduction per mg protein per min after the addition of decylubiquinol. Decylubiquinol was synthesized by the sodium borohydride ($NaBH_4$) reduction of decylubiquinone and extraction with diethyl ether/iso-octane (2:1 v/v). The organic phase was washed with 2 M NaCl and evaporated to dryness under a N_2 stream. Decylubiquinol was resuspended in 1 mL ethanol with the addition of 10 μL 0.1 N HCl.

In parallel to complex III assays, TAMH cell viability was determined by a sulforhodamine B (SRB) optical density assay of cell culture protein (Skehan *et al.* 1990). Briefly, TAMH cells in 200 μL growth media were seeded on 96-well cell culture microtiter plates, including a serial dilution as standard. Cultures were grown for 24 h then treated with the appropriate treatment for the designated time. Cells were fixed to the plate by the drop-wise addition of 50 μL of 4°C trichloroacetic acid (TCA-50%

(w/v)). After 30 min of fixation, plates were washed five times with tap water to remove all residual acid and were dried either with a heat gun or at room temperature. Fixed protein was stained with 100 μL of 0.4% (w/v) SRB in 1% acetic acid for 30 min at room temperature. SRB stain was removed by 4 washes with 4°C 1% acetic acid and dried completely. Bound SRB dye was solubilized for optical density measurement by the addition of 100 μL 10 mM Tris-base with shaking for 5 min. Optical density was recorded at 520 nm on a Molecular Devices Thermo Max microtiter plate reader and reported as percent viability as compared to control treatment on each plate.

Complex III activities were reported as mean rate of cytochrome *c* reduction (μmol cyt *c* reduced/mg protein/min of reaction time) ± standard error as well as percentage of the control rate. Viability results were presented as percent viability (mean ± standard error). Statistical analysis for either complex III activity or SRB viability was by two tailed, Student's t-test. A p value less than or equal to 0.1 was considered significant.

3.3 Results

3.3.1 Western Blots using Cytochrome *b* antibody

Peptide antibodies designed for cytochrome *b*, both FRAG and LOOP, demonstrated a high antibody titer by ELISA as measured against free peptide coated plates (1:100K dilution). Although the peptide specific titers appeared to be high, the recognition of cytochrome *b* in cell lysates was not as clear as anticipated (Fig. 3.2). The bovine cytochrome *b* as part of the bc_1 complex used as a positive control also appeared in slightly different locations between the FRAG and LOOP antibodies. The FRAG antibody also detected multiple bands within the control lane and although there are a

total of eleven subunits, theoretically we did not expect any cross reactivity with any subunits other than cytochrome *b*.

TAMH cell lysates screened with either FRAG or LOOP antibodies demonstrated multiple bands of immunoreactivity and high background both in the control and treatment groups (Fig. 3.2). Although many immunoreactive bands were observed both in the control and treatment groups, there were a few bands of interest recognized by the LOOP antibody. Treatment with either APAP or AMAP caused a strong increase in immunoreactivity around 48 and 69 kDa consistent with epitope unmasking. The FRAG antibody also detected drug-related increases in immunoreactivity that were less intense (see around 45 kDa). Antibodies were also screened against APAP dosed mouse liver homogenate (wild type as described in Chapter 4) with no observable changes between control (0 h) and treatments (6 and 24 h) (Fig. 3.3).

To check for experimental reproducibility, several different passage numbers of TAMH were exposed to 5 mM APAP for 48 h and screened for epitope appearance with the LOOP antibody. This blot is seen in the upper panel of Figure 3.4. Although there are slight differences between treatment groups, there is a clear trend in the bands around 54 kDa and 42 kDa as calculated based on migration. The immunoreactivity observed at 69 kDa in the initial blot was not reproducible. Because of the high background and possible lack of specificity, the LOOP antibody was back-adsorbed against a column loaded with untreated TAMH cell lysate. This purified antibody slightly reduced the presence of non-specific bands while maintaining the characteristic epitope unmasking seen in the previous gels (lower panel of Fig. 3.4). The identity and significance, if any,

of these epitope unmasking proteins was not clear, so mass spectrometry was utilized to help identify the proteins as described in the following section.

3.3.2 Epitope Unmasking identification

A DEAE column was used to separate 5 mM APAP-treated TAMH lysate proteins that were detected by UV absorbance at 280 nm as shown in Figure 3.5. The odd numbered fractions were screened by Western blot to determine the fractions containing the epitope change. Of the 28 fractions screened, only fractions 25, 27, 29, 31, and 33 demonstrated any immunoreactivity (data not shown). The odd numbered fractions with immunoreactivity were combined with the next even numbered fraction and concentrated. After concentration, protein content of the fraction was determined and the fractions were screened again for immunoreactivity by Western blot (Fig. 3.6). Fractions 31-33 were not included in this screen because total protein content was insufficient to run two gel lanes of 50 μg each. The most intense immunoreactivity was observed in the combined fractions 29 and 30 with apparent molecular weights calculated to be 47 and 54 kDa. The silver stained gel also had heavy bands in the molecular weight region associated with the immunoreactivity (* notations in Fig. 3.6). A repeat gel was prepared because an electrophoresis irregularity in the first gel prevented the precise band excision required for tryptic digest and MS analysis. In the repeat gel, only fractions 29 and 30 were separated in various concentrations to allow for multiple analyses if needed (Fig. 3.7). Protein bands corresponding to the immunoreactivity at approximately 47 and 54 kDa (* notations in Fig. 3.7) were excised from the gel and subjected to trypsin digest for tandem MS analysis as described in the methods.

During the HPLC separation of peptide fragments and subsequent introduction into the MS, selected peptides identified in the survey scans were analyzed to determine peptide sequence. The resultant data was searched against both the NCBI non-redundant database and the Swiss Prot database using the Mascot program as described in the methods. Multiple significant hits were identified for each band and are listed in Tables 3.1 and 3.2. The major component of the 54 kDa band was identified with 26 peptides covering 45% of the protein sequence for protein disulfide isomerase (PDI, Figures 3.8, 3.9, and 3.10). The major component of the 47 kDa band was the β-subunit of ATP synthase identified with 18 unique peptides covering 43% of the protein sequence (Figures 3.11, 3.12, and 3.13). In both cases, the database predicted protein mass was higher than the mass estimated by comparison of mobility to electrophoresis standards. The database estimated MW for PDI was 57 kDa but 54 kDa was the apparent MW, while ATP synthase β-subunit was estimated by the database at 56 kDa, its apparent MW was 45 kDa.

3.3.3 Complex III activities *in vitro*

In order to determine a possible role for cytochrome *b* in the mitochondrial to nuclear communication pathway, the functional status of complex III (bc_1 complex containing cytochrome *b*) and viability were examined in TAMH cells dosed with APAP, TFEC, or $NaAsO_2$. Cytochrome *b* is critical to the electron flow through Complex III required to reduce cytochrome *c*; therefore, complex III activity was measured by monitoring the antimycin A-sensitive rate of cytochrome *c* reduction. Antimycin A specifically inhibits electron flow through complex III by binding to cytochrome *b* near the heme closest to the mitochondrial matrix (Iwata *et al.* 1998). In 5 mM APAP dosed

TAMH cells, the antimycin A-sensitive complex III rate increased significantly after 24 and 48 h of treatment. Concurrently, viability determined by SRB assay decreased significantly within 6 h of treatment (Fig. 3.14). A dose-related trend between 0 and 2.5 mM APAP was observed although the difference was not statistically significant (Fig 3.15). Complex III activities in TAMH cells dosed with 0.25 mM TFEC were statistically lower after 4 and 12 h. The initial drop (4 h) in complex III activity preceded the statistically significant drop in viability observed at 8 h by SRB assay (Fig. 3.16). The observed changes to complex III activity induced by APAP and TFEC appeared to be distinctive, since the pro-apoptotic treatment with $NaAsO_2$ had no significant effect although the trend was similar to TFEC treatment (Fig. 3.17).

3.4 Discussion

3.4.1 Physical Characterization of Cytochrome *b* with specific antibodies

Although the peptide antibodies to LOOP and the isolated FRAG of cytochrome *b* had a high titer when measured against the free peptide, there was a lack of sensitivity to identify cytochrome *b* either from *in vitro* cell lysates or from *in vivo* homogenates (Fig. 3.2 and 3.3). This was expected since cytochrome *b* has traditionally been difficult to raise antibodies against because it is highly conserved across species. Even with this limitation, other treatment-specific bands were observed by Western blot analysis. MS/MS peptide sequencing and database searching were utilized to identify immunoreacitve bands that may offer some insight into the cellular response to APAP-induced toxicity.

The 54 kDa immunoreacitve band was identified as mouse protein disulfide isomerase (Fig. 3.8). Protein disulfide isomerase (PDI), also known as prolyl 4-

hydroxylase β-subunit and the cellular thyroid hormone binding protein, is primarily responsible for protein disulfide bond formation, reduction, and isomerization to form native structures. PDI is traditionally thought to be localized to the ER, and more recently, has been proposed to function as part of a multiprotein complex containing a large number of protein chaperones that assist in the proper assembly of immunoglobulin heavy chains (Meunier *et al.* 2002).

In addition to the logical and classical localization of PDI to the ER, other subcellular sites have been identified, and PDI may play critical roles in several cellular processes. For example, PDI has been localized to the cellular surface and may contribute to platelet adhesion (Essex and Li 1999; Lahav *et al.* 2000; Essex *et al.* 2001) and the internalization of HIV from the cell surface (Ryser *et al.* 1994). PDI has also been found in the liver cytosol of humans and monkeys and may function together with insulin-degrading enzyme in insulin disulfide cleavage and proteolysis (Wroblewski *et al.* 1992). An enzyme with PDI activity has also been localized to the mitochondria and may function as a mediator of MPTP *via* calcium binding (Rigobello *et al.* 2000). Furthermore, a complex of mitochondrial PDI (Q2) and mtHSP70 has been found to have β-lyase activity (Cooper *et al.* 2001).

PDI was previously identified as an APAP-adducted protein after microsomal incubations with ^{14}C labeled APAP (Zhou *et al.* 1996). In addition to PDI, also known as Q5, two other proteins, another thiol:protein disulfide oxidoreductase Q2 and calreticulin, were adducted by APAP. Since calreticulin is a major calcium storage protein and Q2 and Q5 are involved in calcium regulation in addition to protein folding, the authors suggested that APAP toxicity could be related to the inhibition of proper protein folding

or disruption of calcium homeostasis because of the participation of the identified proteins in these pathways. Also of interest is the observation that metabolic activation of halothane also results in that adduction of Q2, Q5, and calreticulin *in vivo* although subsequent hepatotoxicity is proposed to work *via* an immune-mediated process rather than a necrotic process like APAP (Martin *et al.* 1991; Pohl *et al.* 1991; Butler *et al.* 1992).

The role that PDI plays in APAP-toxicity is not clear, but proteomic techniques have previously observed an up-regulation of PDI after treatment. Up-regulation of PDI also has been observed after either ionizing radiation (Prasad *et al.* 1999) or hypoxia (Tanaka *et al.* 2000). It is proposed that this accumulation of PDI is a cellular stress response much like the observed up-regulation of ER lumenal stress proteins (HSP90, grp94, and grp78) through the UPR (Little *et al.* 1994; Kaufman 1999).

In addition to PDI, the 54 kDa immunoreactive band also included two subunits of the T-Complex protein-1 (TCP-1 δ and TCP-1 η) and vimentin as minor components. TCP-1, also called chaperonin containing TCP-1 or TCP-1 ring complex, is a large multisubunit cytosolic complex that acts to facilitate protein folding much like mitochondrial HSP60 (Dunn *et al.* 2001). Vimentin is a type III intermediate filament protein expressed in mesenchymal cells. Although vimentin is a cytoskeletal protein, its exact function is unclear because of a subtle phenotype observed in knockout mice and the various proteins with which it has been isolated (Evans 1998). At this point, it is not clear what, if any, role these proteins play in APAP-induced toxicity as they have never been previously investigated in relation to APAP treatment. Additionally, mass spectral ion scores for each of theses components were much lower than the score for PDI (from

66 to 290 versus 1312 for PDI). Ion scores are based upon the fit of the MS/MS data with the predicted fragmentation pattern for the identified peptide. An ion score greater than 45 indicates identity or extensive homology ($p<0.05$).

The primary protein observed in the 47 kDa immunoreactive band was identified as the β-subunit of F_1F_0-type ATP synthase, also called ATPase. The F_1F_0-type ATP synthase is also called electron transport chain Complex V and utilizes the proton gradient generated by ETC across the inner mitochondrial membrane to produce ATP. It can also work in reverse to cleave ATP and produce a proton gradient. The F_1 unit is localized within the mitochondrial matrix and consists of 9 polypeptides from five unique subunits (α_3, β_3, γ, δ, and ε) while the F_0 unit is imbedded within the MIM and consists of three subunits (a_1, b_2, and $c_{10\text{-}14}$). It is currently accepted that the F_1 and F_0 portions of the ATP synthase work together in a rotary motor type mechanism to produce ATP. The substrate-binding site of ATP synthase is on the β-subunit of the F_1 unit within the intermembrane space (Capaldi and Aggeler 2002) and is the subunit identified by MS analyses in these studies as the immunoreactive band at 47 kDa.

This is not the first time alteration in the ATP synthase complex have been observed or suggested after APAP treatment. Katyare and Satav (1989) demonstrated altered ATPase activity in rat liver mitochondria though not a complete inhibition. The change in activity was supported by 2D-GE studies after ^{14}C-APAP dosing. In these experiments the α-subunit of ATP synthase was identified as an APAP-adducted protein and therefore would be predicted to have an altered activity (Qiu *et al.* 1998). A more recent 2D-GE study also demonstrated a significant decrease in the protein content of the ATP synthase α-subunit but no dramatic changes in the β-subunit (Ruepp *et al.* 2002).

The identification of the ATP synthase is also of interest because of its localization within the mitochondria and its close association with the ETC.

Other minor components identified within the 47 kDa band included glutathione synthetase, elongation factor 1-α (EF1-α), HLA-B associated transcript-1, and vimentin. The significance of these hits is also questionable since ion scores for these proteins are in the range of 116 to 169 while the ion score for ATP synthase β-subunit is 1113. EF1-α is one of the most abundant proteins in eukaryotic cells, second only to actin (Slobin 1980; Dharmawardhane *et al.* 1991; Derventzi *et al.* 1993), and is known to function in mRNA translation. The HLA-B associated transcript-1 is a probable ATP-dependent RNA helicase of the DEAD family of helicases (Peelman *et al.* 1995) that may have a regulatory function in inflammatory processes (Allcock *et al.* 2001). The identification of vimentin in both immunoreactive bands is curious and may indicate an artifact of the homogenization process or a non-specific association with the other proteins.

To define the exact role, if any, these proteins play in APAP-induced cell death requires more direct study of the individual targets. It is not inconceivable that PDI and ATP synthase could be contributing to or responding to APAP-induced cell death but their contribution requires more investigation.

3.4.2 Functional Characterization measuring enzymatic activities

Based on our hypothesis, changes in cytochrome *b* either by differences in expression or peptidase cleavage would perturb the delicate structural interactions required for efficient electron transfer through the bc_1 complex ultimately affecting respiration (O_2 consumption). A functional ETC reduces O_2 and generates the membrane potential ($\Delta\Psi$) that is utilized for ATP production. To elucidate changes in the different

complexes of the ETC rather than determine respiratory competency overall, different substrates are given to introduce reducing equivalents into the ETC at different locations. Some of the more commonly used include succinate as an electron donor to complex II and glutamate, pyruvate & malate, or β-hydroxybutyrate as generators of NADH through the TCA cycle that ultimately donates electrons to complex I. Also, electrons can be introduced to complex IV by the addition of ascorbate and *N,N,N,N*-tetramethyl-*p*-phenylenediamine (TMPD) thereby directly covering each of the ETC complexes except complex III. In these studies we desired a direct complex III activity so an assay independent on the other ETC processes was chosen. Using a method published by Gudz *et al.* (1997), we measured the antimycin A-sensitive rate of cytochrome *c* reduction after the addition of decylubiquinol (the electron donor).

TAMH cells dosed with TFEC demonstrated a decrease in complex III activity (Fig. 3.16) that agrees with previous reports of TFEC-induced inhibition of O_2 consumption (Hayden and Stevens 1990; Groves *et al.* 1993). The historically proposed site of inhibition of many cysteine conjugates differs from the complex III inhibition we observed with TFEC treatment. Specifically, *S*-(1,2-dichlorovinyl)-L-cysteine (DCVC), *S*-(2-benyothiazolyl)-L-cysteine (BTC) and several other cysteine or glutathione conjugates inhibit state 3 respiration universally (Hayden and Stevens 1990) and often this inhibition is greatest in studies monitoring O_2 consumption after the addition of succinate as the electron donor (Lash *et al.* 1986; Lash and Anders 1986, 1987). The addition of ADP to coupled mitochondria causes an increase in the respiratory rate that is called state 3 respiration. Changes were not observed in state 4, resting, ADP-limited,

respiration or with the addition of glutamate & malate (complex I) or ascorbate & TMPD (complex IV).

Previously, the possibility of complex III inhibition has been suggested but not directly observed as we have here. Lash and Anders (1987) observed state 3 respiration inhibition with the addition of succinate measured by O_2 consumption but pointed out that complex III could be responsible as explained below in a quote from their paper.

> Because the rate of electron transfer from glutamate & malate is much slower than that from succinate, inhibition of flux through complex III with the former respiratory substrates as electron donors may not be detected by measurement of oxygen consumption (Lash and Anders 1987).

Our results indicate this may be the case since we were able to measure complex III activity directly and show a decreased rate. The complex III activity is not totally ablated but inhibited, therefore agreeing with the observation of inhibited O_2 consumption. These observations support the role of mitochondria in cell death and may help to further elucidate the process of cell death.

The same complex III measurement technique was applied to APAP-treated TAMH cells to evaluate a possible role for cytochrome *b* in that form of cell death. In contrast to the decrease observed with TFEC treatment, APAP treatment caused a statistically significant increase in complex III activity after 24 and 48 h. The increased complex III activities we observed after APAP treatment appear contrary to the published results of groups who investigated respiration by measuring O_2 consumption. Many of these groups have reported an overall inhibition of respiration by APAP and its metabolites (Meyers *et al.* 1988; Esterline *et al.* 1989; Katyare and Satav 1989; Ramsay *et al.* 1989; Burcham and Harman 1990, 1991). These reports may not be in direct

disagreement with our observations, since it appears that the effects were localized to either complex I or complex II and the direct effects on complex III were never measured (Meyers *et al.* 1988; Katyare and Satav 1989; Ramsay *et al.* 1989).

Investigations into the effects of APAP on respiration have demonstrated that APAP itself reversibly inhibits respiration in isolated mouse hepatocytes, most notably at complex I (Esterline *et al.* 1989). Although this reversible effect by APAP has been characterized, metabolism of APAP to NAPQI or direct exposure of mitochondria to NAPQI is required for irreversible inhibition of glutamate & malate induced state 3 respiration (Meyers *et al.* 1988; Esterline *et al.* 1989; Ramsay *et al.* 1989). In systems exposed to metabolites, either through metabolism or metabolite addition, respiratory inhibition was observed with both generators of NADH and succinate (Katyare and Satav 1989; Ramsay *et al.* 1989; Burcham and Harman 1990, 1991). Two different groups proposed the possibility of complex III inhibition. First Ramsay *et al.* (Ramsay *et al.* 1989) proposed the binding of quinone metabolites of both APAP and AMAP to complex III after direct exposure of isolated mouse liver mitochondria to the quinones thereby inhibiting electron transfer. The inability of the quinone metabolites of AMAP to cause toxicity *in vivo* may be the result of an apparent inability of AMAP metabolites to access the mitochondria (Tirmenstein and Nelson 1989; Qiu *et al.* 2001). Another proposed mechanism of complex III involvement is the unexplained decrease in cytochrome *b* measured spectrophotometrically after toxic APAP doses in rats (Katyare and Satav 1989). Our observations appear to be in direct contrast to these two previous reports, since we observed an increase in complex III activity.

The possibility of model differences was considered to explain the apparent discrepancy. The TAMH cell model has been well characterized with APAP treatment (Pierce *et al.* 2002). TAMH cells are both able to metabolize APAP and die in a process that is similar to APAP toxicity *in vivo* (Pierce *et al.* 2002). There is a possibility that the protein content of cell lysate used to determine complex III activity is underestimated and may account for the differences in activities. This explanation seems unlikely since a normalization of complex III activities to cell number yielded similar increases in activity (data not shown).

One other concern about this data is the fact that cell viability decreases before increased complex III activity is observed (Fig. 3.14). This may be an indication that what we are observing is a secondary response to the APAP-induced toxicity rather than an initiating event as we have observed with TFEC-induced toxicity. APAP is known to cause ATP depletion (Tirmenstein and Nelson 1990) and the association of ATP depletion with necrosis in lieu of apoptosis (Leist *et al.* 1997; Leist *et al.* 1999) suggests we may be observing the effects of necrosis at 24 and 48 h. Therefore, the relevance of increased complex III activity after APAP dosing is at present unknown.

Recently, Armstrong and Jones (2002) have suggested a role for complex III in apoptosis by modulating the MPTP. HL60 cells overexpressing BCL-2 and depleted of glutathione by L-buthionine S,R-sulfoximine (BSO) or diethyl maleate (DEM) exhibit an antimycin A-sensitive opening of the MPTP and apoptosis. The ability of antimycin A to inhibit MPTP opening suggests a role for complex III, since antimycin A is specific for complex III. The most likely contribution from complex III is the production of reactive oxygen species. Although this is not direct evidence that APAP works though such a

process, it is a conceivable and testable hypothesis, since APAP is known to deplete glutathione and generate a general state of oxidative stress (Tirmenstein and Nelson 1989; Adamson and Harman 1993). In this scenario, the possibility of increased complex III activity seems plausible although not actually demonstrated in the results published so far (Armstrong and Jones 2002).

Further support for the direct role of cytochrome *b* in apoptosis comes from a clinical investigation of hemangioma regression (Hasan *et al.* 2001). In this study, the expression levels of cytochrome *b* in hemangiomas in different stages were evaluated. Interestingly, cytochrome *b* transcripts were the highest in tumors during either spontaneous or steroid induced regression. The investigators suggested a primary role for cytochrome *b* in the apoptotic initiation of regression but offer no direct proof (Hasan *et al.* 2001).

Several different investigations listed above, including ours, have suggested a potential role for cytochrome *b* or complex III in the process of cell death although the exact role, just like most cell death processes, is still unknown. Like the growth of interest in the mitochondria, the growth in interest related to cytochrome *b* will undoubtedly yield more enlightening information over the years to come.

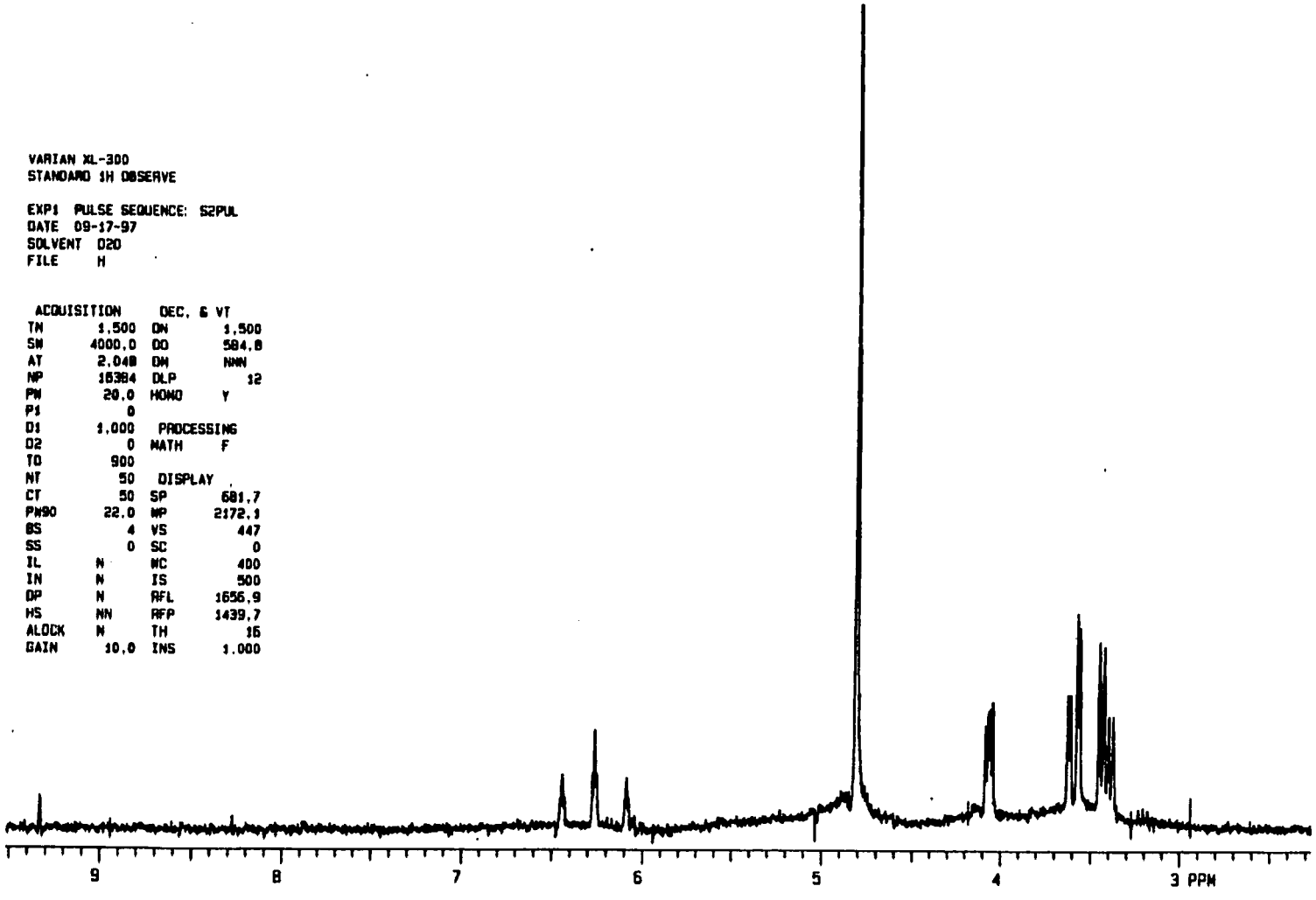

Figure 3.1. Nuclear magnetic resonance of tetrafluoroethyl cysteine in D_2O.

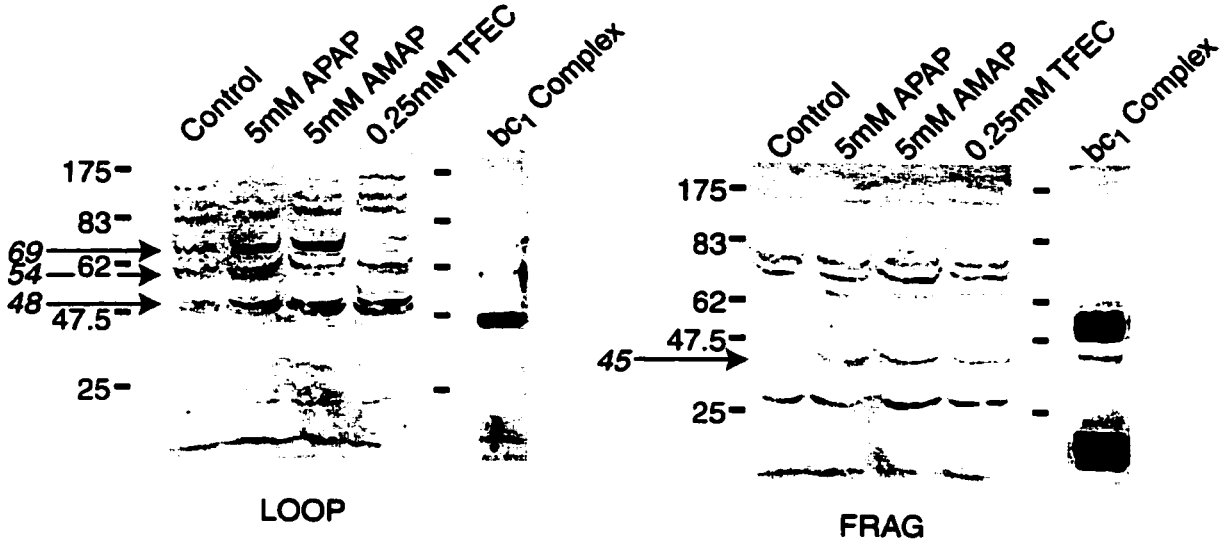

Figure 3.2. Initial Peptide Antibody Screening against TAMH cells.

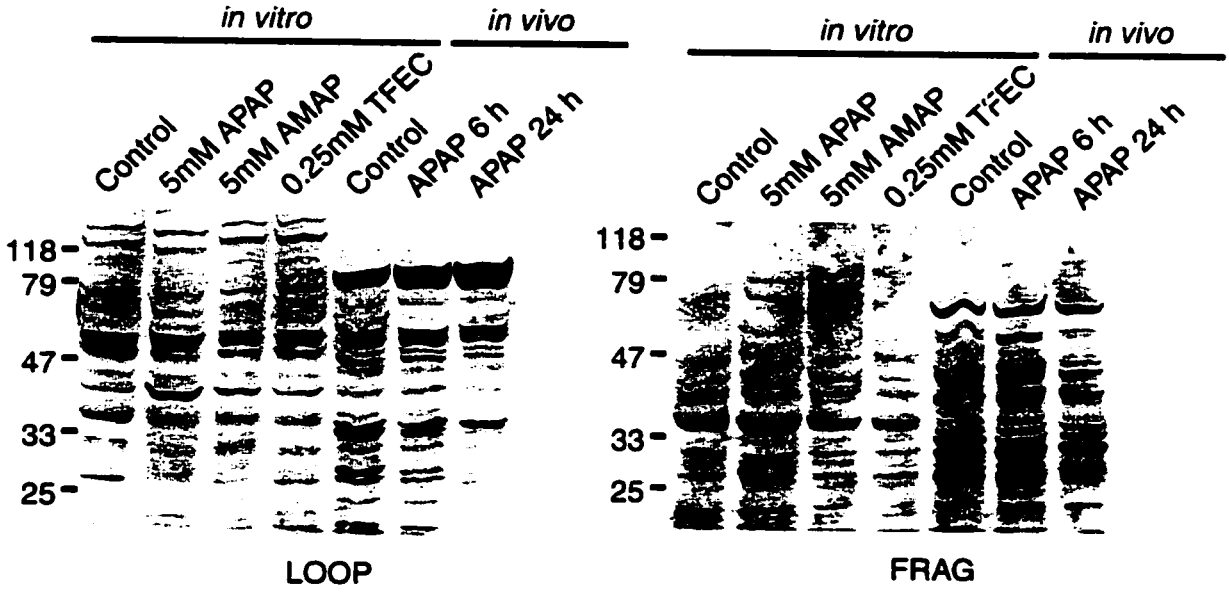

Figure 3.3. Peptide antibody screening both *in vivo* and *in vitro*.

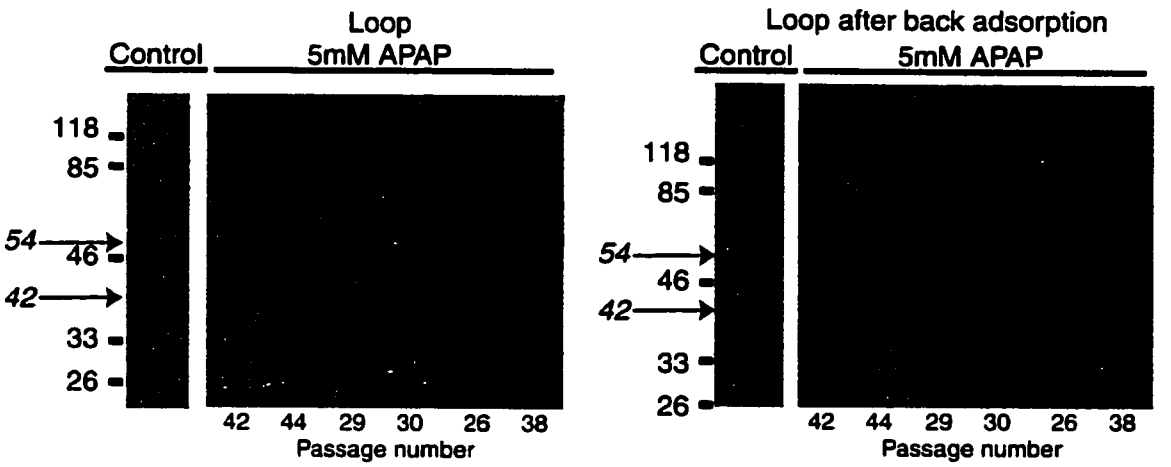

Figure 3.4. Peptide antibody screened against different passage numbers of TAMH cells.

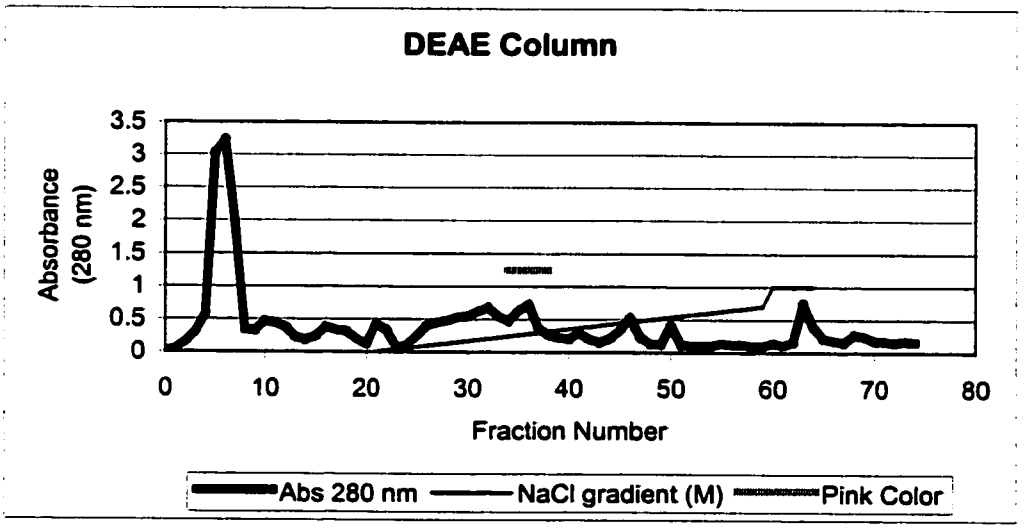

Figure 3.5. DEAE column elution profile.

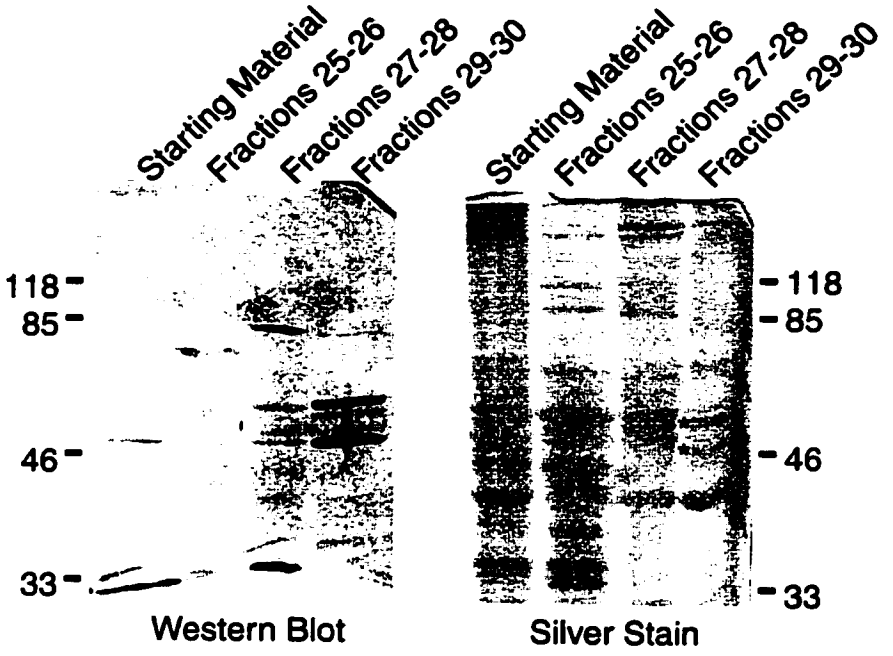

Figure 3.6. DEAE fractions screened with LOOP antibody and silver stained gel. Bands of interest in the silver stained gel are indicated with (*).

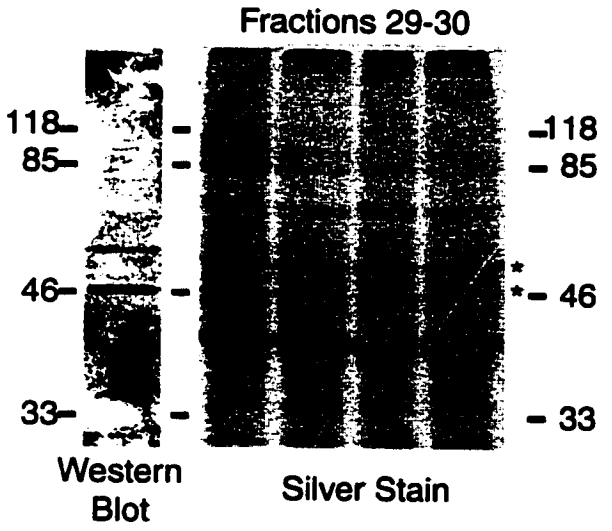

Figure 3.7. Silver Stained gel for trypsin digest. Bands of interest in the silver stained gel are indicated with (*).

Table 3.1. Proteins identified from the 54 kDa immunoreactive band.

Protein Identified	Predicted MW	% Protein Coverage	Number of Peptides	Database[a]
Protein Disulfide Isomerase	57 kDa	45	26	SP & nr
T-Complex protein-1 δ	58 kDa	10	4	SP & nr
Vimentin	54 kDa	11	5	SP & nr
T-Complex protein-1 η	59 kDa	11	2	SP & nr

a-SP is SwissProt and nr is NCBI non-redundant databases.

Table 3.2. Proteins identified from the 47 kDa immunoreactive band.

Protein Identified	Predicted MW	% Protein Coverage	Number of Peptides	Database[a]
ATP synthase β-subunit	56 kDa	43	18	SP & nr
Glutathione synthetase	52 kDa	10	4	SP & nr
Elongation Factor 1-α	50 kDa	6	3	SP & nr
HLA-B associated transcript-1	49 kDa	6	3	SP & nr
Vimentin	54 kDa	6	3	SP & nr

a-SP is SwissProt and nr is NCBI non-redundant databases.

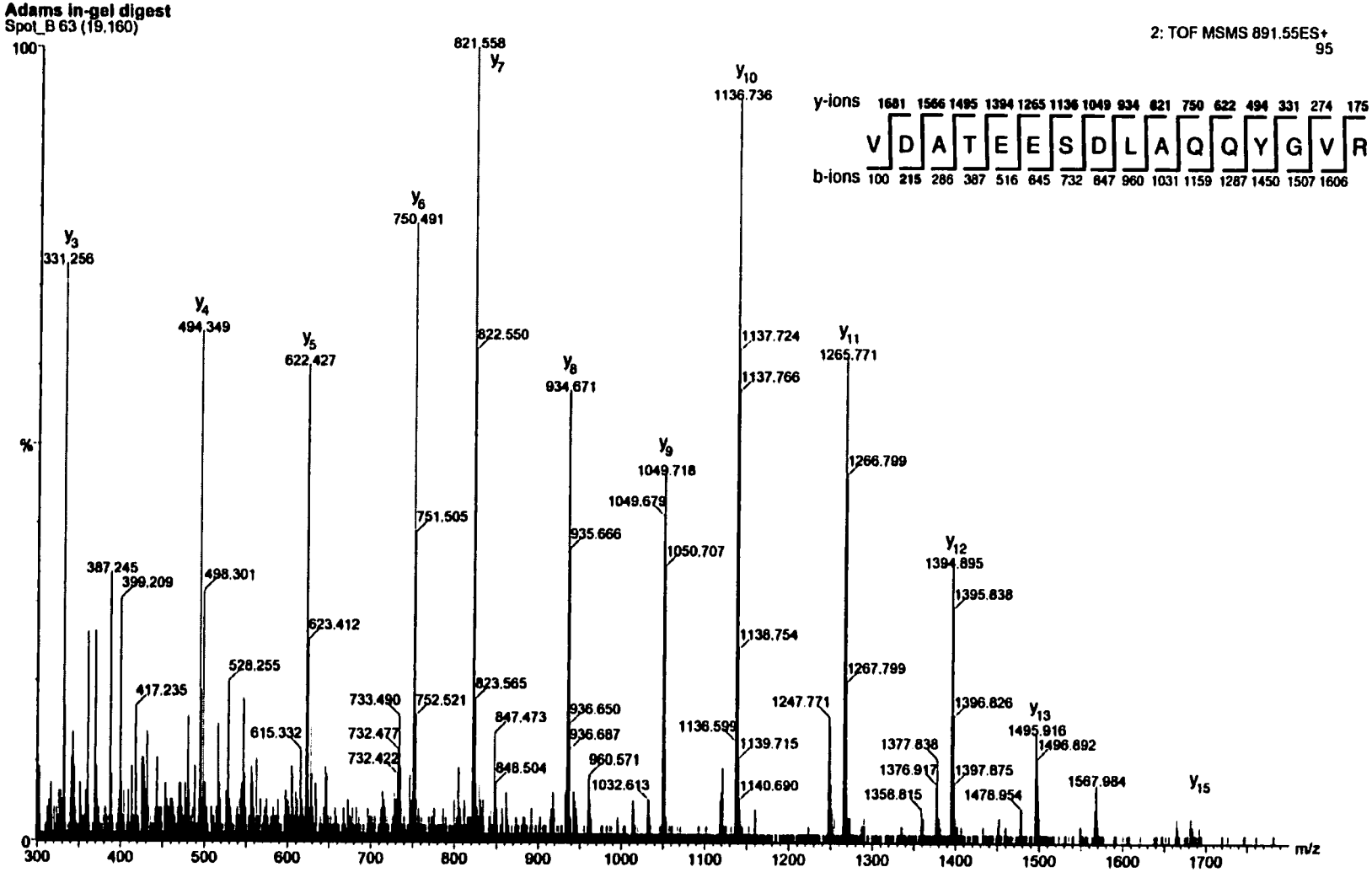

Figure 3.8. Mass Spectrum of 54 kDa band. Tandem mass (MS/MS) spectrum for collision-induced dissociation of the $(M+ 2H)^{2+}$ precursor, *m/z* 891 and the computer match sequence that was searched using Mascot to identify PDI.

```
  1 MLSRALLCLA LAWAARVGAD ALEEEDNVLV LKKSNFEEAL AAHKYLLVEF
 51 YAPWCGHCKA LAPEYAKAAA KLKAEGSEIR LAKVDATEES DLAQQYGVRG
101 YPTIKFFKNG DTASPKEYTA GREADDIVNW LKKRTGPAAT TLSDTAAAES
151 LVDSSEVTVI GFFKDVESDS AKQFLLAAEA IDDIPFGITS NSGVFSKYQL
201 DKDGVVLFKK FDEGRNNFEG EITKEKLLDF IKHNQLPLVI EFTEQTAPKI
251 FGGEIKTHIL LFLPKSVSDY DGKLSSFKRA AEGFKGKILF IFIDSDHTDN
301 QRILEFFGLK KEECPAVRLI TLEEEMTKYK PESDELTAEK ITEFCHRFLE
351 GKIKPHLMSQ EVPEDWDKQP VKVLVGANFE EVAFDEKKNV FVEFYAPWCG
401 HCKQLAPIWD KLGETYKDHE NIIIAKMDST ANEVEAVKVH SFPTLKFFPA
451 SADRTVIDYN GERTLDGFKK FLESGGQDGA GDDEDLDLEE ALEPDMEEDD
501 DQKAVKDEL
```

Figure 3.9. Protein sequence for Protein Disulfide Isomerase precursor (mouse). There are 26 unique peptides covering 45% of the protein sequence. (Accession number P09103-00-00-01).

	Start - End	Observed	Mr(expt)	Mr(calc)	Delta	Sequence
1	33 - 44	448.96	1343.86	1343.68	0.17	KSNFEEALAAHK
2	34 - 44	608.89	1215.76	1215.59	0.18	SNFEEALAAHK
2	34 - 44	608.88	1215.75	1215.59	0.16	SNFEEALAAHK
2	34 - 44	406.26	1215.75	1215.59	0.16	SNFEEALAAHK
3	72 - 80	501.84	1001.67	1001.55	0.12	LKAEGSEIR
4	84 - 99	891.04	1780.05	1779.83	0.23	VDATEESDLAQQYGVR
4	84 - 99	891.04	1780.06	1779.83	0.24	VDATEESDLAQQYGVR
5	123 - 132	601.89	1201.76	1201.60	0.16	EADDIVNWLK
5	123 - 132	601.89	1201.76	1201.60	0.17	EADDIVNWLK
5	123 - 132	601.89	1201.77	1201.60	0.17	EADDIVNWLK
5	123 - 132	601.90	1201.78	1201.60	0.18	EADDIVNWLK
5	123 - 132	601.89	1201.76	1201.60	0.16	EADDIVNWLK
5	123 - 132	601.89	1201.76	1201.60	0.16	EADDIVNWLK
6	198 - 209	712.99	1423.97	1423.77	0.20	YQLDKDGVVLFK
6	198 - 209	475.66	1423.96	1423.77	0.18	YQLDKDGVVLFK
7	203 - 209	389.29	776.56	776.44	0.12	DGVVLFK
8	216 - 224	526.33	1050.64	1050.50	0.14	NNFEGEITK
9	225 - 232	503.37	1004.73	1004.59	0.14	EKLLDFIK
10	227 - 232	374.79	747.56	747.45	0.11	LLDFIK
11	233 - 249	983.16	1964.30	1964.04	0.26	HNQLPLVIEFTEQTAPK
11	233 - 249	655.77	1964.29	1964.04	0.26	HNQLPLVIEFTEQTAPK
12	250 - 265	609.46	1825.34	1825.09	0.26	IFGGEIKTHILLFLPK
13	257 - 265	541.41	1080.81	1080.67	0.14	THILLFLPK
13	257 - 265	541.42	1080.82	1080.67	0.15	THILLFLPK
13	257 - 265	541.42	1080.82	1080.67	0.15	THILLFLPK
14	303 - 310	483.85	965.69	965.56	0.13	ILEFFGLK
14	303 - 310	483.85	965.68	965.56	0.12	ILEFFGLK
15	303 - 311	547.91	1093.81	1093.65	0.15	ILEFFGLKK
16	319 - 328	603.90	1205.79	1205.62	0.17	LITLEEEMTK
16	319 - 328	603.91	1205.80	1205.62	0.18	LITLEEEMTK
17	329 - 340	705.44	1408.86	1408.67	0.18	YKPESDELTAEK
17	329 - 340	470.63	1408.88	1408.67	0.21	YKPESDELTAEK
18	353 - 368	651.41	1951.21	1950.95	0.26	IKPHLMSQEVPEDWDK
19	373 - 387	834.04	1666.06	1665.82	0.24	VLVGANFEEVAFDEK
19	373 - 387	834.03	1666.05	1665.82	0.23	VLVGANFEEVAFDEK
20	373 - 388	599.06	1794.16	1793.92	0.24	VLVGANFEEVAFDEKK
21	404 - 411	485.84	969.67	969.53	0.14	QLAPIWDK
22	412 - 426	582.06	1743.16	1742.92	0.24	LGETYKDHENIIIAK
23	427 - 438	647.39	1292.76	1292.59	0.16	MDSTANEVEAVK
24	439 - 446	464.83	927.65	927.52	0.13	VHSFPTLK
25	447 - 454	455.78	909.55	909.43	0.12	FFPASADR
25	447 - 454	455.79	909.56	909.43	0.13	FFPASADR
25	447 - 454	455.79	909.56	909.43	0.12	FFPASADR
26	455 - 463	533.84	1065.65	1065.51	0.15	TVIDYNGER

Figure 3.10. Peptides from 54 kDa band identified as Protein Disulfide Isomerase.

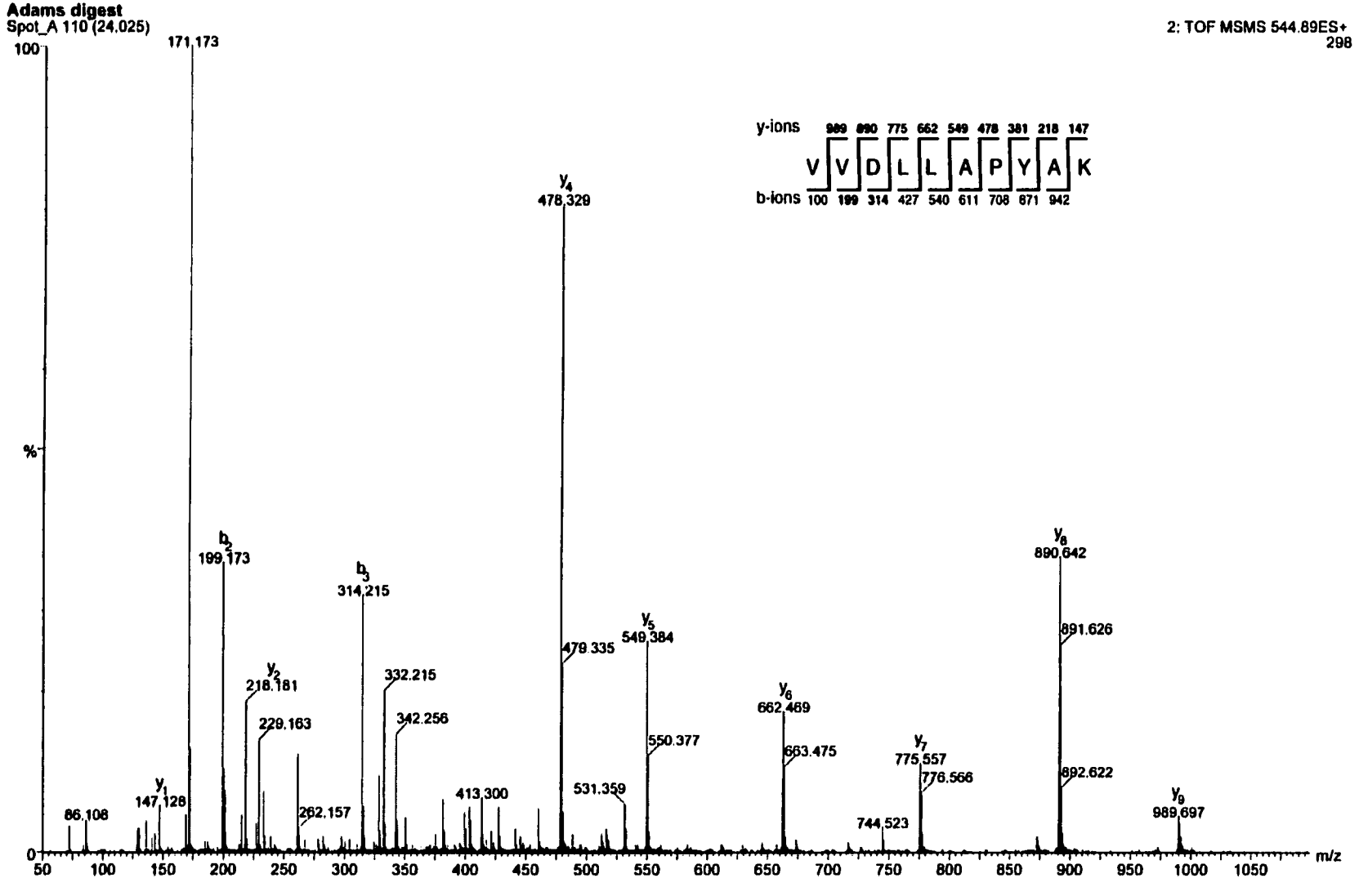

Figure 3.11. Mass spectrum of 46 kDa band. Tandem mass (MS/MS) spectrum for collision-induced dissociation of the $(M+ 2H)^{2+}$ precursor, *m/z* 544 and the computer match sequence that was searched using Mascot to identify ATP synthase β-subunit.

```
  1 MLSLVGRVAS ASASGALRGL SPSAALPQAQ LLLRAAPAGV HPARDYAAQA
 51 SAAPKAGTAT GRIVAVIGAV VDVQFDEGLP PILNALEVQG RDSRLVLEVA
101 QHLGESTVRT IAMDGTEGLV RGQKVLDSGA PIKIPVGPET LGRIMNVIGE
151 PIDERGPIKT KQFAPIHAEA PEFIEMSVEQ EILVTGIKVV DLLAPYAKGG
201 KIGLFGGAGV GKTVLIMELI NNVAKAHGGY SVFAGVGERT REGNDLYHEM
251 IESGVINLKD ATSKVALVYG QMNEPPGARA RVALTGLTVA EYFRDQEGQD
301 VLLFIDNIFR FTQAGSEVSA LLGRIPSAVG YQPTLATDMG TMQERITTTK
351 KGSITSVQAI YVPADDLTDP APATTFAHLD ATTVLSRAIA ELGIYPAVDP
401 LDSTSRIMDP NIVGNEHYDV ARGVQKILQD YKSLQDIIAI LGMDELSEED
451 KLTVSRARKI QRFLSQPFQV AEVFTGHMGK LVPLKETIKG FQQILAGEYD
501 HLPEQAFYMV GPIEEAVAKA DKLAEEHGS
```

Figure 3.12. Protein sequence for ATP synthase β-subunit, mitochondrial precursor (E.C. 3.6.3.14) (mouse). There are 18 unique peptides covering 43% of the protein sequence. (Accession number P56480).

	Start	-	End	Observed	Mr(expt)	Mr(calc)	Delta	Sequence
1	95	-	109	826.08	1650.14	1649.91	0.23	LVLEVAQHLGESTVR
1	95	-	109	826.09	1650.16	1649.91	0.25	LVLEVAQHLGESTVR
1	95	-	109	551.05	1650.12	1649.91	0.21	LVLEVAQHLGESTVR
1	95	-	109	826.08	1650.15	1649.91	0.24	LVLEVAQHLGESTVR
2	110	-	121	631.91	1261.80	1261.63	0.16	TIAMDGTEGLVR
2	110	-	121	631.91	1261.80	1261.63	0.16	TIAMDGTEGLVR
2	110	-	121	631.91	1261.81	1261.63	0.17	TIAMDGTEGLVR
3	125	-	133	450.33	898.65	898.51	0.13	VLDSGAPIK
4	125	-	143	640.45	1918.33	1918.09	0.24	VLDSGAPIKIPVGPETLGR
5	134	-	143	519.87	1037.72	1037.59	0.13	IPVGPETLGR
6	144	-	155	693.45	1384.88	1384.70	0.18	IMNVIGEPIDER
6	144	-	155	693.46	1384.90	1384.70	0.19	IMNVIGEPIDER
6	144	-	155	693.45	1384.88	1384.70	0.18	IMNVIGEPIDER
7	189	-	198	544.89	1087.77	1087.63	0.14	VVDLLAPYAK
7	189	-	198	544.90	1087.77	1087.63	0.15	VVDLLAPYAK
8	202	-	212	488.34	974.67	974.55	0.12	IGLFGGAGVGK
9	213	-	225	729.51	1457.01	1456.83	0.18	TVLIMELINNVAK
9	213	-	225	729.52	1457.03	1456.83	0.19	TVLIMELINNVAK
10	226	-	239	703.94	1405.86	1405.67	0.18	AHGGYSVFAGVGER
11	265	-	279	801.52	1601.01	1600.80	0.21	VALVYGQMNEPPGAR
11	265	-	279	801.52	1601.02	1600.80	0.22	VALVYGQMNEPPGAR
12	282	-	294	720.49	1438.96	1438.78	0.18	VALTGLTVAEYFR
13	311	-	324	718.47	1434.92	1434.75	0.17	FTQAGSEVSALLGR
14	325	-	345	1133.69	2265.36	2265.08	0.28	IPSAVGYQPTLATDMGTMQER
15	388	-	406	994.66	1987.30	1987.03	0.27	AIAELGIYPAVDPLDSTSR
15	388	-	406	994.66	1987.30	1987.03	0.27	AIAELGIYPAVDPLDSTSR
16	407	-	422	615.05	1842.11	1841.87	0.24	IMDPNIVGNEHYDVAR
17	463	-	480	675.09	2022.26	2022.00	0.26	FLSQPFQVAEVFTGHMGK
18	481	-	489	520.91	1039.81	1039.66	0.14	LVPLKETIK

Figure 3.13. Peptides from 46 kDa band identified as ATP synthetase, β-subunit.

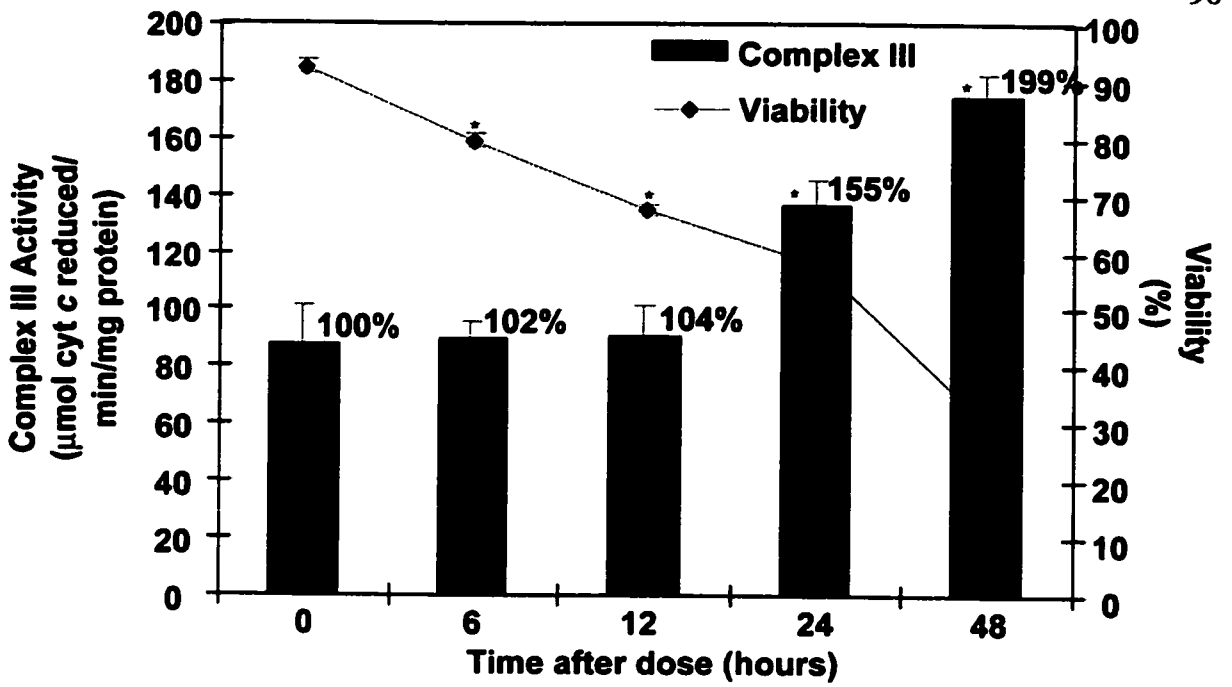

Figure 3.14. Complex III activities and Viability of TAMH cells after APAP (5 mM) dosing.

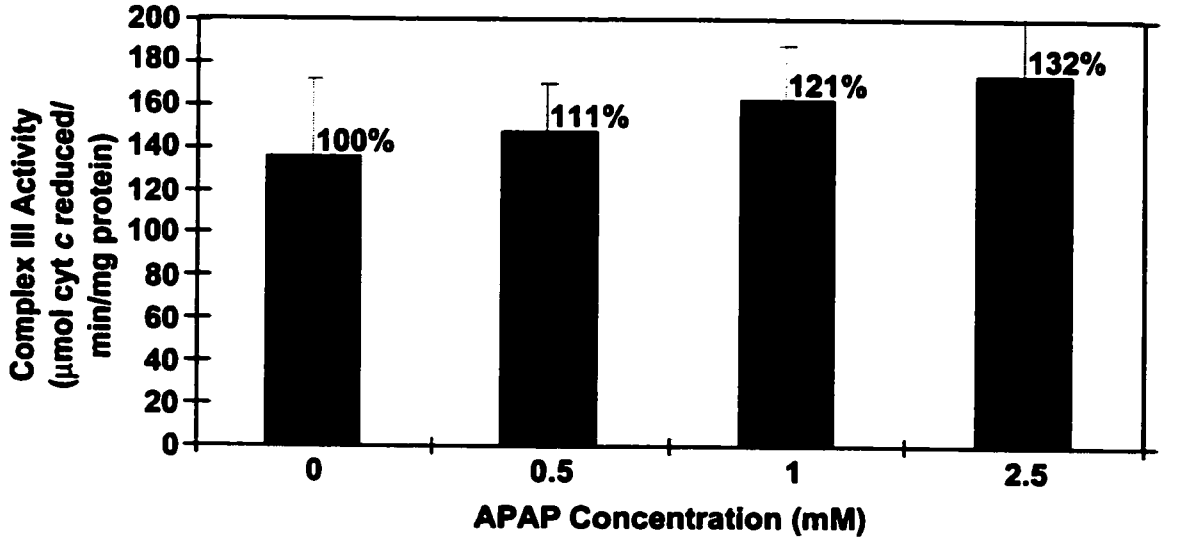

Figure 3.15. Dose response of Complex III activities after TAMH cells were dosed with APAP for 48 h.

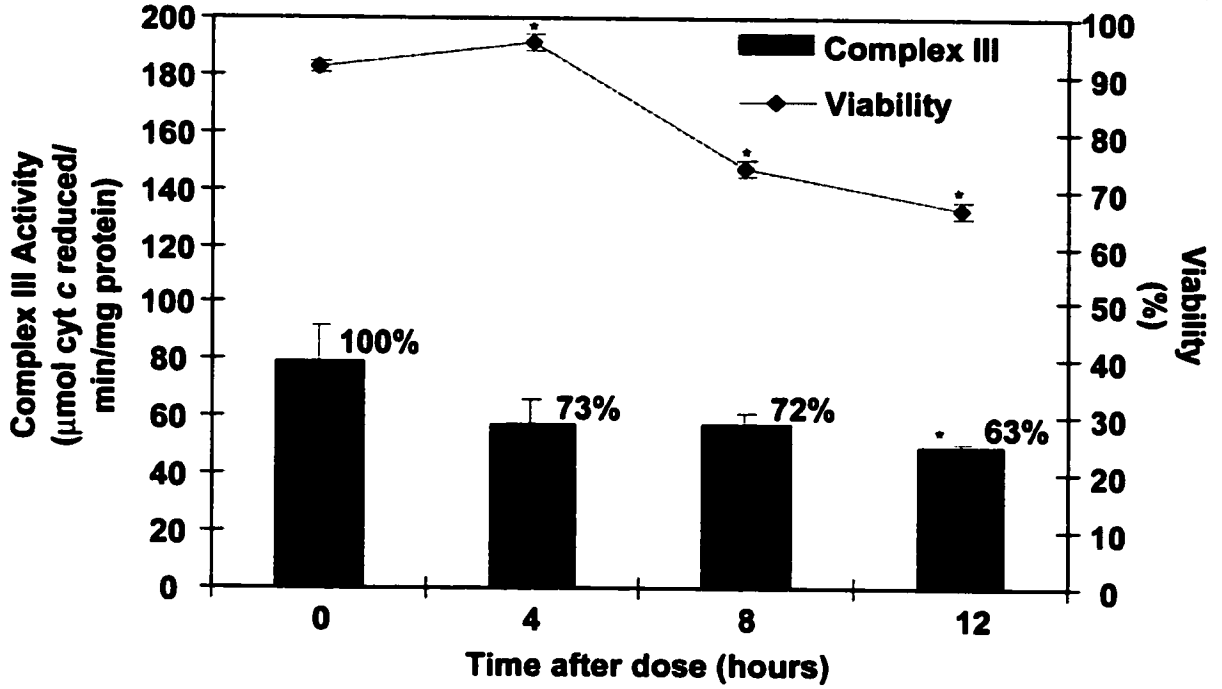

Figure 3.16. Complex III activities and Viability of TAMH cells after TFEC (0.25 mM) dosing.

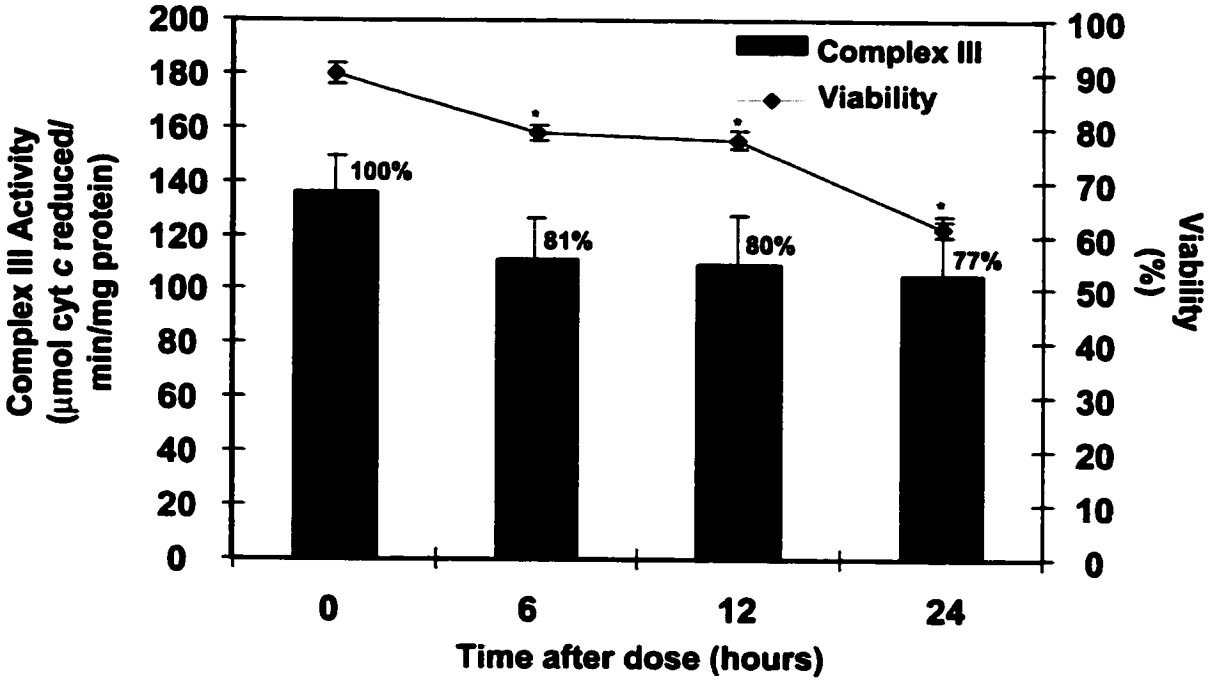

Figure 3.17. Complex III activities and Viability of TAMH cells after $NaAsO_2$ (10 µM) dosing.

Chapter 4

Enhanced Acetaminophen Hepatotoxicity in Transgenic Mice Overexpressing BCL-2[1]

4.1 Introduction

The *in vivo* functional characterization of complex III activity in relation to hepatotoxicity is a natural extension of our *in vitro* observations discussed in Chapter 3. Reports link the requirement of an active ETC for apoptosis initiation by either oxygen deprivation or growth factor withdrawal (Vander Heiden *et al.* 2001; McClintock *et al.* 2002). These effects are dependent on either BAX or BAK mitochondrial translocation induced cytochrome *c* release and can be inhibited by the overexpression of BCL-x_L (Vander Heiden *et al.* 2001; McClintock *et al.* 2002). The observation that changes in cellular metabolism, either glucose deprivation or inhibition of ETC, can initiate cell death indicates a role for ETC, and maybe more specifically complex III, in the early processes of cell death.

The contribution of the mitochondria to apoptosis and drug-induced cell death has been studied extensively. Despite extensive study with APAP, the exact contribution of this organelle in APAP-induced liver injury and cell death is still unclear, but alterations to mitochondrial respiration with APAP treatment have been demonstrated (Meyers *et al.* 1988; Esterline *et al.* 1989; Ramsay *et al.* 1989; Burcham and Harman 1991). Mechanistically, the arylation of free thiols (Dahlin *et al.* 1984; Tirmenstein and Nelson 1990; Qiu *et al.* 1998;) as well as oxidative stress (Tirmenstein and Nelson 1989;

Adamson and Harman 1993; Prescott 1996) have been proposed to play roles in the toxicity of APAP but the consequences of these changes remain uncertain (Jollow *et al.* 1973; Pumford and Halmes 1997; Boulares *et al.* 1999). More recent studies have identified proteins covalently modified by APAP, or its less hepatotoxic isomer N-acetyl-*m*-aminophenol (AMAP), and indicate that an important component of the differential toxicity of these compounds is mediated at the level of the mitochondrion (Qiu *et al.* 1998, 2001).

The hepatotoxicity of APAP has been traditionally thought of as a centrilobular necrotic event (Pumford and Halmes 1997). Other studies have attempted to define an apoptotic component to APAP-mediated cell death but these investigations have not been entirely definitive (Ray *et al.* 1996; Lawson *et al.* 1999). Consequently, we have addressed the possibility that the BCL-2 family of proteins may have a functional role in the progression of liver damage after APAP overdose. The BCL-2 protein family consists of both proapoptotic (e.g., BAX, BAK) and antiapoptotic (e.g., BCL-2, BCL-x_L) members, which play an important role in the determination of apoptosis in response to many physiological and pathological effectors (Desagher *et al.* 1999). This pro- versus anti-apoptotic balance may be controlled through dimerization of BCL-2 family members (Sato *et al.* 1994; Yin *et al.* 1994; Rosse *et al.* 1998) and/or by phosphorylation (Haldar *et al.* 1998). Although there is an extensive literature on the antiapoptotic properties of BCL-2, its mechanism of cytoprotection is still unknown. It has been proposed that the cytoprotective action of BCL-2 may lie in its ability to act as an antioxidant (Hockenbery *et al.* 1993), to block cytochrome *c* release (Cai and Jones 1998), or to inhibit caspase activity after cytochrome *c* release (Rosse *et al.* 1998). Further studies are consequently

required to address this uncertainty in BCL-2 function, particularly with recent reports indicating that BAX translocation to mitochondria is not prevented in apoptotic neurons despite overexpression of BCL-2 (Putcha *et al.* 1999). Although the BCL-2 family has multiple members, it appears that proteins with similar function may have some redundancy in their mechanism of action (Plas and Thompson 2002); therefore, it is not unreasonable to investigate the effects of hBCL-2 overexpression in mouse liver while the major liver isoform is actually BCL-x_L (Tzung *et al.* 1997).

Based on observations that APAP-induced cell death is partly apoptotic (Ray *et al.* 1996; Lawson *et al.* 1999), we examined APAP-mediated hepatotoxicity for alterations in the subcellular distribution of BAX, a BCL-2 family member implicated as a central effector of mitochondrially-mediated apoptotic cell death (Wei *et al.* 2001). We report here that BAX is redistributed with APAP treatment and, consequently, may play an early role in APAP-mediated hepatotoxicity. In addition, we hypothesized that overexpression of BCL-2 protein should offer protection to liver tissue exposed to doses of APAP which would otherwise cause centrilobular necrosis. Our results indicate a more pronounced liver injury produced by APAP in BCL-2 overexpressing animals, with morphological and biochemical evidence of increased damage shifting from centrilobular to throughout the entire lobule (panlobular). These unexpected findings provide a basis for the further elucidation of the role of mitochondria in APAP-induced liver injury and cell death.

4.2 Materials and Methods

4.2.1 Materials

Human *bcl-2* transgenic mice (C57/B6C3H background) were kindly provided by Dr. S. J. Korsmeyer (Dana-Farber Cancer Institute, Harvard Medical School).

4.2.2 Animal care and dosing protocols

Animals were housed in a temperature and humidity controlled SPF facility maintained on a 12 h light/dark cycle with free access to food and water. Animals were genotyped using tail DNA in a PCR assay. Briefly, tail snips were digested in proteinase K overnight at 55°C. Proteinase K was then heat inactivated at 95°C for 10 min. PCR was preformed using 1 μL of the crude extract as a template and primers spanning an intron in *bcl-2* to yield a 300 bp product from the human gene. BCL-2 expression is under the inducible control of a metallothionein promoter. Male mice 16 weeks old (22-28 g) were given 25 mM $ZnSO_4$ in drinking water for 5-7 days prior to dosing and BCL-2 levels were evaluated by immunoblot. Animals were fasted for 16 h prior to dosing with APAP or AMAP (500 mg/kg i.p.) or vehicle (saline). In order to exclude nonspecific metal effects, $ZnSO_4$ supplemented water was freely available to all animals during the fast and after dosing. Liver tissue and plasma samples were taken 6 h and 24 h after injection for histopathological, immunoblotting, and other biochemical determinations.

4.2.3 Isolation of subcellular fractions and immunoblotting procedures

BAX subcellular localization studies were with fractions prepared by standard differential centrifugation procedures from wild type $B6C3F_1$ (Fig. 4.1) or Swiss-Webster mice (data not presented) receiving 600 mg/kg (i.p.) APAP, AMAP or vehicle control (saline) at 2 and/or 4 h after dosing as previously described (Tonge *et al.* 1998). The

relative purity of subcellular fractions was assessed by monitoring lactate dehydrogenase (cytosol) and succinate cytochrome *c* reductase (mitochondria) marker enzyme activities. Subcellular fractions or total homogenized liver tissue (50 μg per lane) were resolved on SDS-PAGE minigels (10-15%, Mini-Protean, II, BioRad, Hercules, CA) and transferred to nitrocellulose (1 h, 15V, Trans-Blot SD Semi-Dry Transfer Cell, BioRad). Immunodetection, using antibodies to BAX (B9; Santa Cruz Biotechnology, Santa Cruz, CA), BCL-2 (N19; Santa Cruz Biotechnology), catalase (Calbiochem, San Diego, CA), cytochrome *c* (Pharmingen, San Diego, CA), mouse albumin (ICN Pharmaceuticals, Costa Mesa, CA), GAPDH (Dietze *et al.* 1997), or anti-APAP protein adducts (Tonge *et al.* 1998) was preformed by standard procedures and detected by chemiluminescence (SuperSignal® ULTRA, Pierce, Rockford, IL).

4.2.4 Transaminase activities

Alanine aminotransferase (ALT) and aspartate aminotransferase (AST) were assessed spectrophotometrically using either the *Dimension Clinical Chemistry System* (Dade Behring, Deerfield, IL) analyzer on plasma samples diluted with DADE™ diluent to within the linear range of the analyzer (typically 1:40-1:50) or standard commercial methods (Sigma Diagnostics INFINITY™, Procedure No. 122-UV or No. 152-UV) exactly as described by the manufacturer. In both cases aminotransferase activities are presented as units per liter (U/L).

4.2.5 Assessment of hepatotoxicity by histopathology

Liver tissue sections from animals dosed with APAP, AMAP, or saline were fixed in formalin and embedded in paraffin. Sections of 5 μm thickness were stained with hematoxylin and eosin using standard procedures. Sections were independently

evaluated without prior knowledge of treatment regime and digital photomicrographs were taken at 100X or 200X magnification.

4.2.6 Assessment of cellular morphology by electron microscopy

Liver sections from animals dosed with APAP, AMAP, or saline were fixed in Karnovsky's fixative (1/2 strength glutaraldehyde-formaldehyde), embedded and stained with uranyl acetate and Reynold's lead citrate. Specimens were examined using a Philips 410 Transmission Electron Microscope at 12,000 or 6,000X magnification.

4.2.7 Determination of reduced (GSH) and oxidized (GSSG) liver glutathione

Hepatic glutathione levels were determined as previously described (Luderer *et al.* 2001). Briefly, liver tissue was homogenized in 5% (w/v) sulfosalicylic acid then immediately processed independently for either GSH or GSSG. For GSSG, free GSH was derivatized with 2-vinylpyridine at room temperature and excess 2-vinylpyridine extracted into the organic phase with chloroform. GSSG was then reduced by the addition of 50 µl of 1 mM NADPH and 20 units/ml GSH reductase for 1 hour at room temperature followed by derivatization with 20 µl of 12.5 mM monobromobimane in the dark for 30 minutes prior to HPLC analysis (Shimadzu LC-6A HPLC equipped with an Alltech 15 x 0.5-cm C18 reverse-phase column using a binary gradient [solvent A = 1.0 mM tetrabutylammonium phosphate; pH 3.0 and solvent B = methanol] at a flow-rate of 1.5 ml/min with starting conditions of 95% A/5% B). Eluted peaks were monitored fluorimetrically at λex = 375 nm and λem = 475 nm. Reduced GSH was assessed by further dilution (1:10) with 5% (w/v) SSA. A 100 µl of the diluted sample was then combined with 50 µl 10% (v/v) triethanolamine, mixed, and a 100 µl of the mixture was

added to 200 µl buffer (100 mM NaH_2PO_4, 1 mM EDTA) prior to derivatization and HPLC as described above for GSSG.

4.2.8 Caspase activation

Caspase activation was determined as previously described (Franklin *et al.* 1998). Briefly, 50 µg of liver tissue homogenate were incubated for 60 min at 37°C in 100 µl of caspase assay buffer (50 mM HEPES, pH 7.4, 100 mM sodium chloride, 2 mM EDTA, 20% sucrose (w/v), 0.2% CHAPS (w/v), 10 mM DTT) with 20 µM Ac-DEVD-amc (Alexis Biochemicals, San Diego, CA) and fluorescence monitored on a Packard Fluorocount (Packard Instrument Company, Meriden, CT) microplate fluorometer with an excitation wavelength of 360 nm and an emission wavelength of 460 nm. Data are presented as fold activation over extracts from untreated cells.

4.2.9 Determination of mitochondrial respiration

Oxidative phosphorylation activity, *via* complex III, ubiquinol:ferricytochrome *c* oxidoreductase (E. C. 1.10.2.2), was assayed as previously described (Gudz *et al.* 1997). In brief, the rate of reduction of cytochrome *c* in isolated mitochondria was monitored spectrophotometrically (Cary 3E UV-Vis Spectrophotometer, Varian, Australia) with or without antimycin A, a specific complex III inhibitor, for 1 min at 550 nm after the addition of decylubiquinol substrate. The antimycin A sensitive rate is then calculated using the extinction coefficient of 19.1 mM^{-1} cm^{-1} (Gudz *et al.* 1997) and reported as µmol cytochrome *c* reduced per min per mg mitochondrial protein.

4.2.10 Statistical analysis

Results are calculated as mean ± SE. Statistical significance was determined for transaminase and caspase activities using two-tailed, unpaired t-test analysis and for

GSH/GSSG contents using paired, two-tailed, t-test. The statistical significance of complex III activities was determined by Mann-Whitney U test. p values ≤ 0.05 were considered significant.

4.3 Results

4.3.1 Altered processing and subcellular levels of BAX after drug treatment

Increased immunoreactivity of proapoptotic BAX was found in the mitochondrial fraction after APAP or AMAP treatment of wild type $B6C3F_1$ mice (Fig. 4.1, upper panels). On the basis of molecular mass calculations the data indicated that in these nontransgenic animals the beta (β) splice variant of BAX represented the active isoform. Similarly, a loss of BAX immunoreactivity from the cytosol, consistent with the BAX-α isoform, was observed (Fig. 4.1, lower panels). Moreover, at these early time points the extent of BAX-α loss appeared to correlate well with the relative hepatotoxic potential of the two compounds being completely absent in the cytosol of APAP treatments only. Drug-induced increases to BAX-β mitochondrial levels, however, were only associated with release of cytochrome *c* into the cytosol in 2 h APAP treated animals and not observed with AMAP treatment (Fig. 4.1).

4.3.2 Assessment of liver damage

Liver damage was assessed histologically and by determining plasma ALT and AST activities. WT (-/-) and *bcl-2* (-/+) transgenic animals induced with Zn demonstrated no alterations to hepatic morphologies (Fig. 4.2C,D cf. 4.2A) and no significant differences in plasma ALT and AST levels (data not shown). Consequently, WT (-/-) animals were used as the basis for comparison to treatment groups. At 6 h after injection, all treatment transaminase levels were elevated as compared to vehicle treated

controls (Table 4.1). The 24 h ALT and AST enzyme levels were significantly raised in APAP-treated *bcl-2* (-/+) transgenic mice (55.8 and 18 fold higher, respectively) versus control (vehicle-treated) WT mice. In comparison, APAP-treatment in WT mice resulted in considerably smaller elevations of plasma ALT and AST activities versus control (vehicle-treated) WT mice (22 and 6.6 fold, respectively; Table 4.1). These 24 h data indicate a previously unreported difference in the biological response to APAP between WT and *bcl*-2 (-/+) animals with a more severe form of liver damage found in BCL-2 overexpressing mice.

In contrast to APAP treatment, AMAP-treated transgenic animals showed only early elevations in liver enzymes (6 h), which returned to uninjured (control) levels within 24 h indicating a lack of progression to fulminant hepatotoxicity with this nonhepatotoxic isomer (Table 4.1). In order to exclude the possibility of increased metabolism and bioactivation of APAP in *bcl-2* (-/+) animals, we confirmed the extent of protein adduct formation at 6 and 24 h by immunoblot as previously described (Tonge *et al.* 1998). These data indicate that alterations to APAP-induced hepatotoxicity in BCL-2 overexpressing animals are not a result of increased production of the APAP reactive metabolite, NAPQI, as no difference in the extent of protein modification was detected (data not presented).

4.3.3 Histopathological analyses

In comparison to vehicle treated controls (Fig. 4.2A) APAP treatment in WT mice resulted in a clear centrilobular (zone 3) necrosis with areas of focal bridging necrosis and hemorrhage (Fig. 4.2B). In places where the hepatocytes were less obscured by

blood, i.e., at the edges of the lesion, microvesicular steatosis was also identified in intact centrilobular hepatocytes (data not shown).

Evidence of zone 3 necrosis and microvesicular steatosis was also observed after 6 h in *bcl-2* (-/+) transgenic mice treated with APAP (Fig. 4.2E). The pronounced microvesicular steatosis found at this time point was suggestive of an early injury marker presumably involving the endoplasmic reticulum and mitochondria (Redlich *et al.* 1990). In contrast to the more typical centrilobular injury of WT animals (Fig. 4.2B) APAP-induced damage in *bcl-2* (-/+) mice progressed to massive confluent necrosis and hemorrhagic infiltration by 24 h (Fig. 4.2F). Consequently, the extent of lobular involvement was much greater in BCL-2 overexpressing animals indicating that BCL-2 overexpression was not hepatoprotective but instead exacerbated APAP-initiated liver damage.

BCL-2 overexpressing animals dosed with AMAP also developed microvesicular steatosis 6 h after treatment but did not progress to extensive necrosis (Fig. 4.2G & H). Based on the extent of histopathologic changes we conclude that AMAP is significantly less hepatotoxic in comparison to APAP in *bcl-2* (-/+) transgenic mice in keeping with previous reports using other mouse strains (Tirmenstein and Nelson 1991).

BCL-2 overexpression *per se* had little effect on overall cellular morphology as observed by electron microscopy except for the presence of electron dense cytoplasmic aggregates in all *bcl-2* (-/+) mice induced with $ZnSO_4$ supplemented water (Fig. 4.3A, C, & D). Treatment of WT mice with APAP resulted in nuclear condensation and margination as well as mitochondrial proliferation (Fig. 4.3B). Increased lipid deposits were also apparent at 6 h after treatment with APAP consistent with the hepatic steatosis

observed by light microscopy (Fig. 4.3B). Liver tissue morphology of BCL-2 overexpressing mice treated with APAP was distinctive, however, with mitochondrial/endoplasmic reticulum associations commonly observed (Fig. 4.3C). In addition, ringed mitochondria, which are often associated with hepatotoxicity in the rat (Ghadially 1997), were observed (Fig. 4.3C). The functional significance of these structures are unknown but may be related to autophagy of this organelle (Dunn 1990).

4.3.4 Further characterizations of BCL-2 overexpression

To further assess the effects of BCL-2 overexpression *per se* several biochemical parameters were determined in addition to liver morphology. Early, APAP-specific, increases in mitochondrial BAX content (and most likely BAX-α) were reproducibly observed in *bcl-2* (-/+) transgenic mice by chemiluminescent immunoblot analysis but required extended, overnight, exposures to be detected (Fig. 4.4A, upper panel). In comparison, no differences in saline-treated mitochondrial BAX content were observed between *bcl-2* (-/-) and *bcl-2* (-/+) animals (Fig. 4.4A, upper panel). However, APAP-specific BAX mitochondrial translocations in *bcl-2* (-/+) mice failed to induce cytochrome *c* release into the cytosol (Fig. 4.4A-center panel) despite apparently excellent subcellular fractionations of mitochondria from the cytosol (cytochrome *c* vs. GAPDH; Fig. 4.4A-center & lower panels).

Overexpression of BCL-2 was observed to marginally, but significantly, increase hepatic GSSG levels ($p < 0.05$) without significant alterations to reduced GSH (Fig. 4.4B). These data suggest that BCL-2 expression alone, without APAP treatment, may result in a basal oxidative stress, which does not manifest as overt injury by either morphological criteria or plasma transaminase elevations (Figs. 4.2 & 4.3, Table 4.1,

refer Discussion). Furthermore, although alterations were not observed in total cellular catalase or mitochondrial Cu/Zn-SOD (data not presented) increases in peroxisomal catalase content were found in the heavy membrane (mitochondrial) fraction after APAP treatment in both *bcl-2* (-/-) and *bcl-2* (-/+) animals (Fig. 4.4C).

4.3.5 Immunoblot detection of BCL-2

Expression of human *bcl-2* transgene was confirmed by immunoblotting mouse liver tissue homogenates with commercially available antisera directed to the N-terminal region of BCL-2 (N19, refer Methods), which recognizes both human and endogenous mouse BCL-2. The data demonstrated clearly an overexpression of the human *bcl-2* transgene in transgenic animals whereas little or no endogenous murine BCL-2 was detected in WT mice (Fig. 4.5A, upper panel). Immunoblotting also revealed apparent decreases in BCL-2 protein content in APAP-, but not AMAP-, treated transgenic mice relative to GAPDH loading controls (Fig. 4.5A, upper cf. lower panel). These slight decreases in BCL-2 protein appeared to correlate with an increased breakdown of mouse hepatic albumin in APAP-treated groups (Fig. 4.5A, upper cf. center panel) and not be attributed to general sample proteolysis as the GAPDH loading standards remained unaffected (Fig. 4.5A, lower panel).

4.3.6 Caspase activation

BCL-2 degradation is generally associated with a proapoptotic state and increased activity of the effector caspase, caspase-3. To further examine the possibility of BCL-2 cleavage to its proapoptotic form by caspase-3, the activation of caspase-3-like enzymes in liver tissue homogenates was evaluated. Only modest increases in DEVD-amc cleavage were observed after either APAP- or AMAP-treatment of *bcl-2* (-/+) transgenic

or WT mice (Fig. 4.5B). For example, at 6 h after treatment, AMAP-treated transgenic mice had the highest change in caspase-3-like activity (1.28 fold increase vs. control, $p \leq 0.05$) while at 24 h after treatment, APAP-treated transgenic mice were highest with a 1.47 fold increase in activity versus control ($p \leq 0.05$). These changes are in agreement with our previous studies indicating only slight caspase-3-like activation after APAP-treatment *in vitro* and *in vivo* (Pierce *et al.* 2002). Although statistically significant the biological relevance of low-level DEVD-amc cleavage activity in APAP- and AMAP-treated mice observed in these studies is unclear.

4.3.7 Complex III activities

In order to evaluate overall mitochondrial respiratory chain activity, ubiquinol:ferricytochrome *c* oxidoreductase (complex III) activity was determined in control and treatment groups. At 6 h, and prior to overt liver damage, all three treatment groups demonstrated a statistically significant decrease in complex III activity compared to control levels (Fig. 4.6). The extent of inhibition correlated well with eventual liver damage as APAP-treated transgenic mice were most adversely affected (with the exception of AMAP-treatment, refer below). The same trend was also seen in APAP-treated transgenic animals at 24 h when liver damage was well advanced but the absolute level of complex III inhibition was less. This may be a consequence of the differential centrifugation procedures used to isolate mitochondria from damaged tissue with the selection of intact, and relatively functional, organelles.

In comparison to APAP-treated animals, however, AMAP-treated transgenic complex III activities had returned to control levels after 24 h in agreement with histopathological observations (Fig. 4.2). This provides further support for a transient

complex III loss and subsequent recovery of mitochondrial function by this non-hepatotoxic isomer (Fig. 4.6). Observed changes in complex III activities at 24 h correlated well with plasma AST (r^2=0.89) and ALT (r^2=0.87) levels at the same time point supporting the conclusion that mitochondrial function, and especially complex III activity, is an indicator of APAP-induced hepatotoxicity.

4.4 Discussion

The cell death and liver injury produced by APAP has been studied extensively for over 20 years. Necrosis has usually been associated with APAP-induced hepatotoxicity but more recently a role for apoptosis has been proposed but not supported by extensive data (Ray *et al.* 1996; Lawson *et al.* 1999). For example, studies have concluded that APAP-associated hepatotoxicity is a mixed necrotic and apoptotic event with approximately 40% of cells undergoing apoptosis based on oligosomal DNA laddering while 60% undergo necrosis as determined by plasma transaminase elevations (Ray *et al.* 1996). The data presented here suggest an early role for BAX in APAP-induced liver injury indicating that necrotic cell death in these circumstances may be initiated at the mitochondrion in a proapoptotic manner. Nonetheless, the precise relationship between APAP-mediated protein modifications, mitochondrial BAX content, and cell death has yet to be fully determined.

Mitochondria play an important role in APAP-mediated cell death. This has been deduced from many studies that indicate preferential mitochondrial glutathione depletion, calcium deregulation (Tirmenstein and Nelson 1989, 1991), and selective protein modifications within the mitochondrion (Qiu *et al.* 1998, 2001) after APAP - but not AMAP - treatment. Consistent with general mitochondrial dysfunction both decreased

oxygen utilization and ATP levels have been associated with APAP overdosing (Tirmenstein and Nelson 1990; Burcham and Harman 1991). In a related observation, it has been previously proposed that ATP levels are critical in determining the path to cell death (i.e., apoptosis versus necrosis) (Leist *et al.* 1997).

Most studies have used protective agents to elucidate the mechanism by which APAP elicits its toxicity (e.g., antioxidants, calcium chelators, etc.). Our studies have focused on the events downstream of APAP-protein adduction and examined the cellular responses to such modifications that ultimately lead to cell death. BAX has been shown to regulate the release of mitochondrial cytochrome *c via* components of the permeability transition pore (Shimizu *et al.* 1999). Consequently, APAP- and AMAP-mediated cell death and liver injury may be, at least in part, attributable to this mechanism. Other contributing factors appear to be required, however, as mitochondrial BAX localization does not always correlate with cytochrome *c* loss into the cytosol (Figs. 1 & 4A, (Putcha *et al.* 1999)). In this regard, it should be noted that BAX-dependent mitochondrial cytochrome *c* release is insufficient to account for the capacity to undergo apoptosis in a trophic factor withdrawal model of sympathetic neuron cell death (Deshmukh and Johnson 1998). An alternative explanation for the absence of cytochrome *c* in the cytosol, despite mitochondrial BAX localization, can be found with a recent report which indicates that the absolute levels of intracellular BAX may determine the extent and even reversibility of mitochondrial cytochrome *c* release (Pastorino *et al.* 1999). Finally, BAX-induced apoptosis requires a functional F_0F_1-ATPase proton pump in mammalian cells (Matsuyama *et al.* 1998), which may explain recent findings indicating that F_0F_1-ATPase inhibition protects against APAP-mediated damage (Banerjee *et al.* 1998).

It has also been recognized that BCL-2 itself, as well as other members like BCL-x_L (the BCL-2 functional homologue expressed in hepatocytes; (Tzung *et al.* 1997), heterodimerize with BAX (Sato *et al.* 1994; Yin *et al.* 1994). BCL-2 dimerization with BAX is thought to mediate its antiapoptotic action (Yin *et al.* 1994; Rosse *et al.* 1998). Recognizing the function of BAX translocation as an initiating mitochondrial event in many apoptotic systems (Wei *et al.* 2001), and the potential for regulatory control by BCL-2, we have attempted to determine whether BCL-2 overexpression may protect against APAP-induced hepatotoxicity as reported for other stimuli (Rosse *et al.* 1998; Putcha *et al.* 1999). In this manner, perturbing the balance between BAX and BCL-2 in favor of BCL-2, should be hepatoprotective.

The liver damage we have observed in APAP-treated *bcl-2 (-/+)* transgenic animals was considerably greater than that found with WT animals contrary to our expectations (Fig. 4.2, Table 4.1). Moreover, we were able to detect APAP-specific localization of BAX to mitochondria in *bcl-2 (-/+)* animals (Fig. 4.4A). However, these levels appeared to be considerably lower than comparably treated nontransgenic mice as determined by immunoblot sensitivity. The only measurable difference we have observed between control BCL-2 overexpressing and WT animals is an elevation of hepatic oxidized glutathione (GSSG) in *bcl-2* (-/+) animals (Fig. 4.4B). Although an antioxidant function has been attributed to BCL-2 our findings are in agreement with a previous report proposing a prooxidant capacity for BCL-2 in mammalian cells (Steinman 1995). In addition, it has also been observed that BCL-2 overexpression fails to prevent the action of classical inducers of permeability transition in isolated mouse liver mitochondria (Yang *et al.* 2000). Moreover, our caspase-3-like activities (DEVD-

amc cleavage) were much lower than that observed with most other apoptosis models (Fig. 4.5B). This low-level caspase activation was expected based on previous reports of no caspase activation (Lawson *et al.* 1999) and our observations of low caspase activation in APAP- and AMAP-treated mice (Pierce *et al.* 2002). These observations are consistent with a proapoptotic initiation of liver damage during APAP overdose and subsequent advance to death *via* necrosis.

Disruption of oxidative phosphorylation, specifically at complex I and complex II, after direct exposure to NAPQI, the APAP reactive intermediate, has been previously reported (Burcham and Harman 1991) but an inhibition of complex III *in vivo* has not been observed. However, *in vitro* studies have demonstrated decreased complex III activity after NAPQI exposure to inverted membrane particles (Ramsay *et al.* 1989). From the studies presented here we conclude that alterations to complex III activities can be a sensitive and early marker of the eventual extent of liver damage.

The generation of a proapoptotic BCL-2 cleavage fragment by caspase-3 or other proteolytic cleavage activity may offer an explanation for the enhanced APAP-induced hepatotoxicity we have observed (Cheng *et al.* 1997; Kirsch *et al.* 1999). Although our studies suggest that BCL-2 protein levels were decreased 24 h after APAP treatments, we have not detected BCL-2 fragments consistent with cleavage by caspase-3 to the proapoptotic form (Fig. 4.5A). Our data (i.e., low caspase activation and no evidence for a specific cleavage product) suggest that BCL-2 disappearance in 24 h APAP-treated animals may be attributable to another cellular proteolytic activity (e.g., proteasome; (Breitschopf *et al.* 2000; Pierce *et al.* 2002)). Further experiments will be required to determine the mechanism of BCL-2 loss in APAP-treated animals. An alternative

explanation for enhanced APAP-induced hepatotoxicity in BCL-2 overexpressing animals is the observation that APAP inhibits proteasomal activity transiently (Qiu *et al.* 1998; Pierce *et al.* 2002). As recently suggested, this inhibition may perturb the balance between BCL-2 and BAX thereby resulting in decreased BAX degradation and a shift to a more proapoptotic state (Li and Dou 2000).

In conclusion, our studies indicate that the overexpression of human BCL-2 in C57/B6C3H mice significantly enhances APAP-induced hepatotoxicity. Biochemical and morphological evidence also confirms a key role for mitochondria in the progression of this damage. These novel findings allow for new avenues to approach and define the mechanism of APAP-mediated hepatotoxicity.

4.5 End Notes

1-Parts of the chapter were previously published as:

Adams, M. L., Pierce, R. H., Vail, M. E., White, C. C., Tonge, R. P., Kavanagh, T. J., Fausto, N., Nelson, S. D., and Bruschi, S. A. (2001). Enhanced acetaminophen hepatotoxicity in transgenic mice overexpressing BCL-2. *Mol Pharmacol* **60**, 907-15.

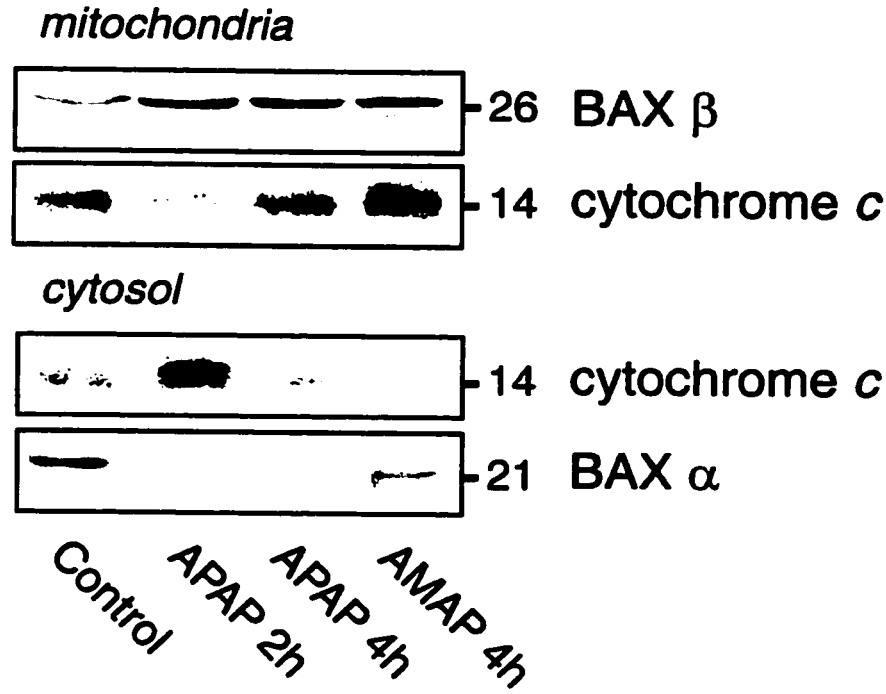

Figure 4.1: Mitochondrial alterations induced by APAP and the nonhepatotoxic positional isomer, AMAP. Subcellular fractions from $B6C3F_1$ mice were isolated at various times after control (vehicle), APAP, or AMAP treatment (600 mg/kg, i.p) and immunoblotted using standard procedures. **(Upper two panels)** Mitochondrial fractions immunoblotted for BAX and cytochrome *c* content indicated early and sustained BAX-β relocalization to mitochondria in all treatments with transient cytochrome *c* depletion in APAP treatments.
(Lower two panels) Cytosolic fractions immunoblotted for BAX and cytochrome *c* release indicated release of cytochrome *c* from mitochondria of APAP-treated animals and either an absence of BAX-α immunoreactivity in APAP treatments or a relative depletion of BAX-α in AMAP treated animals. Molecular mass of immunoreactive proteins, in kDa, is indicated on the right of each panel.

Table 4.1. Plasma Transaminase Activities in wild-type (-/-) and *bcl-2* (-/+) transgenic mice treated with 500 mg/kg acetaminophen or *N*-acetyl-*m*-aminophenol.

	AST[a]				ALT[a]			
	6 h	f. c.[b]	24 h	f. c.[b]	6 h	f. c.[b]	24 h	f. c.[b]
control (-/-)[c]	531 (361)	---	1175 (446)	---	211 (31)	---	626 (262)	---
APAP (-/-)	5745 (1004)[d]	10.8	7787 (2380)[d,e]	6.6	6258 (1587)	29.7	13746 (3374)[d,e]	22.0
APAP (-/+)	3764 (1123)[d]	7.1	21196 (882)[f,g,h]	18.0	3278 (1006)[d]	15.5	34920 (5604)[d,g,h]	55.8
AMAP (-/+)	1010 (178)	1.9	564 (141)	0.5	725 (222)	3.4	543 (126)	0.9

a - Values reported as Units per liter. [mean (SE)]. n=3-6 for each treatment group
b - Fold Change as compared to control values.
c – No significant differences were observed between bcl-2 (-/-) and (-/+) in either plasma AST or ALT levels
d - $p \leq 0.05$ versus control (-/-)
e - Dosed 6 animals, 3 survived.
f - $p \leq 0.001$ versus control (-/-)
g - Dosed 7 animals, 3 survived
h – $p \leq 0.05$ versus APAP (-/-) 24 h

Figure 4.2. Assessment of hepatotoxicity by morphology. Hematoxylin and eosin stained liver sections 6 h and 24 h after dosing with APAP or AMAP (500 mg/kg, i.p.). All animals were induced with 25 mM $ZnSO_4$ in the drinking water for 5-7 days prior to dosing. (**A**) control WT (-/-) treated with saline only showing normal hepatic morphology. (**B**) WT (-/-) animals 24 h after dosing with APAP showing distinct areas of centrilobular necrosis. (**C-D**) Zn-induced *bcl-2* (-/+) animals dosed with saline only at either 100X (C) or 200X (D) magnification showing typical hepatic lobule structure and no evidence of damage. (**E-F**) *bcl-2* (-/+) animals 6 h (E) and 24 h (F) after dosing with APAP. At 6 h, microvesicular steatosis (hollow arrowheads, D) is observed but by 24 h, a massive confluent necrosis is evident (solid arrowheads, F) with considerable hemorrhage. (**G-H**) AMAP-treated animals developed a qualitatively more pronounced microvesicular steatosis at 6 h (hollow arrowheads, G). In contrast to APAP, AMAP-treated *bcl-2* (-/+) animals did not progress to extensive damage (H). All photographs are 100X magnification, except (D) at 200X. Central vein indicated by CV.

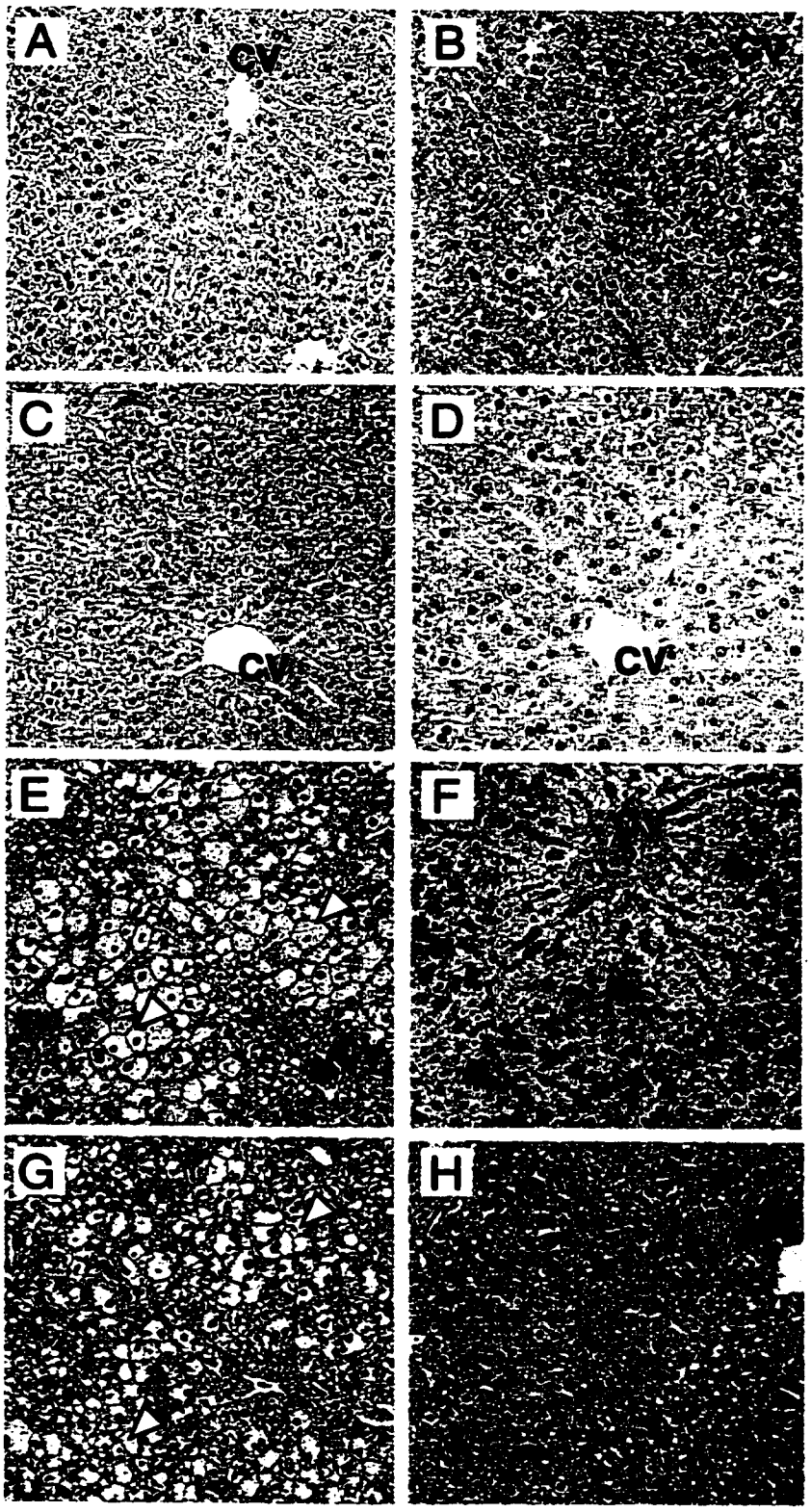
A
CV
B
CV
C
CV
D
CV
E
F
G
H

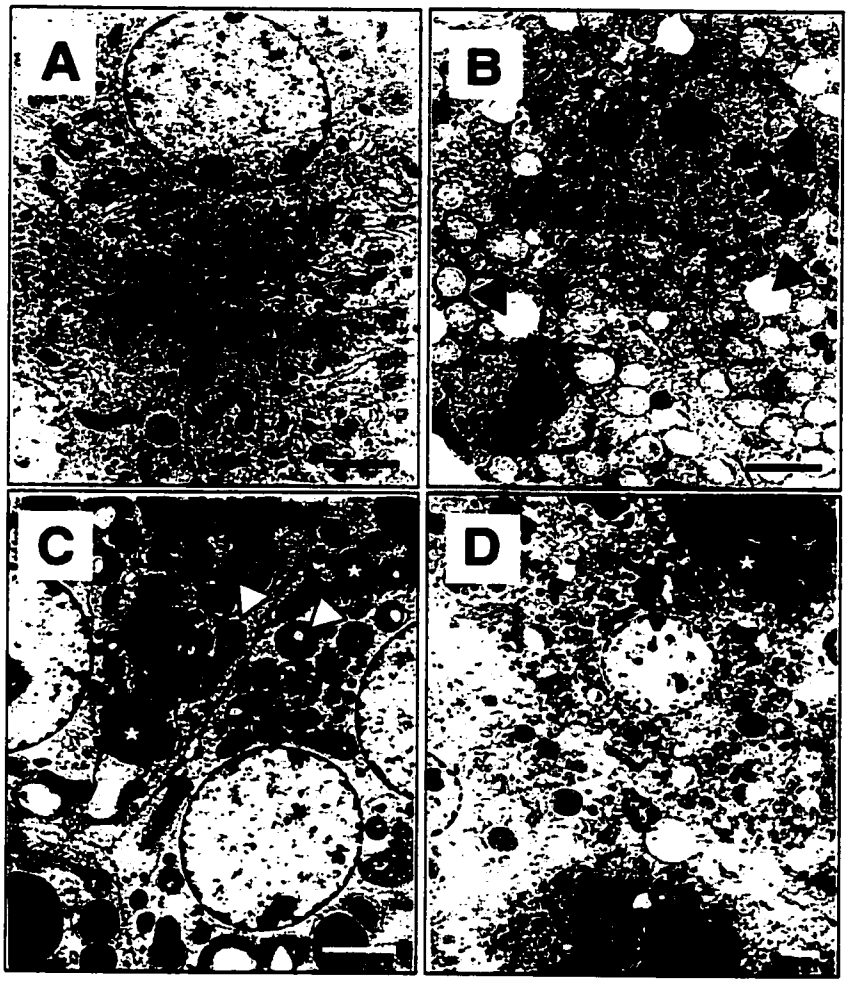

Figure 4.3. Assessment of cellular morphology changes by electron microscopy. Liver sections were fixed in Karnovsky's fixative and stained with Reynold's lead citrate 6 h after dosing with APAP and AMAP 500 mg/kg i.p. **(A)** Control *bcl-2* (-/+) treated only with $ZnSO_4$ showing normal hepatocyte morphology. **(B)** WT (-/-) animals 6 h after dosing with APAP showing lipid deposition (solid arrowheads), mitochondrial proliferation and nuclear condensation. **(C-D)** *bcl-2* (-/+) animals 6 h after dosing with APAP and AMAP, respectively. APAP-treatment (C) shows association of the endoplasmic reticulum with the mitochondria and ring-shaped mitochondria (hollow arrowhead) while AMAP-treatment (D) shows almost normal morphology with the exception of electron dense aggregates which are seen in all *bcl-2* (-/+) animals (*). All magnifications are ~12,000X except (D) at ~6,000X. Bar equals 5 μm.

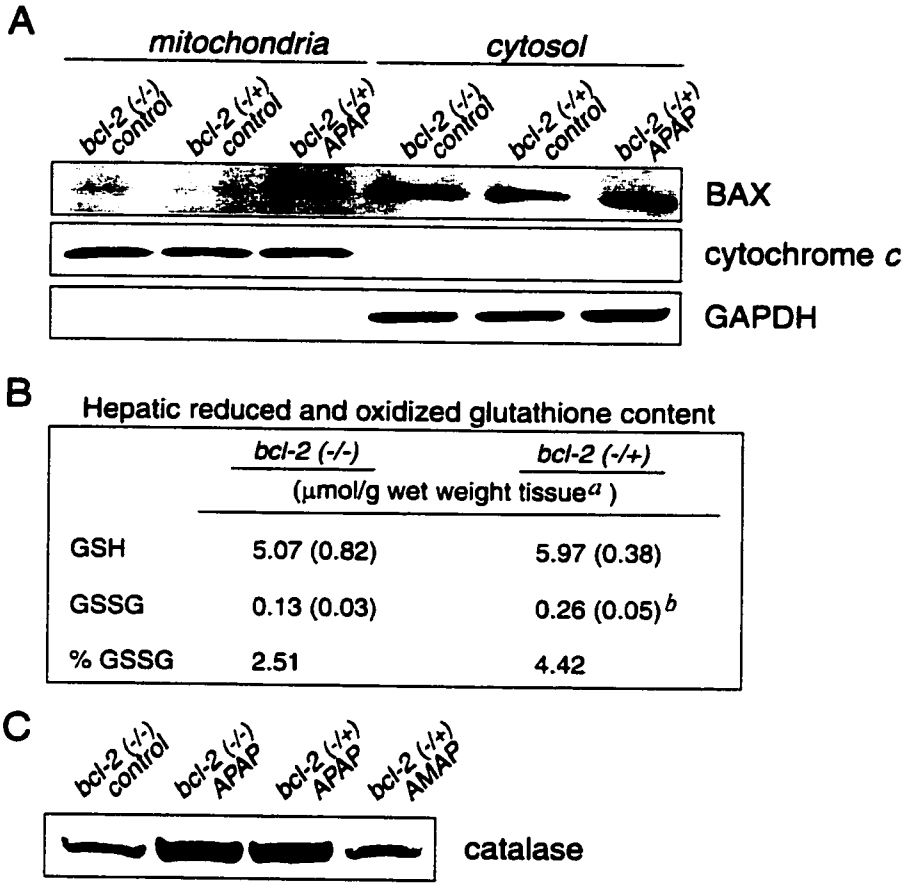

Figure 4.4. Biochemical characterizations of control, APAP-treated *bcl-2* (-/+), and WT (-/-) transgenic animals. **(A)** Subcellular BAX content from mitochondrial and cytosolic fractions prepared from *bcl-2* (-/-) and *bcl-2* (-/+) animals 2 h after treatment with vehicle only (saline/control) or APAP (500 mg/kg, i.p.) as described in *Methods*. APAP-specific BAX translocation to the mitochondrial fraction was observed in BCL-2 overexpressing animals (upper panel). Cytochrome *c* and GAPDH remained in the mitochondria and cytosol, respectively, in all treatment groups (lower 2 panels). **(B)** Hepatic reduced (GSH) and oxidized (GSSG) glutathione contents of *bcl-2* (-/-) and *bcl-2* (-/+) mice induced with $ZnSO_4$ in the drinking water for 5-7 days and dosed with saline vehicle only as described in *Methods*. (***a***) Total GSH or GSSG content reported as mean ± SE (n=4), (***b***) Significant increase ($p < 0.05$) in GSSG in *bcl-2* (-/+) transgenic animals. **(C)** APAP-specific elevations of hepatic catalase content in "heavy membrane" (mitochondria + peroxisomes) fractions of *bcl-2* (-/-) and *bcl-2* (-/+) animals isolated 6 h after vehicle or drug treatment.

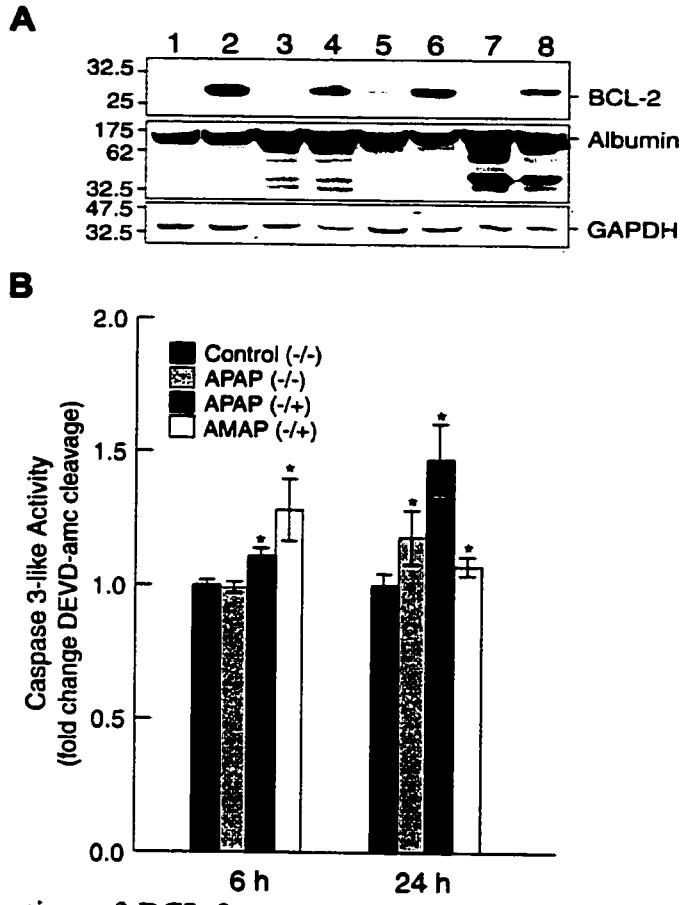

Figure 4.5. Confirmation of BCL-2 transgene overexpression in control and APAP-dosed WT (-/-) and *bcl-2* (-/+) animals. **(A)** Confirmation by immunoblot analysis of liver BCL-2 content in tissue homogenates from control, APAP or AMAP (500 mg/kg, i.p.) treatments prepared as described in *Methods*. The blot was probed with antisera to BCL-2 (N19) (Santa Cruz), GAPDH, and albumin (ICN) using standard procedures. Molecular weight markers (kDa) are indicated to the left of the panel. Samples were taken at 6 h (lanes 1-4) and 24 h (lanes 5-8) after treatment. Endogenous murine BCL-2 was not detected in saline injected WT animals (lanes 1 & 5) or APAP-treated WT animals (lanes 3 & 7) using BCL-2 (N19) antiserum. High levels of BCL-2 expression were confirmed in *bcl-2* (-/+) animals treated with $ZnSO_4$ and dosed with AMAP (lane 2 & 6) or APAP (lane 4 & 8). Degradation of albumin was observed most predominantly in the APAP treated animals. Equal loading of samples was demonstrated by GAPDH content after membrane stripping, blocking and reprobing. **(B)** The activation of caspase-3-like enzymes was evaluated as described in *Methods*. Activity is represented as fold change in DEVD-amc cleavage versus untreated animals after 60 min incubation in caspase assay buffer. Error bars represent SE of mean expressed as a percentage of absolute activity and range from 1.1% to 6.2% of total activity. n=3-6 animals for each treatment group. * $p < 0.05$ (compared to control values).

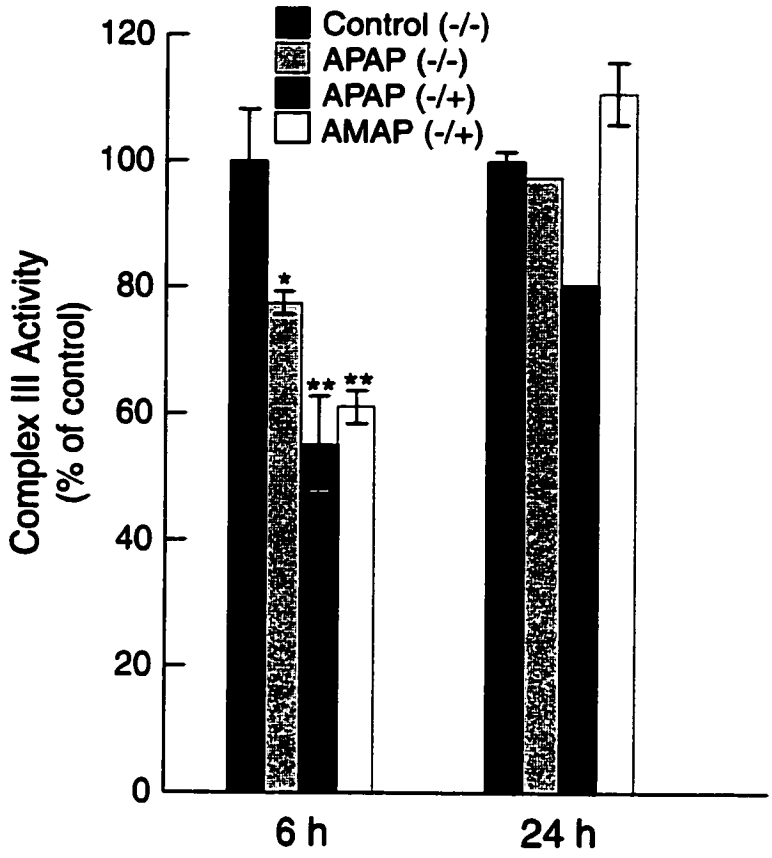

Figure 4.6. Complex III Activity. Complex III (ubiquinol:ferricytochrome *c* oxidoreductase) activities for each treatment group (APAP or AMAP, 500 mg/kg i.p.) were determined as described in *Methods*. Values are reported as percentage of mean control rate (μmol cytochrome *c* reduced per min per mg mitochondrial protein). Errors, expressed as % SE, ranged from 1.4 to 7% for controls and 3.5 to 10.5% for treatment groups. n=3-6 for all treatment groups except APAP (-/+) 24 h and APAP (-/-) 24 h for which n=2. *p = 0.05, **p < 0.05 (compared to control values).

References

Abraham, D. G., Patel, P. P., and Cooper, A. J. (1995). Isolation from rat kidney of a cytosolic high molecular weight cysteine- S-conjugate beta-lyase with activity toward leukotriene E4. *J Biol Chem* **270**, 180-8.

Adamson, G. M., and Harman, A. W. (1993). Oxidative stress in cultured hepatocytes exposed to acetaminophen. *Biochem Pharmacol* **45**, 2289-94.

Allcock, R. J., Williams, J. H., and Price, P. (2001). The central MHC gene, BAT1, may encode a protein that down-regulates cytokine production. *Genes Cells* **6**, 487-94.

Ameisen, J. C., and Capron, A. (1991). Cell dysfunction and depletion in AIDS: the programmed cell death hypothesis. *Immunol Today* **12**, 102-5.

Anders, M. W., and Dekant, W. (1998). Glutathione-dependent bioactivation of haloalkenes. *Annu Rev Pharmacol Toxicol* **38**, 501-37.

Antonsson, B., Conti, F., Ciavatta, A., Montessuit, S., Lewis, S., Martinou, I., Bernasconi, L., Bernard, A., Mermod, J. J., Mazzei, G., Maundrell, K., Gambale, F., Sadoul, R., and Martinou, J. C. (1997). Inhibition of BAX channel-forming activity by BCL-2. *Science* **277**, 370-2.

Armstrong, J. S., and Jones, D. P. (2002). Glutathione depletion enforces the mitochondrial permeability transition and causes cell death in BCL-2 overexpressing HL60 cells. *FASEB J* **16**, 1263-5.

Baehrecke, E. H. (2002). How death shapes life during development. *Nat Rev Mol Cell Biol* **3**, 779-87.

Bakhshi, A., Jensen, J. P., Goldman, P., Wright, J. J., McBride, O. W., Epstein, A. L., and Korsmeyer, S. J. (1985). Cloning the chromosomal breakpoint of t(14;18) human lymphomas: clustering around JH on chromosome 14 and near a transcriptional unit on 18. *Cell* **41**, 899-906.

Banerjee, A., Linscheer, W. G., Chiji, H., Murthy, U. K., Cho, C., Nandi, J., and Chan, S. H. (1998). Induction of an ATPase inhibitor protein by propylthiouracil and protection against paracetamol (acetaminophen) hepatotoxicity in the rat. *Br J Pharmacol* **124**, 1041-7.

Barres, B. A., Hart, I. K., Coles, H. S., Burne, J. F., Voyvodic, J. T., Richardson, W. D., and Raff, M. C. (1992). Cell death and control of cell survival in the oligodendrocyte lineage. *Cell* **70**, 31-46.

Bartolone, J. B., Birge, R. B., Bulera, S. J., Bruno, M. K., Nishanian, E. V., Cohen, S. D., and Khairallah, E. A. (1992). Purification, antibody production, and partial amino acid sequence of the 58-kDa acetaminophen-binding liver proteins. *Toxicol Appl Pharmacol* **113**, 19-29.

Beere, H. M., Wolf, B. B., Cain, K., Mosser, D. D., Mahboubi, A., Kuwana, T., Tailor, P., Morimoto, R. I., Cohen, G. M., and Green, D. R. (2000). Heat-shock protein 70 inhibits apoptosis by preventing recruitment of procaspase-9 to the Apaf-1 apoptosome. *Nat Cell Biol* **2**, 469-75.

Bossy-Wetzel, E., Newmeyer, D. D., and Green, D. R. (1998). Mitochondrial cytochrome *c* release in apoptosis occurs upstream of DEVD- specific caspase activation and independently of mitochondrial transmembrane depolarization. *EMBO J* **17**, 37-49.

Boulares, H. A., Giardina, C., Navarro, C. L., Khairallah, E. A., and Cohen, S. D. (1999). Modulation of serum growth factor signal transduction in Hepa 1-6 cells by acetaminophen: an inhibition of c-myc expression, NF-kappaB activation, and Raf-1 kinase activity. *Toxicol Sci* **48**, 264-74.

Braun, H. P., Emmermann, M., Kruft, V., and Schmitz, U. K. (1992). The general mitochondrial processing peptidase from potato is an integral part of cytochrome *c* reductase of the respiratory chain. *EMBO J* **11**, 3219-27.

Breitschopf, K., Haendeler, J., Malchow, P., Zeiher, A. M., and Dimmeler, S. (2000). Posttranslational modification of BCL-2 facilitates its proteasome- dependent degradation: molecular characterization of the involved signaling pathway. *Mol Cell Biol* **20**, 1886-96.

Brodie, B. B., Reid, W. D., Cho, A. K., Sipes, G., Krishna, G., and Gillette, J. R. (1971). Possible mechanism of liver necrosis caused by aromatic organic compounds. *Proc Natl Acad Sci U S A* **68**, 160-4.

Bruschi, S., Crabb, J. W., and Stevens, J. L. (1994). The E3 subunit of 2-oxoglutarate, branched-chain alpha-keto acid, and malate dehydrogenase are adducted during nephrotoxic cysteine-conjugate injury. *Toxicologist* **14**, 428.

Bruschi, S. A., Lindsay, J. G., and Crabb, J. W. (1998). Mitochondrial stress protein recognition of inactivated dehydrogenases during mammalian cell death. *Proc Natl Acad Sci U S A* **95**, 13413-8.

Bruschi, S. A., West, K. A., Crabb, J. W., Gupta, R. S., and Stevens, J. L. (1993). Mitochondrial HSP60 (P1 protein) and a HSP70-like protein (mortalin) are major targets for modification during *S*-(1,1,2,2-tetrafluoroethyl)- L-cysteine-induced nephrotoxicity. *J Biol Chem* **268**, 23157-61.

Bulera, S. J., Birge, R. B., Cohen, S. D., and Khairallah, E. A. (1995). Identification of the mouse liver 44-kDa acetaminophen-binding protein as a subunit of glutamine synthetase. *Toxicol Appl Pharmacol* **134**, 313-20.

Burcham, P. C., and Harman, A. W. (1990). Mitochondrial dysfunction in paracetamol hepatotoxicity: in vitro studies in isolated mouse hepatocytes. *Toxicol Lett* **50**, 37-48.

Burcham, P. C., and Harman, A. W. (1991). Acetaminophen toxicity results in site-specific mitochondrial damage in isolated mouse hepatocytes. *J Biol Chem* **266**, 5049-54.

Butler, L. E., Thomassen, D., Martin, J. L., Martin, B. M., Kenna, J. G., and Pohl, L. R. (1992). The calcium-binding protein calreticulin is covalently modified in rat liver by a reactive metabolite of the inhalation anesthetic halothane. *Chem Res Toxicol* **5**, 406-10.

Butow, R. A., Docherty, R., and Parikh, V. S. (1988). A path from mitochondria to the yeast nucleus. *Philos Trans R Soc Lond B Biol Sci* **319**, 127-33.

Cai, J., and Jones, D. P. (1998). Superoxide in apoptosis. Mitochondrial generation triggered by cytochrome *c* loss. *J Biol Chem* **273**, 11401-4.

Calder, I. C., Hart, S. J., Healey, K., and Ham, K. N. (1981). N-hydroxyacetaminophen: a postulated toxic metabolite of acetaminophen. *J Med Chem* **24**, 988-93.

Capaldi, R. A., and Aggeler, R. (2002). Mechanism of the F_1F_0-type ATP synthase, a biological rotary motor. *Trends Biochem Sci* **27**, 154-60.

Chautan, M., Chazal, G., Cecconi, F., Gruss, P., and Golstein, P. (1999). Interdigital cell death can occur through a necrotic and caspase- independent pathway. *Curr Biol* **9**, 967-70.

Chelstowska, A., Liu, Z., Jia, Y., Amberg, D., and Butow, R. A. (1999). Signalling between mitochondria and the nucleus regulates the expression of a new D-lactate dehydrogenase activity in yeast. *Yeast* **15**, 1377-91.

Cheng, E. H., Kirsch, D. G., Clem, R. J., Ravi, R., Kastan, M. B., Bedi, A., Ueno, K., and Hardwick, J. M. (1997). Conversion of BCL-2 to a BAX-like death effector by caspases. *Science* **278**, 1966-8.

Choi, D. W. (1992). Excitotoxic cell death. *J Neurobiol* **23**, 1261-76.

Clarke, A. R., Purdie, C. A., Harrison, D. J., Morris, R. G., Bird, C. C., Hooper, M. L., and Wyllie, A. H. (1993). Thymocyte apoptosis induced by p53-dependent and independent pathways. *Nature* **362**, 849-52.

Cleary, M. L., and Sklar, J. (1985). Nucleotide sequence of a t(14;18) chromosomal breakpoint in follicular lymphoma and demonstration of a breakpoint-cluster region near a transcriptionally active locus on chromosome 18. *Proc Natl Acad Sci U S A* **82**, 7439-43.

Commandeur, J. N., De Kanter, F. J., and Vermeulen, N. P. (1989). Bioactivation of the cysteine-S-conjugate and mercapturic acid of tetrafluoroethylene to acylating reactive intermediates in the rat: dependence of activation and deactivation activities on acetyl coenzyme A availability. *Mol Pharmacol* **36**, 654-63.

Cooper, A., Bruschi, S., and Anders, M. (2002). Toxic, halogenated cysteine S-conjugates and targeting of mitochondrial enzymes of energy metabolism. *Biochem Pharmacol* **64**, 553.

Cooper, A. J., Wang, J., Gartner, C. A., and Bruschi, S. A. (2001). Co-purification of mitochondrial HSP70 and mature protein disulfide isomerase with a functional rat kidney high-M(r) cysteine S-conjugate β-lyase. *Biochem Pharmacol* **62**, 1345-53.

Crompton, M. (1999). The mitochondrial permeability transition pore and its role in cell death. *Biochem J* **341**, 233-49.

Dahlin, D. C., Miwa, G. T., Lu, A. Y., and Nelson, S. D. (1984). N-acetyl-*p*-benzoquinone imine: a cytochrome P-450-mediated oxidation product of acetaminophen. *Proc Natl Acad Sci U S A* **81**, 1327-31.

Dahlin, D. C., and Nelson, S. D. (1982). Synthesis, decomposition kinetics, and preliminary toxicological studies of pure N-acetyl-*p*-benzoquinone imine, a proposed toxic metabolite of acetaminophen. *J Med Chem* **25**, 885-6.

Darrouzet, E., Moser, C. C., Dutton, P. L., and Daldal, F. (2001). Large scale domain movement in cytochrome bc_1: a new device for electron transfer in proteins. *Trends Biochem Sci* **26**, 445-51.

de Jong, D., Prins, F. A., Mason, D. Y., Reed, J. C., van Ommen, G. B., and Kluin, P. M. (1994). Subcellular localization of the BCL-2 protein in malignant and normal lymphoid cells. *Cancer Res* **54**, 256-60.

Deng, K., Zhang, L., Kachurin, A. M., Yu, L., Xia, D., Kim, H., Deisenhofer, J., and Yu, C. A. (1998). Activation of a matrix processing peptidase from the crystalline cytochrome bc_1 complex of bovine heart mitochondria. *J Biol Chem* **273**, 20752-7.

Derventzi, A., Rattan, S. I., and Clark, B. F. (1993). Phorbol ester PMA stimulates protein synthesis and increases the levels of active elongation factors EF-1 α and EF-2 in ageing human fibroblasts. *Mech Ageing Dev* **69**, 193-205.

Desagher, S., and Martinou, J. C. (2000). Mitochondria as the central control point of apoptosis. *Trends Cell Biol* **10**, 369-77.

Desagher, S., Osen-Sand, A., Nichols, A., Eskes, R., Montessuit, S., Lauper, S., Maundrell, K., Antonsson, B., and Martinou, J. C. (1999). BID-induced conformational change of BAX is responsible for mitochondrial cytochrome *c* release during apoptosis. *J Cell Biol* **144**, 891-901.

Deshmukh, M., and Johnson, E. M., Jr. (1998). Evidence of a novel event during neuronal death: development of competence-to-die in response to cytoplasmic cytochrome *c*. *Neuron* **21**, 695-705.

Dharmawardhane, S., Demma, M., Yang, F., and Condeelis, J. (1991). Compartmentalization and actin binding properties of ABP-50: the elongation factor-1 α of Dictyostelium. *Cell Motil Cytoskeleton* **20**, 279-88.

Dietze, E. C., Schafer, A., Omichinski, J. G., and Nelson, S. D. (1997). Inactivation of glyceraldehyde-3-phosphate dehydrogenase by a reactive metabolite of acetaminophen and mass spectral characterization of an arylated active site peptide. *Chem Res Toxicol* **10**, 1097-103.

Du, C., Fang, M., Li, Y., Li, L., and Wang, X. (2000). SMAC, a mitochondrial protein that promotes cytochrome *c*-dependent caspase activation by eliminating IAP inhibition. *Cell* **102**, 33-42.

Dunn, A. Y., Melville, M. W., and Frydman, J. (2001). Review: cellular substrates of the eukaryotic chaperonin TRiC/CCT. *J Struct Biol* **135**, 176-84.

Dunn, W. A., Jr. (1990). Studies on the mechanisms of autophagy: formation of the autophagic vacuole. *J Cell Biol* **110**, 1923-33.

Eriksson, A., Sjoling, S., and Glaser, E. (1994). The ubiquinol cytochrome *c* oxidoreductase complex of spinach leaf mitochondria is involved in both respiration and protein processing. *Biochim Biophys Acta* **1186**, 221-231.

Esposti, M. D., De Vries, S., Crimi, M., Ghelli, A., Patarnello, T., and Meyer, A. (1993). Mitochondrial cytochrome *b*: evolution and structure of the protein. *Biochim Biophys Acta* **1143**, 243-71.

Essex, D. W., and Li, M. (1999). Protein disulphide isomerase mediates platelet aggregation and secretion. *Br J Haematol* **104**, 448-54.

Essex, D. W., Li, M., Miller, A., and Feinman, R. D. (2001). Protein disulfide isomerase and sulfhydryl-dependent pathways in platelet activation. *Biochemistry* **40**, 6070-5.

Esterline, R. L., Ray, S. D., and Ji, S. (1989). Reversible and irreversible inhibition of hepatic mitochondrial respiration by acetaminophen and its toxic metabolite, N-acetyl-*p*-benzoquinoneimine (NAPQI). *Biochem Pharmacol* **38**, 2387-90.

Evans, R. M. (1998). Vimentin: the conundrum of the intermediate filament gene family. *Bioessays* **20**, 79-86.

Franklin, C. C., Srikanth, S., and Kraft, A. S. (1998). Conditional expression of mitogen-activated protein kinase phosphatase- 1, MKP-1, is cytoprotective against UV-induced apoptosis. *Proc Natl Acad Sci U S A* **95**, 3014-9.

Friberg, H., Ferrand-Drake, M., Bengtsson, F., Halestrap, A. P., and Wieloch, T. (1998). Cyclosporin A, but not FK 506, protects mitochondria and neurons against hypoglycemic damage and implicates the mitochondrial permeability transition in cell death. *J Neurosci* **18**, 5151-9.

Garrett, R., and Grisham, C. M. (1995). *Biochemistry*. Saunders College Pub., Fort Worth.

Gemborys, M. W., Gribble, G. W., and Mudge, G. H. (1978). Synthesis of N-hydroxyacetaminophen, a postulated toxic metabolite of acetaminophen, and its phenolic sulfate conjugate. *J Med Chem* **21**, 649-52.

Ghadially, F. N. (1997). Mitochondria. In *Ultrastructural pathology of the cell and matrix*, 4th ed., Vol. 1, pp. 195-342. Butterworth-Heinemann, Boston.

Gougeon, M. L., and Montagnier, L. (1993). Apoptosis in AIDS. *Science* **260**, 1269-70.

Gross, A., Jockel, J., Wei, M. C., and Korsmeyer, S. J. (1998). Enforced dimerization of BAX results in its translocation, mitochondrial dysfunction and apoptosis. *EMBO J* **17**, 3878-85.

Gross, A., McDonnell, J. M., and Korsmeyer, S. J. (1999a). BCL-2 family members and the mitochondria in apoptosis. *Genes Dev* **13**, 1899-911.

Gross, A., Yin, X. M., Wang, K., Wei, M. C., Jockel, J., Milliman, C., Erdjument-Bromage, H., Tempst, P., and Korsmeyer, S. J. (1999b). Caspase cleaved BID targets mitochondria and is required for cytochrome *c* release, while BCL-x_L prevents this release but not tumor necrosis factor-R1/Fas death. *J Biol Chem* **274**, 1156-63.

Groux, H., Torpier, G., Monte, D., Mouton, Y., Capron, A., and Ameisen, J. C. (1992). Activation-induced death by apoptosis in CD4+ T cells from human immunodeficiency virus-infected asymptomatic individuals. *J Exp Med* **175**, 331-40.

Groves, C. E., Hayden, P. J., Lock, E. A., and Schnellmann, R. G. (1993). Differential cellular effects in the toxicity of haloalkene and haloalkane cysteine conjugates to rabbit renal proximal tubules. *J Biochem Toxicol* **8**, 49-56.

Gudz, T. I., Tserng, K. Y., and Hoppel, C. L. (1997). Direct inhibition of mitochondrial respiratory chain complex III by cell-permeable ceramide. *J Biol Chem* **272**, 24154-8.

Gupta, S., Rogers, L. K., Taylor, S. K., and Smith, C. V. (1997). Inhibition of carbamyl phosphate synthetase-I and glutamine synthetase by hepatotoxic doses of acetaminophen in mice. *Toxicol Appl Pharmacol* **146**, 317-27.

Haldar, S., Basu, A., and Croce, C. M. (1998). Serine-70 is one of the critical sites for drug-induced BCL-2 phosphorylation in cancer cells. *Cancer Res* **58**, 1609-15.

Halestrap, A. P., Doran, E., Gillespie, J. P., and O'Toole, A. (2000). Mitochondria and cell death. *Biochem Soc Trans* **28**, 170-7.

Halestrap, A. P., Kerr, P. M., Javadov, S., and Woodfield, K. Y. (1998). Elucidating the molecular mechanism of the permeability transition pore and its role in reperfusion injury of the heart. *Biochim Biophys Acta* **1366**, 79-94.

Halmes, N. C., Hinson, J. A., Martin, B. M., and Pumford, N. R. (1996). Glutamate dehydrogenase covalently binds to a reactive metabolite of acetaminophen. *Chem Res Toxicol* **9**, 541-6.

Harding, H. P., Zhang, Y., and Ron, D. (1999). Protein translation and folding are coupled by an endoplasmic-reticulum- resident kinase. *Nature* **397**, 271-4.

Hasan, Q., Tan, S. T., Gush, J., and Davis, P. F. (2001). Altered mitochondrial cytochrome *b* gene expression during the regression of hemangioma. *Plast Reconstr Surg* **108**, 1471-6; discussion 1477-8.

Hayden, P., Schaeffer, V. H., Larsen, G., and Stevens, J. L. (1987). Cysteine S-conjugates. *Methods Enzymol* **143**, 228-34.

Hayden, P. J., Ichimura, T., McCann, D. J., Pohl, L. R., and Stevens, J. L. (1991). Detection of cysteine conjugate metabolite adduct formation with specific mitochondrial proteins using antibodies raised against halothane metabolite adducts. *J Biol Chem* **266**, 18415-8.

Hayden, P. J., and Stevens, J. L. (1990). Cysteine conjugate toxicity, metabolism, and binding to macromolecules in isolated rat kidney mitochondria. *Mol Pharmacol* **37**, 468-76.

Healey, K., Calder, I. C., Yong, A. C., Crowe, C. A., Funder, C. C., Ham, K. N., and Tange, J. D. (1978). Liver and kidney damage induced by N-hydroxyparacetamol. *Xenobiotica* **8**, 403-11.

Heintz, N. (1993). Cell death and the cell cycle: a relationship between transformation and neurodegeneration? *Trends Biochem Sci* **18**, 157-9.

Hinson, J. A., Nelson, S. D., and Gillette, J. R. (1979a). Metabolism of [*p*-^{18}O]-phenacetin: the mechanism of activation of phenacetin to reactive metabolites in hamsters. *Mol Pharmacol* **15**, 419-27.

Hinson, J. A., Pohl, L. R., and Gillette, J. R. (1979b). N-Hydroxyacetaminophen: a microsomal metabolite of N-hydroxyphenacetin but apparently not of acetaminophen. *Life Sci* **24**, 2133-8.

Hinson, J. A., Pohl, L. R., Monks, T. J., Gillette, J. R., and Guengerich, F. P. (1980). 3-Hydroxyacetaminophen: a microsomal metabolite of acetaminophen. Evidence against an epoxide as the reactive metabolite of acetaminophen. *Drug Metab Dispos* **8**, 289-94.

Hockenbery, D. M., Oltvai, Z. N., Yin, X. M., Milliman, C. L., and Korsmeyer, S. J. (1993). BCL-2 functions in an antioxidant pathway to prevent apoptosis. *Cell* **75**, 241-51.

Hong, M., Cohen, S. D., and Khairallah, E. A. (1994). Translocation of the major cytosolic acetaminophen (APAP) protein adducts into the nucleus. *Toxicologist* **14**, 427.

Hsu, Y. T., Wolter, K. G., and Youle, R. J. (1997). Cytosol-to-membrane redistribution of BAX and BCL-X_L during apoptosis. *Proc Natl Acad Sci U S A* **94**, 3668-72.

Isacson, O. (1993). On neuronal health. *Trends Neurosci* **16**, 306-8.

Iwata, S., Lee, J. W., Okada, K., Lee, J. K., Iwata, M., Rasmussen, B., Link, T. A., Ramaswamy, S., and Jap, B. K. (1998). Complete structure of the 11-subunit bovine mitochondrial cytochrome bc_1 complex. *Science* **281**, 64-71.

James, E. A., Gygi, S. P., Adams, M. L., Pierce, R. H., Fausto, N., Aebersold, R. H., Nelson, S. D., and Bruschi, S. A. (2002). Mitochondrial aconitase modification, functional inhibition, and evidence for a supramolecular complex of the TCA cycle by the renal toxicant *S*-(1,1,2,2-tetrafluoroethyl)-L-cysteine. *Biochemistry* **41**, 6789-97.

Jia, Y., Rothermel, B., Thornton, J., and Butow, R. A. (1997). A basic helix-loop-helix-leucine zipper transcription complex in yeast functions in a signaling pathway from mitochondria to the nucleus. *Mol Cell Biol* **17**, 1110-7.

Jollow, D. J., Mitchell, J. R., Potter, W. Z., Davis, D. C., Gillette, J. R., and Brodie, B. B. (1973). Acetaminophen-induced hepatic necrosis. II. Role of covalent binding *in vivo*. *J Pharmacol Exp Ther* **187**, 195-202.

Katyare, S. S., and Satav, J. G. (1989). Impaired mitochondrial oxidative energy metabolism following paracetamol-induced hepatotoxicity in the rat. *Br J Pharmacol* **96**, 51-8.

Kaufman, R. J. (1999). Stress signaling from the lumen of the endoplasmic reticulum: coordination of gene transcriptional and translational controls. *Genes Dev* **13**, 1211-33.

Kirsch, D. G., Doseff, A., Chau, B. N., Lim, D. S., de Souza-Pinto, N. C., Hansford, R., Kastan, M. B., Lazebnik, Y. A., and Hardwick, J. M. (1999). Caspase-3-dependent cleavage of BCL-2 promotes release of cytochrome *c*. *J Biol Chem* **274**, 21155-61.

Klambt, C., Jacobs, J. R., and Goodman, C. S. (1991). The midline of the Drosophila central nervous system: a model for the genetic analysis of cell fate, cell migration, and growth cone guidance. *Cell* **64**, 801-15.

Kratochwil, K., and Schwartz, P. (1976). Tissue interaction in androgen response of embryonic mammary rudiment of mouse: identification of target tissue for testosterone. *Proc Natl Acad Sci U S A* **73**, 4041-4.

Kroemer, G., and Reed, J. C. (2000). Mitochondrial control of cell death. *Nat Med* **6**, 513-9.

Lahav, J., Gofer-Dadosh, N., Luboshitz, J., Hess, O., and Shaklai, M. (2000). Protein disulfide isomerase mediates integrin-dependent adhesion. *FEBS Lett* **475**, 89-92.

Landin, J. S., Cohen, S. D., and Khairallah, E. A. (1996). Identification of a 54-kDa mitochondrial acetaminophen-binding protein as aldehyde dehydrogenase. *Toxicol Appl Pharmacol* **141**, 299-307.

Lash, L. H., and Anders, M. W. (1986). Cytotoxicity of *S*-(1,2-dichlorovinyl)glutathione and *S*-(1,2- dichlorovinyl)-L-cysteine in isolated rat kidney cells. *J Biol Chem* **261**, 13076-81.

Lash, L. H., and Anders, M. W. (1987). Mechanism of *S*-(1,2-dichlorovinyl)-L-cysteine- and *S*-(1,2- dichlorovinyl)-L-homocysteine-induced renal mitochondrial toxicity. *Mol Pharmacol* **32**, 549-56.

Lash, L. H., Elfarra, A. A., and Anders, M. W. (1986). Renal cysteine conjugate β-lyase. Bioactivation of nephrotoxic cysteine S-conjugates in mitochondrial outer membrane. *J Biol Chem* **261**, 5930-5.

Lawson, J. A., Fisher, M. A., Simmons, C. A., Farhood, A., and Jaeschke, H. (1999). Inhibition of Fas receptor (CD95)-induced hepatic caspase activation and apoptosis by acetaminophen in mice. *Toxicol Appl Pharmacol* **156**, 179-86.

Lee, J. M., and Bernstein, A. (1993). p53 mutations increase resistance to ionizing radiation. *Proc Natl Acad Sci U S A* **90**, 5742-6.

Leist, M., Single, B., Castoldi, A. F., Kuhnle, S., and Nicotera, P. (1997). Intracellular adenosine triphosphate (ATP) concentration: a switch in the decision between apoptosis and necrosis. *J Exp Med* **185**, 1481-6.

Leist, M., Single, B., Naumann, H., Fava, E., Simon, B., Kuhnle, S., and Nicotera, P. (1999). Inhibition of mitochondrial ATP generation by nitric oxide switches apoptosis to necrosis. *Exp Cell Res* **249**, 396-403.

Li, B., and Dou, Q. P. (2000). BAX degradation by the ubiquitin/proteasome-dependent pathway: involvement in tumor survival and progression. *Proc Natl Acad Sci U S A* **97**, 3850-5.

Li, H., Zhu, H., Xu, C. J., and Yuan, J. (1998). Cleavage of BID by caspase 8 mediates the mitochondrial damage in the Fas pathway of apoptosis. *Cell* **94**, 491-501.

Li, P., Nijhawan, D., Budihardjo, I., Srinivasula, S. M., Ahmad, M., Alnemri, E. S., and Wang, X. (1997). Cytochrome c and dATP-dependent formation of Apaf-1/caspase-9 complex initiates an apoptotic protease cascade. *Cell* **91**, 479-89.

Liao, X., and Butow, R. A. (1993). RTG1 and RTG2: two yeast genes required for a novel path of communication from mitochondria to the nucleus. *Cell* **72**, 61-71.

Liao, X. S., Small, W. C., Srere, P. A., and Butow, R. A. (1991). Intramitochondrial functions regulate nonmitochondrial citrate synthase (CIT2) expression in *Saccharomyces cerevisiae*. *Mol Cell Biol* **11**, 38-46.

Little, E., Ramakrishnan, M., Roy, B., Gazit, G., and Lee, A. S. (1994). The glucose-regulated proteins (GRP78 and GRP94): functions, gene regulation, and applications. *Crit Rev Eukaryot Gene Expr* **4**, 1-18.

Liu, X., Kim, C. N., Yang, J., Jemmerson, R., and Wang, X. (1996). Induction of apoptotic program in cell-free extracts: requirement for dATP and cytochrome *c*. *Cell* **86**, 147-57.

Liu, Z., and Butow, R. A. (1999). A transcriptional switch in the expression of yeast tricarboxylic acid cycle genes in response to a reduction or loss of respiratory function. *Mol Cell Biol* **19**, 6720-8.

Lock, E. A., and Ishmael, J. (1998). The nephrotoxicity and hepatotoxicity of 1,1,2,2-tetrafluoroethyl-L- cysteine in the rat. *Arch Toxicol* **72**, 347-54.

Lowe, S. W., Schmitt, E. M., Smith, S. W., Osborne, B. A., and Jacks, T. (1993). p53 is required for radiation-induced apoptosis in mouse thymocytes. *Nature* **362**, 847-9.

Luderer, U., Kavanagh, T. J., White, C. C., and Faustman, E. M. (2001). Gonadotropin regulation of glutathione synthesis in the rat ovary. *Reprod Toxicol* **15**, 495-504.

Luo, X., Budihardjo, I., Zou, H., Slaughter, C., and Wang, X. (1998). BID, a BCL-2 interacting protein, mediates cytochrome *c* release from mitochondria in response to activation of cell surface death receptors. *Cell* **94**, 481-90.

Ma, Y., and Hendershot, L. M. (2001). The unfolding tale of the unfolded protein response. *Cell* **107**, 827-30.

Martin, J. L., Pumford, N. R., LaRosa, A. C., Martin, B. M., Gonzaga, H. M., Beaven, M. A., and Pohl, L. R. (1991). A metabolite of halothane covalently binds to an endoplasmic reticulum protein that is highly homologous to phosphatidylinositol-specific phospholipase C-alpha but has no activity. *Biochem Biophys Res Commun* **178**, 679-85.

Marzo, I., Brenner, C., Zamzami, N., Jurgensmeier, J. M., Susin, S. A., Vieira, H. L., Prevost, M. C., Xie, Z., Matsuyama, S., Reed, J. C., and Kroemer, G. (1998a). BAX and adenine nucleotide translocator cooperate in the mitochondrial control of apoptosis. *Science* **281**, 2027-31.

Marzo, I., Brenner, C., Zamzami, N., Susin, S. A., Beutner, G., Brdiczka, D., Remy, R., Xie, Z. H., Reed, J. C., and Kroemer, G. (1998b). The permeability transition pore complex: a target for apoptosis regulation by caspases and BCL-2-related proteins. *J Exp Med* **187**, 1261-71.

Matsuyama, S., Xu, Q., Velours, J., and Reed, J. C. (1998). The Mitochondrial F_0F_1-ATPase proton pump is required for function of the proapoptotic protein BAX in yeast and mammalian cells. *Mol Cell* **1**, 327-36.

McClintock, D. S., Santore, M. T., Lee, V. Y., Brunelle, J., Budinger, G. R., Zong, W. X., Thompson, C. B., Hay, N., and Chandel, N. S. (2002). BCL-2 family members and functional electron transport chain regulate oxygen deprivation-induced cell death. *Mol Cell Biol* **22**, 94-104.

Meunier, L., Usherwood, Y. K., Chung, K. T., and Hendershot, L. M. (2002). A subset of chaperones and folding enzymes form multiprotein complexes in endoplasmic reticulum to bind nascent proteins. *Mol Biol Cell* **13**, 4456-69.

Meyers, L. L., Beierschmitt, W. P., Khairallah, E. A., and Cohen, S. D. (1988). Acetaminophen-induced inhibition of hepatic mitochondrial respiration in mice. *Toxicol Appl Pharmacol* **93**, 378-87.

Miner, D. J., and Kissinger, P. T. (1979). Evidence for the involvement of N-acetyl-*p*-quinoneimine in acetaminophen metabolism. *Biochem Pharmacol* **28**, 3285-90.

Mitchell, J. R., Jollow, D. J., Gillette, J. R., and Brodie, B. B. (1973a). Drug metabolism as a cause of drug toxicity. *Drug Metab Dispos* **1**, 418-23.

Mitchell, J. R., Jollow, D. J., Potter, W. Z., Davis, D. C., Gillette, J. R., and Brodie, B. B. (1973b). Acetaminophen-induced hepatic necrosis. I. Role of drug metabolism. *J Pharmacol Exp Ther* **187**, 185-94.

Mitchell, J. R., Jollow, D. J., Potter, W. Z., Gillette, J. R., and Brodie, B. B. (1973c). Acetaminophen-induced hepatic necrosis. IV. Protective role of glutathione. *J Pharmacol Exp Ther* **187**, 211-7.

Narita, M., Shimizu, S., Ito, T., Chittenden, T., Lutz, R. J., Matsuda, H., and Tsujimoto, Y. (1998). BAX interacts with the permeability transition pore to induce permeability transition and cytochrome *c* release in isolated mitochondria. *Proc Natl Acad Sci U S A* **95**, 14681-6.

Nelson, S. D., Forte, A. J., and Dahlin, D. C. (1980). Lack of evidence for N-hydroxyacetaminophen as a reactive metabolite of acetaminophen in vitro. *Biochem Pharmacol* **29**, 1617-20.

Nelson, S. D., Tirmenstein, M. A., Rashed, M. S., and Myers, T. G. (1991). Acetaminophen and protein thiol modification. *Adv Exp Med Biol* **283**, 579-88.

National Toxicology Program (NTP) (1997) NTP Technical report on the toxicology and carcinogenesis of tetrafluoroethylene (CAS no 116-14-3) in F344/N rats and B6C3F$_1$ mice (inhalation studies) Technical Report Series No. 450, NIH publication no 97-3366. US Department of Health and Human Services, Public Health Service, National Institutes of Health, Research Triangle Park, NC.

National Toxicology Program (NTP) (2002) 10th Report on Carcinogens published at http://ehp.niehs.nih.gov/roc/toc10.html.

Pastorino, J. G., Tafani, M., Rothman, R. J., Marcinkeviciute, A., Hoek, J. B., Farber, J. L., and Marcinkeviciute, A. (1999). Functional consequences of the sustained or transient activation by BAX of the mitochondrial permeability transition pore. *J Biol Chem* **274**, 31734-9.

Patil, C., and Walter, P. (2001). Intracellular signaling from the endoplasmic reticulum to the nucleus: the unfolded protein response in yeast and mammals. *Curr Opin Cell Biol* **13**, 349-55.

Peelman, L. J., Chardon, P., Nunes, M., Renard, C., Geffrotin, C., Vaiman, M., Van Zeveren, A., Coppieters, W., van de Weghe, A., Bouquet, Y., and *et al.* (1995). The BAT1 gene in the MHC encodes an evolutionarily conserved putative nuclear RNA helicase of the DEAD family. *Genomics* **26**, 210-8.

Perkins, D. N., Pappin, D. J., Creasy, D. M., and Cottrell, J. S. (1999). Probability-based protein identification by searching sequence databases using mass spectrometry data. *Electrophoresis* **20**, 3551-67.

Pierce, R. H., Franklin, C. C., Campbell, J. S., Tonge, R. P., Chen, W., Fausto, N., Nelson, S. D., and Bruschi, S. A. (2002). Cell culture model for acetaminophen-induced hepatocyte death *in vivo*. *Biochemical Pharmacology* **64**, 413-424.

Plas, D. R., and Thompson, C. B. (2002). Cell metabolism in the regulation of programmed cell death. *Trends Endocrinol Metab* **13**, 75-8.

Pohl, L. R., Thomassen, D., Pumford, N. R., Butler, L. E., Satoh, H., Ferrans, V. J., Perrone, A., Martin, B. M., and Martin, J. L. (1991). Hapten carrier conjugates associated with halothane hepatitis. *Adv Exp Med Biol* **283**, 111-20.

Potter, W. Z., Davis, D. C., Mitchell, J. R., Jollow, D. J., Gillette, J. R., and Brodie, B. B. (1973). Acetaminophen-induced hepatic necrosis. III. Cytochrome P-450-mediated covalent binding *in vitro*. *J Pharmacol Exp Ther* **187**, 203-10.

Potter, W. Z., Thorgeirsson, S. S., Jollow, D. J., and Mitchell, J. R. (1974). Acetaminophen-induced hepatic necrosis. V. Correlation of hepatic necrosis, covalent binding and glutathione depletion in hamsters. *Pharmacology* **12**, 129-43.

Prasad, S. C., Soldatenkov, V. A., Kuettel, M. R., Thraves, P. J., Zou, X., and Dritschilo, A. (1999). Protein changes associated with ionizing radiation-induced apoptosis in human prostate epithelial tumor cells. *Electrophoresis* **20**, 1065-74.

Prescott, L. F. (1996). *Paracetamol (acetaminophen): a critical bibliographic review.* Taylor & Francis, London, UK.

Pumford, N. R., and Halmes, N. C. (1997). Protein targets of xenobiotic reactive intermediates. *Annu Rev Pharmacol Toxicol* **37**, 91-117.

Pumford, N. R., Halmes, N. C., Martin, B. M., Cook, R. J., Wagner, C., and Hinson, J. A. (1997). Covalent binding of acetaminophen to N-10-formyltetrahydrofolate dehydrogenase in mice. *J Pharmacol Exp Ther* **280**, 501-5.

Pumford, N. R., Martin, B. M., and Hinson, J. A. (1992). A metabolite of acetaminophen covalently binds to the 56 kDa selenium binding protein. *Biochem Biophys Res Commun* **182**, 1348-55.

Putcha, G. V., Deshmukh, M., and Johnson, E. M., Jr. (1999). BAX translocation is a critical event in neuronal apoptosis: regulation by neuroprotectants, BCL-2, and caspases. *J Neurosci* **19**, 7476-85.

Qiu, Y., Benet, L. Z., and Burlingame, A. L. (1998). Identification of the hepatic protein targets of reactive metabolites of acetaminophen *in vivo* in mice using two-dimensional gel electrophoresis and mass spectrometry. *J Biol Chem* **273**, 17940-53.

Qiu, Y., Benet, L. Z., and Burlingame, A. L. (2001). Identification of hepatic protein targets of the reactive metabolites of the non-hepatotoxic regioisomer of acetaminophen, 3'- hydroxyacetanilide, in the mouse in vivo using two-dimensional gel electrophoresis and mass spectrometry. *Adv Exp Med Biol* **500**, 663-73.

Ramsay, R. R., Rashed, M. S., and Nelson, S. D. (1989). *In vitro* effects of acetaminophen metabolites and analogs on the respiration of mouse liver mitochondria. *Arch Biochem Biophys* **273**, 449-57.

Rashed, M. S., Myers, T. G., and Nelson, S. D. (1990). Hepatic protein arylation, glutathione depletion, and metabolite profiles of acetaminophen and a non-hepatotoxic regioisomer, 3'- hydroxyacetanilide, in the mouse. *Drug Metab Dispos* **18**, 765-70.

Ray, S. D., Mumaw, V. R., Raje, R. R., and Fariss, M. W. (1996). Protection of acetaminophen-induced hepatocellular apoptosis and necrosis by cholesteryl hemisuccinate pretreatment. *J Pharmacol Exp Ther* **279**, 1470-83.

Redlich, C. A., West, A. B., Fleming, L., True, L. D., Cullen, M. R., and Riely, C. A. (1990). Clinical and pathological characteristics of hepatotoxicity associated with occupational exposure to dimethylformamide. *Gastroenterology* **99**, 748-57.

Rigobello, M. P., Donella-Deana, A., Cesaro, L., and Bindoli, A. (2000). Isolation, purification, and characterization of a rat liver mitochondrial protein disulfide isomerase. *Free Radic Biol Med* **28**, 266-72.

Robertson, J. D., and Orrenius, S. (2002). Role of mitochondria in toxic cell death. *Toxicology* **181-182**, 491-6.

Rosse, T., Olivier, R., Monney, L., Rager, M., Conus, S., Fellay, I., Jansen, B., and Borner, C. (1998). BCL-2 prolongs cell survival after BAX-induced release of cytochrome *c*. *Nature* **391**, 496-9.

Ruepp, S. U., Tonge, R. P., Shaw, J., Wallis, N., and Pognan, F. (2002). Genomics and proteomics analysis of acetaminophen toxicity in mouse liver. *Toxicol Sci* **65**, 135-50.

Ryser, H. J., Levy, E. M., Mandel, R., and DiSciullo, G. J. (1994). Inhibition of human immunodeficiency virus infection by agents that interfere with thiol-disulfide interchange upon virus-receptor interaction. *Proc Natl Acad Sci U S A* **91**, 4559-63.

Saito, M., Korsmeyer, S. J., and Schlesinger, P. H. (2000). BAX-dependent transport of cytochrome *c* reconstituted in pure liposomes. *Nat Cell Biol* **2**, 553-5.

Saleh, A., Srinivasula, S. M., Balkir, L., Robbins, P. D., and Alnemri, E. S. (2000). Negative regulation of the Apaf-1 apoptosome by Hsp70. *Nat Cell Biol* **2**, 476-83.

Sato, T., Hanada, M., Bodrug, S., Irie, S., Iwama, N., Boise, L. H., Thompson, C. B., Golemis, E., Fong, L., Wang, H. G., and *et al.* (1994). Interactions among members of the BCL-2 protein family analyzed with a yeast two-hybrid system. *Proc Natl Acad Sci U S A* **91**, 9238-42.

Scaffidi, C., Fulda, S., Srinivasan, A., Friesen, C., Li, F., Tomaselli, K. J., Debatin, K. M., Krammer, P. H., and Peter, M. E. (1998). Two CD95 (APO-1/Fas) signaling pathways. *EMBO J* **17**, 1675-87.

Scarpulla, R. C. (2002). Nuclear activators and coactivators in mammalian mitochondrial biogenesis. *Biochim Biophys Acta* **1576**, 1-14.

Scheffler, I. E. (1999). *Mitochondria*. Wiley-Liss, New York.

Schulte, U., and Weiss, H. (1995). Ubiquinol cytochrome *c* oxidoreductase of *Neurospora crassa*. *Methods Enzymol* **260**, 63-70.

Sekito, T., Thornton, J., and Butow, R. A. (2000). Mitochondria-to-nuclear signaling is regulated by the subcellular localization of the transcription factors RTG1p and RTG3p. *Mol Biol Cell* **11**, 2103-15.

Shen, J., Chen, X., Hendershot, L., and Prywes, R. (2002). ER stress regulation of ATF6 localization by dissociation of BiP/GRP78 binding and unmasking of Golgi localization signals. *Dev Cell* **3**, 99-111.

Shevchenko, A., Wilm, M., Vorm, O., and Mann, M. (1996). Mass spectrometric sequencing of proteins silver-stained polyacrylamide gels. *Anal Chem* **68**, 850-8.

Shimizu, S., Narita, M., and Tsujimoto, Y. (1999). BCL-2 family proteins regulate the release of apoptogenic cytochrome *c* by the mitochondrial channel VDAC. *Nature* **399**, 483-7.

Sidrauski, C., Chapman, R., and Walter, P. (1998). The unfolded protein response: an intracellular signaling pathway with many surprising features. *Trends Cell Biol* **8**, 245-9.

Skehan, P., Storeng, R., Scudiero, D., Monks, A., McMahon, J., Vistica, D., Warren, J. T., Bokesch, H., Kenney, S., and Boyd, M. R. (1990). New colorimetric cytotoxicity assay for anticancer-drug screening. *J Natl Cancer Inst* **82**, 1107-12.

Slobin, L. I. (1980). The role of eucaryotic factor Tu in protein synthesis. The measurement of the elongation factor Tu content of rabbit reticulocytes and other mammalian cells by a sensitive radioimmunoassay. *Eur J Biochem* **110**, 555-63.

Steele, C. M., Masson, H. A., Battershill, J. M., Gibson, G. G., and Ioannides, C. (1983). Metabolic activation of paracetamol by highly purified forms of cytochrome P-450. *Res Commun Chem Pathol Pharmacol* **40**, 109-19.

Steinman, H. M. (1995). The BCL-2 oncoprotein functions as a pro-oxidant. *J Biol Chem* **270**, 3487-90.

Suda, T., Takahashi, T., Golstein, P., and Nagata, S. (1993). Molecular cloning and expression of the Fas ligand, a novel member of the tumor necrosis factor family. *Cell* **75**, 1169-78.

Susin, S. A., Lorenzo, H. K., Zamzami, N., Marzo, I., Snow, B. E., Brothers, G. M., Mangion, J., Jacotot, E., Costantini, P., Loeffler, M., Larochette, N., Goodlett, D. R., Aebersold, R., Siderovski, D. P., Penninger, J. M., and Kroemer, G. (1999). Molecular characterization of mitochondrial apoptosis-inducing factor. *Nature* **397**, 441-6.

Tanaka, S., Uehara, T., and Nomura, Y. (2000). Up-regulation of protein-disulfide isomerase in response to hypoxia/brain ischemia and its protective effect against apoptotic cell death. *J Biol Chem* **275**, 10388-93.

Tetrafluoroethylene (TFE). (1999) *IARC Monogr Eval Carcinog Risks Hum* 71(pt 3): 1143-51.

Thompson, C. B. (1995). Apoptosis in the pathogenesis and treatment of disease. *Science* **267**, 1456-62.

Tirmenstein, M. A., and Nelson, S. D. (1989). Subcellular binding and effects on calcium homeostasis produced by acetaminophen and a nonhepatotoxic regioisomer, 3'-hydroxyacetanilide, in mouse liver. *J Biol Chem* **264**, 9814-9.

Tirmenstein, M. A., and Nelson, S. D. (1990). Acetaminophen-induced oxidation of protein thiols. Contribution of impaired thiol-metabolizing enzymes and the breakdown of adenine nucleotides. *J Biol Chem* **265**, 3059-65.

Tirmenstein, M. A., and Nelson, S. D. (1991). Hepatotoxicity after 3'-hydroxyacetanilide administration to buthionine sulfoximine pretreated mice. *Chem Res Toxicol* **4**, 214-7.

Tonge, R. P., Kelly, E. J., Bruschi, S. A., Kalhorn, T., Eaton, D. L., Nebert, D. W., and Nelson, S. D. (1998). Role of CYP1A2 in the hepatotoxicity of acetaminophen: investigations using Cyp1a2 null mice. *Toxicol Appl Pharmacol* **153**, 102-8.

Tsujimoto, Y., Gorham, J., Cossman, J., Jaffe, E., and Croce, C. M. (1985). The t(14;18) chromosome translocations involved in B-cell neoplasms result from mistakes in VDJ joining. *Science* **229**, 1390-3.

Tzung, S. P., Fausto, N., and Hockenbery, D. M. (1997). Expression of BCL-2 family during liver regeneration and identification of BCL-x as a delayed early response gene. *Am J Pathol* **150**, 1985-95.

Van Loo, G., Saelens, X., Van Gurp, M., MacFarlane, M., Martin, S. J., and Vandenabeele, P. (2002). The role of mitochondrial factors in apoptosis: a Russian roulette with more than one bullet. *Cell Death Differ* **9**, 1031-42.

Vander Heiden, M. G., Chandel, N. S., Schumacker, P. T., and Thompson, C. B. (1999). BCL-X_L prevents cell death following growth factor withdrawal by facilitating mitochondrial ATP/ADP exchange. *Mol Cell* **3**, 159-67.

Vander Heiden, M. G., Plas, D. R., Rathmell, J. C., Fox, C. J., Harris, M. H., and Thompson, C. B. (2001). Growth factors can influence cell growth and survival through effects on glucose metabolism. *Mol Cell Biol* **21**, 5899-912.

Verhagen, A. M., Ekert, P. G., Pakusch, M., Silke, J., Connolly, L. M., Reid, G. E., Moritz, R. L., Simpson, R. J., and Vaux, D. L. (2000). Identification of DIABLO, a mammalian protein that promotes apoptosis by binding to and antagonizing IAP proteins. *Cell* **102**, 43-53.

Wang, X. (2001). The expanding role of mitochondria in apoptosis. *Genes Dev* **15**, 2922-33.

Watanabe-Fukunaga, R., Brannan, C. I., Copeland, N. G., Jenkins, N. A., and Nagata, S. (1992). Lymphoproliferation disorder in mice explained by defects in Fas antigen that mediates apoptosis. *Nature* **356**, 314-7.

Wei, M. C., Lindsten, T., Mootha, V. K., Weiler, S., Gross, A., Ashiya, M., Thompson, C. B., and Korsmeyer, S. J. (2000). tBID, a membrane-targeted death ligand, oligomerizes BAK to release cytochrome *c*. *Genes Dev* **14**, 2060-71.

Wei, M. C., Zong, W. X., Cheng, E. H., Lindsten, T., Panoutsakopoulou, V., Ross, A. J., Roth, K. A., MacGregor, G. R., Thompson, C. B., and Korsmeyer, S. J. (2001).

Proapoptotic BAX and BAK: a requisite gateway to mitochondrial dysfunction and death. *Science* **292**, 727-30.

Weis, M., Morgenstern, R., Cotgreave, I. A., Nelson, S. D., and Moldeus, P. (1992). N-acetyl-*p*-benzoquinone imine-induced protein thiol modification in isolated rat hepatocytes. *Biochem Pharmacol* **43**, 1493-505.

Wolter, K. G., Hsu, Y. T., Smith, C. L., Nechushtan, A., Xi, X. G., and Youle, R. J. (1997). Movement of BAX from the cytosol to mitochondria during apoptosis. *J Cell Biol* **139**, 1281-92.

Wroblewski, V. J., Masnyk, M., Khambatta, S. S., and Becker, G. W. (1992). Mechanisms involved in degradation of human insulin by cytosolic fractions of human, monkey, and rat liver. *Diabetes* **41**, 539-47.

Wu, J. C., Merlino, G., Cveklova, K., Mosinger, B., Jr., and Fausto, N. (1994). Autonomous growth in serum-free medium and production of hepatocellular carcinomas by differentiated hepatocyte lines that overexpress transforming growth factor α-1. *Cancer Res* **54**, 5964-73.

Yang, J. C., Kahn, A., and Cortopassi, G. (2000). BCL-2 does not inhibit the permeability transition pore in mouse liver mitochondria. *Toxicology* **151**, 65-72.

Yin, X. M., Oltvai, Z. N., and Korsmeyer, S. J. (1994). BH1 and BH2 domains of BCL-2 are required for inhibition of apoptosis and heterodimerization with BAX. *Nature* **369**, 321-3.

Zakeri, Z. (1998). The study of cell death by the use of cellular and developmental models. In *When cells die : a comprehensive evaluation of apoptosis and programmed cell death* (R. A. Lockshin, Z. Zakeri and J. L. Tilly, eds.), pp. 97-129. Wiley-Liss, New York.

Zakeri, Z., Quaglino, D., and Ahuja, H. S. (1994). Apoptotic cell death in the mouse limb and its suppression in the hammertoe mutant. *Dev Biol* **165**, 294-7.

Zamzami, N., Susin, S. A., Marchetti, P., Hirsch, T., Gomez-Monterrey, I., Castedo, M., and Kroemer, G. (1996). Mitochondrial control of nuclear apoptosis. *J Exp Med* **183**, 1533-44.

Zhang, J., Huang, W., Chua, S. S., Wei, P., and Moore, D. D. (2002). Modulation of acetaminophen-induced hepatotoxicity by the xenobiotic receptor CAR. *Science* **298**, 422-4.

Zhou, L., McKenzie, B. A., Eccleston, E. D., Srivastava, S. P., Chen, N., Erickson, R. R., and Holtzman, J. L. (1996). The covalent binding of [^{14}C]acetaminophen to mouse

hepatic microsomal proteins: the specific binding to calreticulin and the two forms of the thiol:protein disulfide oxidoreductases. *Chem Res Toxicol* **9**, 1176-82.

Ziv, I., Melamed, E., Nardi, N., Luria, D., Achiron, A., Offen, D., and Barzilai, A. (1994). Dopamine induces apoptosis-like cell death in cultured chick sympathetic neurons--a possible novel pathogenetic mechanism in Parkinson's disease. *Neurosci Lett* **170**, 136-40.

Zong, W. X., Lindsten, T., Ross, A. J., MacGregor, G. R., and Thompson, C. B. (2001). BH3-only proteins that bind pro-survival BCL-2 family members fail to induce apoptosis in the absence of BAX and BAK. *Genes Dev* **15**, 1481-6.

Zoratti, M., and Szabo, I. (1995). The mitochondrial permeability transition. *Biochim Biophys Acta* **1241**, 139-76.

Zou, H., Henzel, W. J., Liu, X., Lutschg, A., and Wang, X. (1997). Apaf-1, a human protein homologous to *C. elegans* CED-4, participates in cytochrome *c*-dependent activation of caspase-3. *Cell* **90**, 405-13.

Zou, H., Li, Y., Liu, X., and Wang, X. (1999). An Apaf-1.cytochrome *c* multimeric complex is a functional apoptosome that activates procaspase-9. *J Biol Chem* **274**, 11549-56.

Vita

Michael Lynn Adams was born in North Carolina. At Campbell University in Buies Creek he earned a Doctor of Pharmacy in 1996. In 2003, he earned a Doctor of Philosophy at the University of Washington in Medicinal Chemistry.